PCCP

PAPER

Cite this: *Phys. Chem. Chem. Phys.*, 2015, **17**, 3081

Formation of complex organic molecules in methanol and methanol–carbon monoxide ices exposed to ionizing radiation – a combined FTIR and reflectron time-of-flight mass spectrometry study†

Surajit Maity, Ralf I. Kaiser* and Brant M. Jones*

Received 16th September 2014,
Accepted 10th November 2014

DOI: 10.1039/c4cp04149f

www.rsc.org/pccp

The radiation induced chemical processing of methanol and methanol–carbon monoxide ices at 5.5 K exposed to ionizing radiation in the form of energetic electrons and subsequent temperature programmed desorption is reported in this study. The endogenous formation of complex organic molecules was monitored *online* and *in situ via* infrared spectroscopy in the solid state and post irradiation with temperature programmed desorption (TPD) using highly sensitive reflectron time-of-flight (ReTOF) mass spectrometry coupled with single photoionization at 10.49 eV. Infrared spectroscopic analysis of the processed ice systems resulted in the identification of simple molecules including the hydroxymethyl radical (CH_2OH), formyl radical (HCO), methane (CH_4), formaldehyde (H_2CO), carbon dioxide (CO_2), ethylene glycol ($HOCH_2CH_2OH$), glycolaldehyde ($HOCH_2CHO$), methyl formate ($HCOOCH_3$), and ketene (H_2CCO). In addition, ReTOF mass spectrometry of subliming molecules following temperature programmed desorption definitely identified several closed shell C/H/O bearing organics including ketene (H_2CCO), acetaldehyde (CH_3COH), ethanol (C_2H_5OH), dimethyl ether (CH_3OCH_3), glyoxal (HCOCOH), glycolaldehyde ($HOCH_2CHO$), ethene-1,2-diol (HOCHCHOH), ethylene glycol ($HOCH_2CH_2OH$), methoxy methanol (CH_3OCH_2OH) and glycerol ($CH_2OHCHOHCH_2OH$) in the processed ice systems. Additionally, an abundant amount of molecules yet to be specifically identified were observed sublimating from the irradiated ices including isomers with the formula $C_3H_{(x=4,6,8)}O$, $C_4H_{(x=8,10)}O$, $C_3H_{(x=4,6,8)}O_2$, $C_4H_{(x=6,8)}O_2$, $C_3H_{(x=4,6)}O_3$, $C_4H_8O_3$, $C_4H_{(x=4,6,8)}O_4$, $C_5H_{(x=6,8)}O_4$ and $C_5H_{(x=6,8)}O_5$. The last group of molecules containing four to five oxygen atoms observed sublimating from the processed ice samples include an astrobiologically important class of sugars relevant to RNA, phospholipids and energy storage. Experiments are currently being designed to elucidate their chemical structure. In addition, several reaction pathways were identified in the irradiated ices of mixed isotopes based upon the results of both *in situ* FTIR analysis and TPD ReTOF gas phase analysis. In general, the results of this study provide crucial information on the formation of a variety of classes of organics including alcohols, ketones, aldehydes, esters, ethers, and sugars within the bulk ices upon exposure to ionizing radiation that are relevant to the molecular clouds within the interstellar medium.

1. Introduction

During the last few decades, cold molecular clouds and star forming regions have been extensively explored for complex organic molecules as these species serve as a 'molecular clock' and thereby aid in an understanding of the chemical evolution of the interstellar medium. In these extreme environments, approximately 60 amongst the currently detected 180 molecules[1] contain six or more atoms with at least one carbon atom and are labelled as complex organic molecules (COMs).[2,3] Furthermore, those molecules containing oxygen such as acetaldehyde (CH_3CHO), acetic acid (CH_3COOH), glycolaldehyde ($HOCH_2CHO$), formamide ($HCONH_2$), and acetamide (CH_3CONH_2) have received considerable interest from the astrochemistry and astrobiology communities[4–6] as these are considered as key precursors and building blocks of biologically important molecules like carbohydrates,[7] amino acids,[8] and polypeptides.[6,9] The discoveries of several sugar related molecules such as dihydroxyacetone (simple sugar), glycerol (sugar alcohol), and glyceric acid (sugar acid)[9]

Department of Chemistry, W.M. Keck Research Laboratory in Astrochemistry, University of Hawai'i at Manoa, Honolulu, HI 96822, USA. E-mail: ralfk@hawaii.edu, brantmj@hawaii.edu

† Electronic supplementary information (ESI) available. See DOI: 10.1039/c4cp04149f

along with amino acids[10,11] in carbonaceous meteorites such as Murchison encouraged the search for their interstellar origin as is hinted by their isotope ratios.[12,13] In addition, glycolaldehyde (the simplest form of a sugar, $HOCH_2CHO$)[14–18] and ethylene glycol (a sugar alcohol, $HOCH_2CH_2OH$)[17,19,20] have been detected in distinct astrophysical environments ranging from hot cores to the molecular clouds in the galactic center. Although searches for higher mass sugars such as glyceraldehyde ($HOCH_2CH(OH)CHO$)[21] and 1,3-dihydroxyacetone ($(HOCH_2)_2CO$)[22–24] have been carried out, these molecules have still remained elusive to date.

A current catalogue of the observed oxygen bearing complex organic molecules is listed in Table S1 of the ESI† along with the locations of their detection and molecular abundance with most of these molecules detected in the Sgr B2(N) hot core. Recently however, Requena-Toress *et al.* detected several of these molecules in the cold molecular clouds (MC G − 0.11–0.08, MC G − 0.02–0.07, and MC G + 0.69–0.03) within the Galactic Center.[17,25] Despite well-established detections of these interstellar molecules, a detailed understanding of the formation pathways has remained elusive. Often, the abundance of complex organics observed toward protostellar cores at temperatures of up to 100 K cannot be explained by networks of gas phase processes *via* neutral–neutral and/or ion–molecule reactions.[2,3,26] For example, the formation of complex organic molecules in the gas phase often requires the involvement of an internally (rovibrationally) excited intermediate, which is highly short lived on the picosecond timescale without a third body for collision induced relaxation.[2] Subsequent models have attempted to boost the production rates of COMs by incorporating grain–surface chemistry, often involving the use of radical–radical reactions on interstellar grains.[27,28] In addition, chemical network models attempting to explain the observed abundance of complex organics in the hot molecular core have acknowledged the requirement to include induced suprathermal chemical reactions within icy mantles *via* UV photons and galactic cosmic rays.[29–33] The significance of non-traditional chemistry within the bulk ice is again emphasized based on the relative abundance of COMs in the *cold* Central Molecular Zone and the Galactic Disk, where observations strongly suggest that the COMs are formed in the icy mantles followed by ejection to the gas phase by shock waves.[17,25] Further, the fractional abundance of molecules such as methyl formate ($HCOOCH_3$) and ethanol (C_2H_5OH) in the outflow of L1157 suggests that the time scale for the gas phase synthesis is too short, *i.e.* less than 2000 years are required for the formation of these COMs following the proposed reaction network and that these complex molecules were therefore most probably formed in the icy mantles followed by desorption due to outflow shocks.[34]

Of the many successes from the Infrared Space Observatory[35,36] and the Spitzer c2d ice survey[37–41] was the confirmation that interstellar grains are coated with an icy mantle consisting mainly of water (H_2O) followed by methanol (CH_3OH), carbon monoxide (CO), carbon dioxide (CO_2), methane (CH_4), ammonia (NH_3), and formaldehyde (H_2CO) holding a thickness of up to a few hundreds of nanometers. The interaction of these ices with energetic ions simulating galactic cosmic rays (GCRs) and with ultraviolet photons (UV) simulating the internal ultraviolet field inside cold molecular clouds has repeatedly been demonstrated to chemically modify ices *via* non-thermal, non-equilibrium chemistry involving radical reactants such as hydrogen, oxygen, nitrogen, and carbon atoms, which are not in thermal equilibrium with the 10 K ices.[42–47] Therefore, in cold molecular clouds, the interaction of ionizing radiation with ice coated nanoparticles is expected to lead to the synthesis of complex organic molecules, which cannot be explained by classical thermal chemistry.[2,3] Once the molecular cloud collapses and transforms to a star-forming region, the elevated temperatures result in the sublimation of these newly formed organic molecules from the grains into the gas phase thereby explaining the abundance of these molecules in the hot cores and corinos. In addition, non-thermal desorption *via* cosmic ray particles, grain–grain collisions, and/or shocks may result in the ejection of COMs into the gas phase of the cold cloud cores.[2,3]

Previous laboratory experiments mimicking interstellar ices exposed to ionizing radiation have provided compelling evidence for the formation of complex organic molecules in the ices at temperatures as low as 5 K. Acetaldehyde for instance has been shown to be formed in methane (CH_4)–carbon monoxide (CO)[48] and ethylene (C_2H_4)–carbon dioxide (CO_2) ices upon electron irradiation at 10 K thus simulating the effects of secondary electrons within the track of GCRs once penetrating the ice coated interstellar grains.[49] The thermodynamically less stable C_2H_4O isomers, vinyl alcohol (CH_2CHOH) and ethylene oxide (c-C_2H_4O), were found as well in the irradiated ethylene (C_2H_4)–carbon dioxide (CO_2) ice.[49] The structural isomers propynal (HCCCHO) and cyclopropenone (c-C_3H_2O) were formed in an icy mixture of acetylene (C_2H_2) and carbon monoxide (CO) at 10 K upon radiolysis.[50] Additionally, formic acid (HCOOH) and acetic acid (CH_3COOH) were found to be endogenous products in water (H_2O)–carbon monoxide (CO)[51] and methane (CH_4)–carbon dioxide (CO_2) ices upon exposure to ionizing radiation, respectively.[52] Following the first detection of glycolaldehyde ($HOCH_2CHO$) in the galactic center,[14] irradiation experiments with ices consisting of methanol (CH_3OH) and methanol (CH_3OH)–carbon monoxide (CO) were conducted in the hope of explaining the origin of this sugar together with the observed isomers, *i.e.*, methyl formate ($HCOOCH_3$) and acetic acid (CH_3COOH), as both methanol (CH_3OH) and carbon monoxide (CO) are the two most abundant species (relative to water) in the interstellar ices.[35–41] Indeed, experiments on methanol[53] ice and a binary ice of methanol and carbon monoxide[54] exposed to ionizing radiation resulted in the identification of glycolaldehyde ($HOCH_2CHO$), methyl formate ($HCOOCH_3$), and ethylene glycol ($HOCH_2CH_2OH$) in addition to the formyl radical (HCO), hydroxyl radical (OH), methane (CH_4), carbon dioxide (CO_2), and formaldehyde (H_2CO) at 10 K. Similar work was conducted utilizing broad band UV photons produced *via* a hydrogen microwave discharge lamp and found evidence of methyl formate ($HCOOCH_3$) and glycolaldehyde ($HOCH_2CHO$) as potential products post photolysis of methanol (CH_3OH) and mixtures with carbon monoxide (CO);[55] a subsequent study on UV processed methanol and methanol–carbon monoxide ices identified methyl formate ($HCOOCH_3$), ethylene glycol ($HOCH_2CH_2OH$), ethanol (C_2H_5OH), and dimethyl ether (CH_3OCH_3).[56] Methoxymethanol (CH_3OCH_2OH) was first identified upon exposure of methanol (CH_3OH) ices to low energy electrons and later confirmed along with other COMs such as ethylene glycol ($HOCH_2CH_2OH$), glycolaldehyde ($HOCH_2CHO$), and possibly glycolic acid ($HOCOCH_2OH$).[57] Additional experiments *via* 200 keV proton bombardment on frozen methanol (CH_3OH) and mixtures with carbon monoxide (CO) resulted once again in the identification of glycolaldehyde ($HOCH_2CHO$),[58,59] methyl formate ($HCOOCH_3$)[58,59] and ethylene glycol ($HOCH_2CH_2OH$).[59] Chen *et al.* reported the formation of dimethylether (CH_3OCH_3), glycolaldehyde ($HOCH_2CHO$), methyl formate ($HCOOCH_3$), acetic acid (CH_3COOH), and ethylene glycol ($HOCH_2CH_2OH$) in irradiated methanol ices using soft X-rays containing peak energies of 300 eV and 550 eV over a broad band spectrum (250–1200 eV).[60] To summarize, multiple experiments have been conducted over the last few decades regarding the chemical modification of methanol ices upon exposure to ionizing radiation simulating astrophysical conditions. Within these studies, a consensus on the formation of small molecules, *e.g.*, carbon monoxide (CO), carbon dioxide (CO_2), formaldehyde (H_2CO), methane (CH_4) and for the most part ethanol (C_2H_5OH), glycolaldehyde ($HOCH_2CHO$), ethylene glycol ($HOCH_2CH_2OH$), methyl formate ($HCOOCH_3$), and acetic acid (CH_3COOH), has been ascertained *via in situ* infrared spectroscopy. Unfortunately, relying only on this technique can often lead to ambiguous assignments of large organics with similar functional groups due to the overlap of their group frequencies, in particular of the important carbonyl group.

Recently, utilizing single photoionization reflectron time-of-flight (ReTOF-PI) mass spectrometry in addition to solid state FTIR spectroscopy, significant progress has been made toward a detailed understanding of several key classes of complex organic molecules carrying the carbonyl functional group.[61,62] Moreover, we have reported on the detection of glycolaldehyde ($HOCH_2CHO$) in irradiated methanol and methanol–carbon monoxide ices exposed to energetic electrons *via* ReTOF-PI mass spectrometry.[63] The continued success of the ReTOF-PI mass spectrometry approach in identifying astrochemically relevant complex organics synthesized in simple ices of methanol and methanol–carbon monoxide is explored here. In this study, we present compelling evidence for the formation of key classes of complex organic molecules synthesized in irradiated ices of methanol (CH_3OH) and methanol (CH_3OH)–carbon monoxide (CO) from infrared spectral data correlated with temperature programmed desorption (TPD) studies exploiting ReTOF-PI gas phase detection at doses relevant to the lifetime of an interstellar icy grain within a cold molecular cloud prior to the warm-up (star formation) phase.

2. Experimental

The experiments were carried out in a novel, contamination-free ultra-high vacuum (UHV) chamber at the W.M. Keck Research Laboratory in Astrochemistry. A detailed description of the instrumentation has been reported previously.[61–64] Briefly, the main chamber was evacuated down to a base pressure of a few 10^{-11} Torr by using oil-free magnetically suspended turbomolecular pumps backed with dry scroll pumps. A closed-cycle helium refrigerator (Sumitomo Heavy Industries, RDK-415E) was used to cool a polished silver substrate mounted on the cold finger to a final temperature of 5.5 ± 0.1 K. The entire cold finger assembly was freely rotatable within the horizontal center plane and translatable in the vertical direction *via* an UHV compatible bellow (McAllister, BLT106) and a differentially pumped rotational feedthrough (Thermoionics Vacuum Products, RNN-600/FA/MCO). The corresponding gases (methanol vapor and premixed methanol–carbon monoxide gas) were then deposited through a glass capillary array with a background pressure reading in the main chamber of about 5×10^{-8} Torr for approximately 3 minutes. This yielded ice samples with thicknesses of 510 ± 10 nm for pristine methanol ices and 495 ± 10 nm for mixed ices of methanol–carbon monoxide. The thickness of the samples was determined *in situ* using laser interferometry[65,66] with a helium–neon (HeNe) laser (CVI Melles-Griot, 25-LHP-213) at 632.8 nm at an incident angle of 4°. From this technique, based upon the ratios of peak to peak intensities,[67] we derived an index of refraction $n_f = 1.34 \pm 0.02$ for pure methanol, in agreement with published data of 1.35,[68] and $n_f = 1.35 \pm 0.02$ for the binary CH_3OH–CO mixture.

In order to determine the ratios of the components in the methanol–carbon monoxide ices, additional calibration experiments were performed. Here, methanol ices with distinct thicknesses were deposited under identical experimental conditions. Subsequently, the ices were annealed at 0.5 K min^{-1} allowing the ices to sublime with gas phase molecules monitored using a quadrupole mass spectrometer (QMS; Extrel, Model 5221) operated as a residual gas analyzer exploiting electron impact ionization with 100 eV electrons at a current of 1 mA. The resultant total QMS signal at m/z = 32 amu (CH_3OH^+) was then integrated and correlated as a function of the deposited molecules determined from the ice thicknesses and the known density of the pure methanol samples. As such, we can determine the total number of methanol molecules in the mixed ices of methanol–carbon monoxide by comparing the QMS ion signal at m/z = 32 amu with the calibration curve. Here, a total of $(4.6 \pm 0.5) \times 10^{17}$ methanol molecules were determined; this results in a thickness of 240 ± 20 nm. In the limit of volume additivity,[69] we can calculate a thickness of (255 ± 30) nm for carbon monoxide by subtracting the methanol thickness (240 ± 20 nm) from the total thickness resulting in an estimated value of $(6.3 \pm 0.6) \times 10^{17}$ carbon monoxide molecules. Consequently, the mixed methanol–carbon monoxide ice was found to be in the ratio of $(4.0 \pm 0.2):(5.0 \pm 0.2)$. Here, the densities of methanol and carbon monoxide ices were used as 1.020 g cm^{-3} and 1.029 g cm^{-3}, respectively.[54] In addition, isotopically labeled CD_3OD, $^{13}CH_3OH$, and $CH_3{}^{18}OH$ ices (Sigma-Aldrich) for pure methanol irradiation experiments and CD_3OD–CO, $^{13}CH_3OH$–CO, $CH_3{}^{18}OH$–CO, CD_3OD–^{13}CO, $CH_3{}^{18}OH$–$C^{18}O$, and $CH_3OH–C^{18}O$ (labelled CO was supplied by Cambridge Isotope Labs) mixed ices for methanol–carbon monoxide irradiation experiments were also used to confirm the identified products *via* isotope shifts of the infrared absorption bands and in the reflectron time-of-flight data.

The ice systems were then irradiated with 5 keV electrons isothermally at 5.5 $\pm$ 0.1 K for one hour at 30 nA over an area of 1.0 $\pm$ 0.1 cm^2 and an angle of incidence of 70° relative to the surface normal of the ice. The total dose deposited in the ice sample was determined from Monte Carlo simulations (CASINO)[70,71] taking into consideration the back scattering coefficient, the energy deposited from the back scattered electrons, and the average penetration depth (ESI,† Table S2). The total energy deposited in the ice was 6.5 $\pm$ 0.8 eV per CH_3OH molecule, and 5.2 $\pm$ 0.8 eV per molecule on average for the irradiation experiments of the binary CH_3OH–CO (4 : 5) ice mixture. It should be noted here that in determining the applied dose of the isotopic analogs both the index of refraction and density were assumed to be similar to that of their respective normal counterparts as most of these data are not empirically available. Furthermore, the density of the CH_3OH–CO ice mixture was calculated as 1.026 g cm^{-3} based on the weighted fraction of the density of the pure components.[69]

For the *online* and *in situ* identification of new molecular band carriers of the ices during irradiation, a Fourier transform infrared spectrometer (Nicolet 6700) was used to monitor the samples throughout the duration of the experiment with an IR spectrum collected every two minutes in the range of 6000–400 cm^{-1} at a resolution of 4 cm^{-1}. Each FTIR spectrum was recorded in the absorption–reflection–absorption mode (reflection angle of 45°) for two minutes resulting in a set of 30 infrared spectra during the radiation exposure (one hour) for each system. After the irradiation, the sample was kept at 5.5 K for one hour; then, temperature programmed desorption (TPD) studies were conducted by heating the irradiated ices at a rate of 0.5 K min^{-1} to 300 K. Throughout the thermal sublimation process, the ice samples were monitored *via* infrared spectroscopy and single photon ionization reflectron time-of-flight mass spectrometry[61,62] separately. The products were ionized upon sublimation *via single photon ionization* exploiting pulsed (30 Hz) coherent vacuum ultraviolet (VUV) light at 118.2 nm (10.49 eV). Here, the third harmonic (354.6 nm) of a high-power pulsed Nd:YAG laser (Spectra Physics, PRO – 250; 30 mJ per pulse) was frequency tripled to produce VUV photons utilizing xenon (Xe) gas as the nonlinear medium.[72] A pulsed valve directed the xenon gas (99.999%; Specialty Gases of America) at a backing pressure of 1266 Torr into a T-shaped stainless steel adapter with a 1 mm diameter hole and 25 mm in length in line with the propagating laser beam. The generated VUV light was then separated and directed to about 1 mm above the ice surface utilizing an off-axis, differentially pumped lithium fluoride (LiF) lens,[73] where the sublimating molecules were then photoionized. The molecular ions were detected utilizing a multichannel plate with a dual chevron configuration following a fast preamplifier (Ortec 9306) and shaped with a 100 MHz discriminator (Advanced Research Instruments, F-100TD). The ReTOF spectra were then recorded with a personal-computer-based multichannel scaler (FAST ComTec, P7888-1 E) using a bin width of 4 ns, triggered at 30 Hz with 3600 sweeps per mass spectrum reflecting a 1 K change in temperature. Additionally, the subliming molecules were also probed *via* a quadrupole mass spectrometer (Extrel, Model 5221) operating in a residual-gas analyzer mode in the mass range of 1–500 amu with an electron impact ionization of 100 eV and an emission current of 1 mA.

To assist in the identification of a specific molecule sublimating in the temperature programmed desorption spectra utilizing ReTOF-PI mass spectrometry, calibration experiments were performed under identical experimental conditions and annealing rates. Here, the vapor of a specific molecule was premixed in pure methanol and/or methanol–carbon monoxide and subsequently deposited onto the substrate kept at 5.5 K. Then, TPD was conducted by heating the premixed ices at the same rate of 0.5 K min^{-1} up to 300 K and subsequently the molecule was detected using ReTOF-PI mass spectrometry. In summary, a total of 12 calibration experiments were performed with 17 different molecules in both methanol and methanol–carbon monoxide ices. The details of the calibration samples and the relative percent amount in the premixed ices are listed in ESI,† Table S3.

3. Results

3.1. Infrared spectroscopy

The infrared spectra of the isotopologue ice systems of methanol (CH_3OH, CD_3OD, $^{13}CH_3OH$ and $CH_3{}^{18}OH$) and mixed ice systems of methanol–carbon monoxide (CH_3OH–CO, CD_3OD–CO, $CH_3{}^{18}OH–C^{18}O$, $^{13}CH_3OH$–CO, $CD_3OD–{}^{13}CO$, $CH_3{}^{18}OH$–CO and $CH_3OH–C^{18}O$) recorded before and after the irradiation are shown in Fig. 1A and B as well as in ESI,† Fig. S1, respectively. The newly formed products are also shown in the 2200–1600 cm^{-1} and 1400–800 cm^{-1} regions of interest along with assignments. Infrared absorption features of the pristine ices and new absorption features that emerged following irradiation are summarized in Tables 1 and 2, respectively. Upon exposure to ionizing radiation several products were observed *in situ* within the bulk ice. Here, in both the methanol and the mixed methanol–carbon monoxide ices the hydroxymethyl radical (CH_2OH) was identified *via* the ν_4 fundamental at 1192 cm^{-1} and 1193 cm^{-1}, respectively; the formyl radical (HCO) was gauged from the ν_3 fundamental at 1842 cm^{-1} in both irradiated ices; methane (CH_4) was detected *via* the ν_4 fundamental at 1304 cm^{-1} and 1303 cm^{-1}. Formation of formaldehyde (H_2CO) was confirmed from the ν_2, ν_3, and ν_4 fundamentals at 1246 cm^{-1}, 1499 cm^{-1} and 1726 cm^{-1} in irradiated CH_3OH ices and at 1249 cm^{-1}, 1497 cm^{-1}, and 1726 cm^{-1} in the irradiated CH_3OH–CO ices. These absorption frequencies are in agreement with previous studies.[53–55,60,74] Formation of carbon monoxide (CO) was confirmed *via* the ν_1 fundamental at 2135 cm^{-1} in the irradiated CH_3OH ice systems. Carbon dioxide (CO_2) was as well observed in both the irradiated CH_3OH and mixed CH_3OH–CO ices as confirmed by the ν_3 band at 2339 cm^{-1} and 2342 cm^{-1}, respectively.

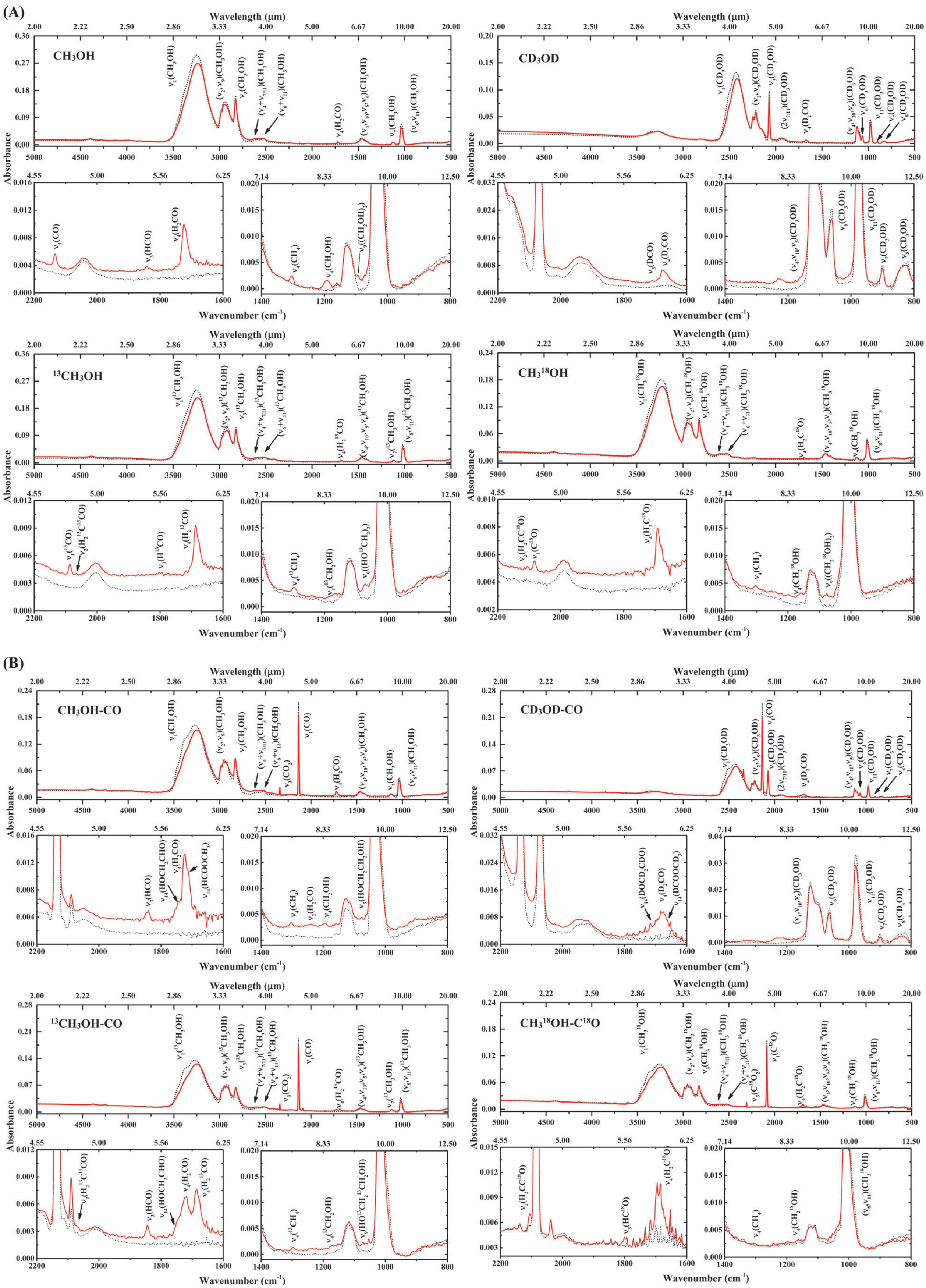
(A)
CH3OH
CD3OD
13CH3OH
CH318OH
(B)
CH3OH-CO
CD3OD-CO
13CH3OH-CO
CH318OH-C18O
Wavelength (μm)
Absorbance
Wavenumber (cm-1)

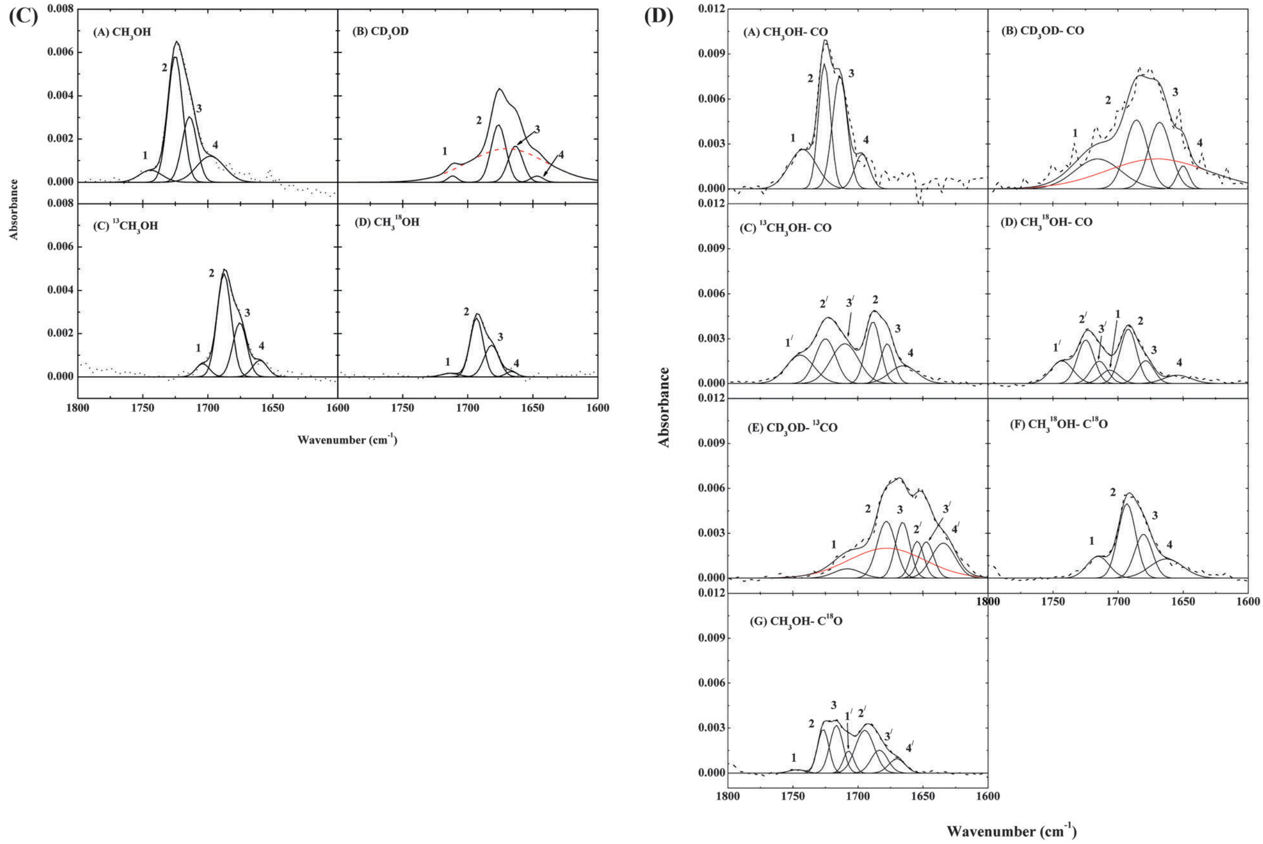

Fig. 1 (A) Infrared absorption spectra of CH_3OH, CD_3OH, $^{13}CH_3OH$ and $CH_3{}^{18}OH$ ices before (dotted trace) and after (solid trace) irradiation at 5.5 K. Newly emerged absorption features in each ice are shown in 2200–1600 cm^{-1} and 1400–800 cm^{-1} regions along with the assignments as listed in Table 2. (B) Infrared absorption spectra of methanol–carbon monoxide mixed ices (CH_3OH–CO, CD_3OD–CO, $CH_3{}^{18}OH$–$C^{18}O$, $^{13}CH_3OH$–CO) before (dotted trace) and after (solid trace) irradiation at 5.5 K. Newly emerged absorption features in each ice are shown in 2200–1600 cm^{-1} and 1400–800 cm^{-1} regions along with the assignments as listed in Table 2. (C) Deconvoluted infrared absorption features in the region of the carbonyl functional group in (A) CH_3OH, (B) CD_3OD, (C) $^{13}CH_3OH$, and (D) $CH_3{}^{18}OH$ ices. The bands marked as (1) and (4) are assigned as the ν_{14} and $2\nu_6$ bands of glycolaldehyde ($HOCH_2CHO$), respectively. The bands marked as (2) and (3) are assigned to formaldehyde (H_2CO) and methyl formate ($HCOOCH_3$). The dotted line in (B) corresponds to $2\nu_8$ of CD_3OD as in the pristine ice.

Ethylene glycol ($HOCH_2CH_2OH$) was identified in both the irradiated ices *via* the ν_9 fundamental at 1094 cm^{-1} based on the assignment of this molecule in previous studies of irradiated methanol ices[53,74] at 1090 cm^{-1} and 1088 cm^{-1}. Note that all other relatively strong infrared absorption bands of ethylene glycol coincidentally overlap with the methanol absorptions[53,54] and therefore are masked. The assignments of these absorptions were also confirmed *via* their isotopic shifts in irradiated ices consisting of CD_3OD, $^{13}CH_3OH$, and $CH_3{}^{18}OH$ and irradiated binary mixed ices consisting of CD_3OD–CO, $CH_3{}^{18}OH$–$C^{18}O$, $^{13}CH_3OH$–CO, CD_3OD–^{13}CO, $CH_3{}^{18}OH$–CO and CH_3OH–$C^{18}O$ as compiled in Table 2. We have also identified ketene (H_2CCO) in $^{13}CH_3OH$ and $CH_3{}^{18}OH$ ices *via* the observation of the ν_2 fundamental at 2067 cm^{-1} ($H_2{}^{13}C^{13}CO$) and 2107 cm^{-1} ($H_2CC^{18}O$), as shown in Fig. 1A. The assignment of ketene agrees with previously reported observations of the ν_2 fundamental at 2071 cm^{-1} for $H_2{}^{13}C^{13}CO$ and 2107 cm^{-1} for $H_2CC^{18}O$.[64,75] In the case of methanol–carbon monoxide ices, ν_2 absorption features of ketene were also identified at 2107 cm^{-1} ($H_2CC^{18}O$) in $CH_3{}^{18}OH$–$C^{18}O$ ice and at 2106 cm^{-1} ($H_2CC^{18}O$) in CH_3OH–$C^{18}O$ ice in agreement with the literature values.[64,75] Note that only isotopologues of ketene are observed as the absorption features of the natural H_2CCO isotopomer and the ν_1 absorption band of carbon monoxide directly overlap at ~2135 cm^{-1}.

3.1.1. Infrared absorption spectra of the carbonyl functional group. The new absorption features connected to the carbonyl functional group in the 1800–1600 cm^{-1} region deserve special attention. These bands are very broad (Fig. 1C and D) and subsequent assignment to only one molecular carrier is erroneous. Further evidence suggesting more than one molecular carrier of this functional group is gained from the additional infrared absorption features of the carbonyl band regions in the irradiated mixed isotopic ice systems of methanol–carbon monoxide ($^{13}CH_3OH$–CO, CD_3OD–^{13}CO, $CH_3{}^{18}OH$–CO and CH_3OH–$C^{18}O$) as shown in Fig. 1D. Therefore, a deconvolution to the absorption features in the 1800–1600 cm^{-1} region was performed with the peak positions and their associated assignments shown in Fig. 1C and D and listed in Tables 2 and 3. In both the irradiated ices of methanol (CH_3OH) and methanol–carbon monoxide (CH_3OH–CO), the deconvolution identified four distinct bands centered at 1743 cm^{-1}, 1726 cm^{-1}, 1714 cm^{-1}, and 1697 cm^{-1}. The band at 1743 cm^{-1} has been

Table 1 Infrared absorption features of the pristine ices of methanol and methanol–carbon monoxide (4 : 5) at 5.5 K

Assignments	CH_3OH	CD_3OD	$^{13}CH_3OH$	$CH_3{}^{18}OH$	CH_3OH–CO	CD_3OD–CO	$CH_3{}^{18}OH$–$C^{18}O$	$^{13}CH_3OH$–CO	CD_3OD–^{13}CO	$CH_3{}^{18}OH$–CO	CH_3OH–$C^{18}O$
$\nu_2/\nu_9 + \nu_4/\nu_6/\nu_{10}$ (CH_3OH)	4399	—	4380	4398	4399	—	4397	4385	—	4395	4403
$\nu_2/\nu_9 + \nu_4$ (CH_3OH)	4274	—	4270	4273	4274	—	4274	4276	—	4276	4277
$2\nu_1$ (CO)	—	—	—	—	4247	4246	4146	4246	4152	4245	4145
$\nu_2/\nu_9 + \nu_8$ (CH_3OH)	4016	—	—	3989	4021	—	3998	3993	—	3994	4023
$\nu_2/\nu_9 + \nu_8$ (CH_3OH)	3987	—	3963	3960	3987	—	3962	3959	—	3960	3987
ν_1 ($CH_3OH\cdots CO$)	—	—	—	—	3623	2674	3608	3621	2674	3609	3620
ν_1 (CH_3OH)	3248	2428	3248	3372	3271	2439	3251	3277	2439	3251	3271
ν_2 (CH_3OH)	2990	2245	2975	2984	2985	2248	2985	2975	2248	2984	2986
ν_9 (CH_3OH)	2958	2216	2945	2956	2956	2217	2952	2949	2218	2956	2956
$\nu_4 + \nu_5/\nu_4 + \nu_{10}/\nu_5 + \nu_{10}/2\nu_4/2\nu_{10}/2\nu_5$ (CH_3OH)	2918	2151	2920	2928	2925	2150	2921	2923, 2906	2150	2928	2925
$\nu_3/2\nu_6$ (CH_3OH)	2825	2071	2824	2825	2828	2073	2828	2824	2073	2828	2828
$\nu_4 + \nu_{11}/\nu_7 + \nu_4/\nu_6/\nu_{10}$ (CH_3OH)	2603	2010	2610	2607	2604	2013	2601	2594	2013	2604	2601
$\nu_6 + \nu_{11}$ (CH_3OH)	2524	—	2511	2526	2524	—	2519	2511	—	2520	2524
$\nu_6 + \nu_8$ (CH_3OH)	2432	—	2412	2419	2438	—	2419	2419	—	2429	2438
$2\nu_{11}/2\nu_7$ (CH_3OH)	2241	1938	2229	2223	2226	1931	2227	2219	1932	2220	2223
ν_1 (CO)	—	—	—	—	2135	2136	2086	2135	2137	2136	2086
$2\nu_8$ (CH_3OH)	2040	1661	2004	1991	2047	1666	2001	2014	1666	1995	2047
ν_4 (CH_3OH)	1475	1124	1475	1475	1475	1124	1474	1475	1124	1475	1476
ν_{10} (CH_3OH)	1460	1062	1458	1461	1461	1063	1458	1458	1063	1461	1460
ν_5 (CH_3OH)	1445	1099	1440	1445	1445	1099	1449	1444	1101	1445	1445
ν_6 (CH_3OH)	1420	1062	1420	1417	1421	1062	1421	1420	1062	1417	1425
ν_7 (CH_3OH)	1130	900	1124	1130	1129	900	1125	1124	900	1123	1129
ν_{11} (CH_3OH)	1040	979	1022	1015	1039	977	1010	1019	978	1011	1039
ν_8 (CH_3OH)	1028	831	1010	—	1028	833	—	—	831	—	—

Table 2 Infrared absorption features of the newly formed products observed in the methanol and methanol–carbon monoxide (4 : 5) ices after irradiation at 5.5 K

Assignments	CH_3OH	CD_3OD	$^{13}CH_3OH$	$CH_3{}^{18}OH$	CH_3OH–CO	CD_3OD–CO	$CH_3{}^{18}OH$–$C^{18}O$	$^{13}CH_3OH$–CO	CD_3OD–^{13}CO	$CH_3{}^{18}OH$–CO	CH_3OH–$C^{18}O$
ν_3 (CO_2)	2339	—	2274	—	2342	2342	2307	2341, 2275	2275	2342, 2324	2342, 2307
ν_2 (H_2CCO)	—	—	2067	2107	—	—	2107	—	—	—	2106
ν_1 (CO)	2135	—	2087	2083	—	2136	2086, 2037	2135, 2089	2137	—	2137
ν_3 (HCO)	1842	1746	1797	1844	1842	—	1799	1844	—	1844	1799
ν_{14} ($HOCH_2CHO$)	1743(1)	1711(1)	1703(1)	1713(1)	1743(1)	1714(1)	1715(1)	— 1743(1′)	1709(1) —	1708(1) 1743(1′)	1747(1) 1707(1′)
ν_4 (H_2CO)	1726(2)	1676(2)	1687(2)	1693(2)	1726(2)	1686(2)	1693(2)	1692(2) 1724(2′)	1678(2) 1655(2′)	1692(2) 1724(2′)	1726(2) 1695(2′)
ν_{14} ($HCOOCH_3$)	1714(3)	1664(3)	1676(3)	1682(3)	1714(3)	1668(3)	1680(3)	1678(3) 1710(3′)	1666(3) 1647(3′)	1680(3) 1714(3′)	1716(3) 1684(3′)
$2\nu_6$ ($HOCH_2CHO$)	1697(4)	1647(4)	1659(4)	1666(4)	1697(4)	1651(4)	1662(4)	1664(4)	1633(4′)	1654(4)	1670(4′)
ν_3 (H_2CO)	1499	—	1499	1496	1497	—	1488	1499	—	1496	1497
ν_4 (CH_4)	1304	—	1296	1304	1303	—	1303	1298	—	1304	1304
ν_2 (H_2CO)	1246	—		—	1249	—	—	—	—	—	—
ν_4 (CH_2OH)	1192	—	1167	1168	1193	—	—	1165	—	1162	1194
ν_9 ($HOCH_2CH_2OH$)	1094	—	1070	1080	1094	—	—	913	—	1089	1087
ν_7 ($HOCH_2CHO$)	—	—		—	1062	—	—		—	—	1062

Notes: the numbers in parentheses are the deconvoluted peak numbers as shown in Fig. 1C and D.

Table 3 Deconvoluted peak positions of the carbonyl absorption bands in methanol and methanol–carbon monoxide ices (Fig. 1C and D) are compared with the assignments reported for the deconvoluted carbonyl bands observed in the irradiated methane–carbon monoxide isotopologue ices reported in ref. 61. Here, RCHO = saturated aldehyde, RCOR′ = saturated ketone, RCOCHCHR′ = α,β-unsaturated aldehyde/ketone

Assignments	CH_3OH			CD_3OD			$CH_3{}^{18}OH$		
	ν (cm^{-1})	Assignments	Ref. 61	ν (cm^{-1})	Assignments	Ref. 60	ν (cm^{-1})	Assignments	Ref. 60
ν_{14} ($HOCH_2CHO$)	1743	ν_{CO} of RCHO	1746	1711	ν_{CO} of CH_3CHO	1715	1713	ν_{CO} of RCHO	1717
ν_4 (H_2CO)	1726	ν_{CO} of CH_3CHO	1727	1676	—	—	1693	ν_{CO} of CH_3CHO	1694
ν_{14} ($HCOOCH_3$)	1714	ν_{CO} of RCOR′	1717	1664	—	—	1682	ν_{CO} of RCOR′	1683
$2\nu_6$ ($HOCH_2CHO$)	1697	ν_{CO} of RCOCHCHR′	1701	1647	—	—	1666	—	—
Assignments	CH_3OH–CO			CD_3OD–CO			$CH_3{}^{18}OH$–$C^{18}O$		
ν_{14} ($HOCH_2CHO$)	1743	ν_{CO} of RCHO	1746	1714	ν_{CO} of CH_3CHO	1715	1715	ν_{CO} of RCHO	1717
ν_4 (H_2CO)	1726	ν_{CO} of CH_3CHO	1727	1686	—	—	1693	ν_{CO} of CH_3CHO	1694
ν_{14} ($HCOOCH_3$)	1714	ν_{CO} of RCOR′	1717	1668	—	—	1680	ν_{CO} of RCOR′	1683
$2\nu_6$ ($HOCH_2CHO$)	1697	ν_{CO} of RCOCHCHR′	1701	1651	—	—	1662	—	—
Assignments	$^{13}CH_3OH$–CO			$CH_3{}^{18}OH$–CO			CH_3OH–$C^{18}O$		
ν_{14} ($HOCH_2CHO$)	—	ν_{CO} of RCHO	—	1708	ν_{CO} of RCHO	1717	1747	ν_{CO} of RCHO	1746
	1743		1746	1743		1746	1707		1717
ν_4 (H_2CO)	1692	ν_{CO} of CH_3CHO	—	1692	ν_{CO} of CH_3CHO	1694	1726	ν_{CO} of CH_3CHO	1727
	1724		1727	1724		1727	1695		1694
ν_{14} ($HCOOCH_3$)	1678	ν_{CO} of RCOR′	—	1680	ν_{CO} of RCOR′	1683	1716	ν_{CO} of RCOR′	1717
	1710		1717	1714		1717	1684		1683
$2\nu_6$ ($HOCH_2CHO$)	1664	—	—	—	—	—	—	ν_{CO} of RCOCHCHR′	—
	—		—	1654		—	1670		1675

assigned to the ν_{14} band of glycolaldehyde ($HOCH_2CHO$) based on the previous identification of this molecule within irradiated methanol ices at 1747 cm^{-1},[53] irradiated methanol–carbon monoxide ices at 1757 cm^{-1},[54] and matrix isolation studies of glycolaldehyde at 1747 cm^{-1}.[76,77] The band at 1714 cm^{-1} was assigned to the ν_{14} fundamental of methyl formate ($HCOOCH_3$), in agreement with previous electron irradiation experiments of methanol and methanol–carbon monoxide ices,[53,54] UV photolysis of methanol ices,[55] and with pure frozen methyl formate at 16 K.[58,59] The absorption at 1726 cm^{-1} has been assigned to the ν_4 fundamental of formaldehyde (H_2CO) again, based on previous literature values.[53–55,58,59] Finally, the band observed at 1697 cm^{-1} can be attributed to the Fermi resonance splitting of the ν_{14} fundamental and the $2\nu_6$ overtone band of glycolaldehyde.[54,60,77] Further support for the above assignments is gained through observation of the frequency shifts in the infrared absorption features of the isotopically labeled ices of CD_3OD, $^{13}CH_3OH$, and $CH_3{}^{18}OH$ and in the binary ices of CD_3OD–CO, $CH_3{}^{18}OH$–$C^{18}O$, $^{13}CH_3OH$–CO, CD_3OD–^{13}CO, $CH_3{}^{18}OH$–CO and CH_3OH–$C^{18}O$ as compiled in Table 3.

Recently, we have reported on the formation of a series of saturated and unsaturated aldehyde/ketones identified in methane–carbon monoxide ices exposed to ionizing radiation.[61] As both irradiated ices in the present study reveal a broad complex structure associated with the carbonyl stretching mode, we present a comparison of the deconvoluted band positions in (i) the pertinent regions observed in the present experiments and (ii) the carbonyl stretching vibrations of the methane–carbon monoxide ices in Table 3. The infrared absorption bands due to the ν_4 fundamental (CO stretching) of formaldehyde (H_2CO) in both CH_3OH and CH_3OH–CO ices were observed at 1726 cm^{-1}. Acetaldehyde (CH_3CHO) was attributed to the band (ν_4) at 1727 cm^{-1} in irradiated CH_4–CO ices;[61] as such, acetaldehyde may contribute to the observed band at 1726 cm^{-1} here as well. Further support for the assignment of acetaldehyde stems from the identification of the ν_4 fundamental of the isotopically labeled acetaldehyde in both the irradiated isotopologue methanol and mixed methanol–carbon monoxide ices. Here, deuterated acetaldehyde (CD_3CDO) was previously observed at 1715 cm^{-1} (ref. 61) and therefore contributes to the infrared absorption bands witnessed here at 1711 cm^{-1} in irradiated CD_3OD ices and at 1714 cm^{-1} in irradiated CD_3OD–CO ices. In addition, acetaldehyde isotopomer ($CH_3CH^{18}O$) was previously assigned at 1694 cm^{-1} (ref. 61) and consequently was attributed to the observed bands at 1693 cm^{-1}, 1693 cm^{-1}, 1692 cm^{-1} and 1695 cm^{-1} in the processed $CH_3{}^{18}OH$, $CH_3{}^{18}OH$–$C^{18}O$, $CH_3{}^{18}OH$–CO and CH_3OH–$C^{18}O$ ices respectively, as well. Further, following irradiation of the ^{18}O isotopically mixed ices, $CH_3{}^{18}OH$–CO and CH_3OH–$C^{18}O$, evidence suggesting the formation of two acetaldehyde isotopomers (CH_3CHO and $CH_3CH^{18}O$) is found in the observed bands at 1724 cm^{-1} and 1694 cm^{-1}, respectively. Further evidence for the formation of acetaldehyde is also confirmed using ReTOF mass spectrometry following TPD studies as discussed below (Section 3.2).

Glycolaldehyde ($HOCH_2CHO$) is observed at 1743 cm^{-1} (ν_{14}) in both irradiated CH_3OH and mixed CH_3OH–CO ices. However, the infrared absorption band at 1743 cm^{-1} may also have contribution from saturated aldehydes such as propanal (CH_3CH_2CHO) and butanal (C_3H_7CHO), as the carbonyl stretching mode of these molecules has been attributed previously at 1746 cm^{-1} as well.[61] Further evidence in support of saturated aldehydes contributing to this carbonyl band again stems from the isotopically labeled irradiated ices and the assignments of the deconvoluted bands of the corresponding carbonyl stretching region (Table 3). Here, the ^{18}O isotope labeled saturated aldehydes ($RCH^{18}O$) were observed at 1717 cm^{-1} in the irradiated methane–carbon monoxide ices as previously reported,[61] and therefore may contribute here to the ν_{14} of glycolaldehyde ($HOCH_2CH^{18}O$) observed at 1713 cm^{-1} in $CH_3{}^{18}OH$, 1715 cm^{-1} in $CH_3{}^{18}OH$–$C^{18}O$, 1708 cm^{-1} in $CH_3{}^{18}OH$–CO and 1707 cm^{-1} in CH_3OH–$C^{18}O$ ices. Similarly, the ν_{14} fundamental of methyl formate ($HCOOCH_3$) observed at 1714 cm^{-1} in both the irradiated CH_3OH and CH_3OH–CO ices can also have contribution from saturated ketones (1717 cm^{-1}), *e.g.* acetone (CH_3COCH_3) and butanone ($C_2H_5COCH_3$). Here, the carbonyl absorption band of ^{18}O labeled saturated ketones (1683 cm^{-1}) was also identified in the isotopically labeled irradiated ices of $CH_3{}^{18}OH$ (1682 cm^{-1}), $CH_3{}^{18}OH$–$C^{18}O$ (1680 cm^{-1}), $CH_3{}^{18}OH$–CO (1680 cm^{-1}) and CH_3OH–$C^{18}O$ (1684 cm^{-1}) (Table 3). In summary, we wish to stress that FTIR spectroscopy can only elucidate particular vibrational modes of complex organics synthesized *in situ* of bulk ices from exposure to ionizing radiation, and very rarely, actual molecular isomers. Consequently, we then turned our attention to a more sensitive technique allowing for the identification of *individual molecules via* their molecular formula, namely, temperature programmed desorption coupled with single photoionization reflectron time-of-flight mass spectrometry.

3.2. Reflectron time-of-flight mass spectra

Following the *in situ* identification of small molecules and vibrational modes of more complex organics as described above, we employed the use of temperature programmed desorption (TPD) to monitor the products sublimating *via* ReTOF-PI mass spectrometry. The full product spectrum of processed methanol and methanol–carbon monoxide isotopologue ices is displayed in Fig. 2A and B, respectively, as a function of temperature during the post-irradiation warm-up stage. In the case of methanol ice, molecules with a mass-to-charge ratio (*m*/*z*) up to 90 amu are observed (Fig. 2A). However, in the case of methanol–carbon monoxide ices, large molecules up to 150 amu are observed (Fig. 2B). This observation alone implies the presence of rich and complex chemistry in the mixed methanol–carbon monoxide ices compared to pure methanol ices despite the similar doses deposited in both the systems.

Products identified utilizing ReTOF mass spectrometry following photoionization at $E_{h\nu}$ = 10.49 eV are described below for the irradiated methanol and mixed methanol–carbon monoxide ices, respectively. Here, the products detected in the methanol ice are also observed in the irradiated methanol–carbon monoxide system. The corresponding mass-to-charge ratios (*m*/*z*) of the identified products and their isotopomers are listed in Tables 4A and B. Note that in the methanol (CH_3OH, CD_3OD, $^{13}CH_3OH$ and $CH_3{}^{18}OH$) ices,

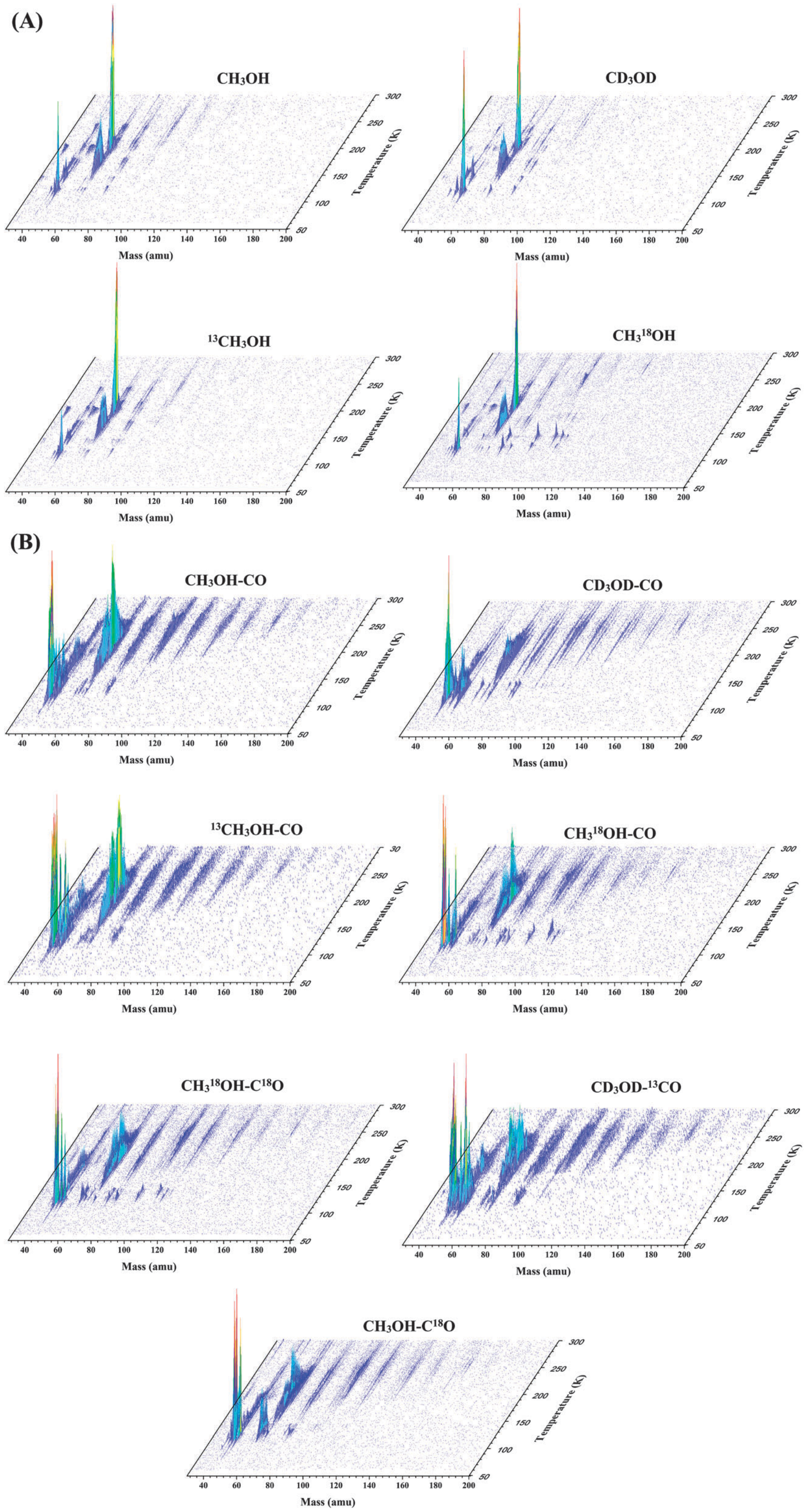

Fig. 2 (A) Reflectron time-of-flight (ReTOF) mass spectra as a function of temperature showing newly formed products subliming into the gas phase from radiation processed methanol isotopologue ices recorded at a photoionization energy of 10.49 eV. (B) Reflectron time-of-flight (ReTOF) mass spectra as a function of temperature showing newly formed products subliming into the gas phase from radiation processed methanol–carbon monoxide isotopologue ices recorded at a photoionization energy of 10.49 eV.

Table 4 (A) Molecular formula and the corresponding mass-to-charge ratios (in amu units) of the products identified in the irradiated methanol isotopologue ices (CH_3OH, CD_3OD, $CH_3{}^{18}OH$ and $^{13}CH_3OH$) during the TPD studies using ReTOF mass spectroscopy. Molecules are grouped into different classes based on the number of oxygen atoms present. The molecule labelled with an asterisk (*) designates a fragment of methoxy methanol (CH_3OCH_2OH) and not a sublimating radical; for further information please see Section 3.2.1. (B) Molecular formula and the corresponding mass-to-charge ratios (*m*/*z* in amu units) of the products identified in the irradiated mixed methanol–carbon monoxide isotopologue ices (CH_3OH–CO, CD_3OD–CO, $CH_3{}^{18}OH$–$C^{18}O$, $^{13}CH_3OH$–CO, CD_3OD–^{13}CO, $CH_3{}^{18}OH$–CO and CH_3OH–$C^{18}O$) during the TPD studies using ReTOF mass spectroscopy. Molecules are grouped into different classes based on the number of oxygen atoms present. In mixed isotopic ices ($^{13}CH_3OH$–CO, CD_3OD–^{13}CO, $CH_3{}^{18}OH$–CO and CH_3OH–$C^{18}O$), the molecules observed are shown in bold letters

(A)

CH_3OH		CD_3OD		$CH_3{}^{18}OH$		$^{13}CH_3OH$	
Formula	*m*/*z*	Formula	*m*/*z*	Formula	*m*/*z*	Formula	*m*/*z*
Products with a single oxygen atom							
C_2H_2O	42	C_2D_2O	44	$C_2H_2{}^{18}O$	44	$^{13}C_2H_2O$	44
C_2H_4O	44	C_2D_4O	48	$C_2H_4{}^{18}O$	46	$^{13}C_2H_4O$	46
C_2H_6O	46	C_2D_6O	52	$C_2H_6{}^{18}O$	48	$^{13}C_2H_6O$	48
C_3H_6O	58	C_3D_6O	64	$C_3H_6{}^{18}O$	60	$^{13}C_3H_6O$	61
C_3H_8O	60	C_3D_8O	68	$C_3H_8{}^{18}O$	62	$^{13}C_3H_8O$	63
C_4H_8O	72	C_4D_8O	80	$C_4H_8{}^{18}O$	74	$^{13}C_4H_8O$	76
Products with two oxygen atoms							
$C_2H_4O_2$	60	$C_2D_4O_2$	64	$C_2H_4{}^{18}O_2$	64	$^{13}C_2H_4O_2$	62
$C_2H_5O_2$*	61	$C_2D_5O_2$	66	$C_3H_5{}^{18}O_2$	65	$^{13}C_2H_5O_2$	63
$C_2H_6O_2$	62	$C_2D_6O_2$	68	$C_2H_6{}^{18}O_2$	66	$^{13}C_2H_6O_2$	64
$C_3H_4O_2$	72	$C_3D_4O_2$	76	$C_3H_4{}^{18}O_2$	76	$^{13}C_3H_4O_2$	75
$C_3H_6O_2$	74	$C_3D_6O_2$	80	$C_3H_6{}^{18}O_2$	78	$^{13}C_3H_6O_2$	77
$C_3H_8O_2$	76	$C_3D_8O_2$	84	$C_3H_8{}^{18}O_2$	80	$^{13}C_3H_8O_2$	79
$C_4H_8O_2$	88	$C_4D_8O_2$	96	$C_4H_8{}^{18}O_2$	92	$^{13}C_4H_8O_2$	92
Products with three oxygen atoms							
$C_3H_6O_3$	90	$C_3D_6O_3$	96	$C_3H_6{}^{18}O_3$	96	$^{13}C_3H_6O_3$	93
$C_3H_8O_3$	92	$C_3D_8O_3$	100	$C_3H_8{}^{18}O_3$	98	$^{13}C_3H_8O_3$	95

(B)

CH_3OH–CO		CD_3OD–CO		$CH_3{}^{18}OH$–$C^{18}O$		$^{13}CH_3OH$–CO		CD_3OD–^{13}CO		$CH_3{}^{18}OH$–CO		CH_3OH–$C^{18}O$	
Formula	*m*/*z*	Formula	*m*/*z*	Formula	*m*/*z*	Formula	*m*/*z*	Formula	*m*/*z*	Formula	*m*/*z*	Formula	*m*/*z*
Products with a single oxygen atom													
C_2H_2O	42	C_2D_2O	44	$C_2H_2{}^{18}O$	44	C_2H_2O	42	$^{13}C_2D_2O$	46	**C_2H_2O**	**42**	**$C_2H_2{}^{18}O$**	**44**
						$^{13}CCH_2O$	**43**	**$^{13}CCD_2O$**	**45**	$C_2H_2{}^{18}O$	44	C_2H_2O	42
						$^{13}C_2H_2O$	44	C_2D_2O	44				
C_2H_4O	44	C_2D_4O	48	$C_2H_4{}^{18}O$	46	C_2H_4O	44	$^{13}C_2D_4O$	50	**C_2H_4O**	**44**	**$C_2H_4{}^{18}O$**	**46**
						$^{13}CCH_4O$	**45**	**$^{13}CCD_4O$**	**49**	$C_2H_4{}^{18}O$	46	C_2H_4O	44
						$^{13}C_2H_4O$	46	C_2D_4O	48				
C_2H_6O	46	C_2D_6O	52	$C_2H_6{}^{18}O$	48	C_2H_6O	46	$^{13}C_2D_6O$	54	C_2H_4O	46	$C_2H_6{}^{18}O$	48
						$^{13}CCH_6O$	47	$^{13}CCD_6O$	53	**$C_2H_6{}^{18}O$**	**48**	**C_2H_6O**	**46**
						$^{13}C_2H_6O$	**48**	**C_2D_6O**	**52**				
C_3H_4O	56	C_3D_4O	60	$C_3H_4{}^{18}O$	58	C_3H_4O	56	$^{13}C_3D_4O$	63	**C_3H_4O**	**56**	**$C_3H_4{}^{18}O$**	**58**
						$^{13}CC_2H_4O$	57	$^{13}C_2CD_4O$	62	$C_3H_4{}^{18}O$	58	C_3H_4O	56
						$^{13}C_2CH_4O$	**58**	**$^{13}CC_2D_4O$**	**61**				
						$^{13}C_3H_4O$	59	C_3D_4O	60				
C_3H_6O	58	C_3D_6O	64	$C_3H_6{}^{18}O$	60	C_3H_6O	58	$^{13}C_3D_6O$	67	**C_3H_6O**	**58**	**$C_3H_6{}^{18}O$**	**60**
						$^{13}CC_2H_6O$	59	$^{13}C_2CD_6O$	66	$C_3H_6{}^{18}O$	60	C_3H_6O	58
						$^{13}C_2CH_6O$	**60**	**$^{13}CC_2D_6O$**	**65**				
						$^{13}C_3H_6O$	61	C_3D_6O	64				
C_3H_8O	60	C_3D_8O	68	$C_3H_8{}^{18}O$	62	C_3H_8O	60	$^{13}C_3D_8O$	71	C_3H_8O	60	$C_3H_8{}^{18}O$	62
						$^{13}CC_2H_8O$	61	$^{13}C_2CD_8O$	70	**$C_3H_8{}^{18}O$**	**62**	**C_3H_8O**	**60**
						$^{13}C_2CH_8O$	62	$^{13}CC_2D_8O$	69				
						$^{13}C_3H_8O$	**63**	**C_3D_8O**	**68**				
C_4H_8O	72	C_4D_8O	80	$C_4H_8{}^{18}O$	74	C_4H_8O	72	$^{13}C_4D_8O$	84	C_4H_8O	72	$C_4H_8{}^{18}O$	74
						$^{13}CC_4H_8O$	73	$^{13}C_3CD_8O$	83	$C_4H_8{}^{18}O$	74	C_4H_8O	72
						$^{13}C_2C_2H_8O$	74	$^{13}C_2C_2D_8O$	82				
						$^{13}C_3CH_8O$	**75**	**$^{13}CC_3D_8O$**	**81**				
						$^{13}C_4H_8O$	76	C_4D_8O	80				
$C_4H_{10}O$	74	$C_4D_{10}O$	84	$C_4H_{10}{}^{18}O$	76	$C_4H_{10}O$	74	$^{13}C_4D_{10}O$	88	$C_4H_{10}O$	74	$C_4H_{10}{}^{18}O$	76
						$^{13}CC_4H_{10}O$	75	$^{13}C_3CD_{10}O$	87	**$C_4H_{10}{}^{18}O$**	**76**	**$C_4H_{10}O$**	**74**
						$^{13}C_2C_2H_{10}O$	76	$^{13}C_2C_2D_{10}O$	86				
						$^{13}C_3CH_{10}O$	77	$^{13}CC_3D_{10}O$	85				
						$^{13}C_4H_{10}O$	**78**	**$C_4D_{10}O$**	**84**				

Table 4 (*continued*)

(B)

$CH_3OH–CO$		$CD_3OD–CO$		$CH_3{}^{18}OH–C^{18}O$		$^{13}CH_3OH–CO$		$CD_3OD–{}^{13}CO$		$CH_3{}^{18}OH–CO$		$CH_3OH–C^{18}O$	
Formula	*m*/*z*	Formula	*m*/*z*	Formula	*m*/*z*	Formula	*m*/*z*	Formula	*m*/*z*	Formula	*m*/*z*	Formula	*m*/*z*
Products with two oxygen atoms													
$C_2H_2O_2$	58	$C_2D_2O_2$	60	$C_2H_2{}^{18}O_2$	62	**$C_2H_2O_2$**	**58**	**$^{13}C_2D_2O_2$**	**62**	**$C_2H_2O_2$**	**58**	**$C_2H_2{}^{18}O_2$**	**62**
						$^{13}CCH_2O_2$	59	$^{13}CCD_2O_2$	61	$C_2H_2{}^{18}OO$	60	$C_2H_2{}^{18}OO$	60
						$^{13}C_2H_2O_2$	60	$C_2D_2O_2$	60	$C_2H_2{}^{18}O_2$	62	$C_2H_2O_2$	58
$C_2H_4O_2$	60	$C_2D_4O_2$	64	$C_2H_4{}^{18}O_2$	64	$C_2H_4O_2$	60	$^{13}C_2D_4O_2$	66	$C_2H_4O_2$	60	$C_2H_4{}^{18}O_2$	64
						$^{13}CCH_4O_2$	**61**	**$^{13}CCD_4O_2$**	**65**	**$C_2H_4{}^{18}OO$**	**62**	**$C_2H_4{}^{18}OO$**	**62**
						$^{13}C_2H_4O_2$	62	$C_2D_4O_2$	64	$C_2H_4{}^{18}O_2$	64	$C_2H_4O_2$	60
$C_2H_5O_2$	61	$C_2D_5O_2$	66	$C_2H_5{}^{18}O_2$	65	$C_2H_5O_2$	61	$^{13}C_2D_5O_2$	68	$C_2H_5O_2$	61	$C_2H_5{}^{18}O_2$	65
						$^{13}CCH_5O_2$	62	$^{13}CCD_5O_2$	67	$C_2H_5{}^{18}OO$	63	$C_2H_5{}^{18}OO$	63
						$^{13}C_2H_5O_2$	**63**	**$C_2D_5O_2$**	**66**	**$C_2H_5{}^{18}O_2$**	**65**	**$C_2H_5O_2$**	**61**
$C_2H_6O_2$	62	$C_2D_6O_2$	68	$C_2H_6{}^{18}O_2$	66	$C_2H_6O_2$	62	$^{13}C_2D_6O_2$	70	$C_2H_6O_2$	62	$C_2H_6{}^{18}O_2$	66
						$^{13}CCH_6O_2$	63	$^{13}CCD_6O_2$	69	$C_2H_6{}^{18}OO$	64	$C_2H_6{}^{18}OO$	64
						$^{13}C_2H_6O_2$	**64**	**$C_2D_6O_2$**	**68**	**$C_2H_6{}^{18}O_2$**	**66**	**$C_2H_6O_2$**	**62**
$C_3H_4O_2$	72	$C_3D_4O_2$	76	$C_3H_4{}^{18}O_2$	76	$C_3H_4O_2$	72	$^{13}C_3D_4O_2$	79	$C_3H_4O_2$	72	$C_3H_4{}^{18}O_2$	76
						$^{13}CC_2H_4O_2$	**73**	**$^{13}C_2CD_4O_2$**	**78**	**$C_3H_4{}^{18}OO$**	**74**	**$C_3H_4{}^{18}OO$**	**74**
						$^{13}C_2CH_4O_2$	74	$^{13}CC_2D_4O_2$	77	$C_3H_4{}^{18}O_2$	76	$C_3H_4O_2$	72
						$^{13}C_3H_4O_2$	75	$C_3D_4O_2$	76				
$C_3H_6O_2$	74	$C_3D_6O_2$	80	$C_3H_6{}^{18}O_2$	78	$C_3H_6O_2$	74	$^{13}C_3D_6O_2$	83	$C_3H_6O_2$	74	$C_3H_6{}^{18}O_2$	78
						$^{13}CC_2H_6O_2$	75	$^{13}C_2CD_6O_2$	82	$C_3H_6{}^{18}OO$	76	$C_3H_6{}^{18}OO$	76
						$^{13}C_2CH_6O_2$	**76**	**$^{13}CC_2D_6O_2$**	**81**	**$C_3H_6{}^{18}O_2$**	**78**	**$C_3H_6O_2$**	**74**
						$^{13}C_3H_6O_2$	77	$C_3D_6O_2$	80				
$C_3H_8O_2$	76	$C_3D_8O_2$	84	$C_3H_8{}^{18}O_2$	80	$C_3H_8O_2$	76	$^{13}C_3D_8O_2$	87	$C_3H_8O_2$	76	$C_3H_8{}^{18}O_2$	80
						$^{13}CC_2H_8O_2$	77	$^{13}C_2CD_8O_2$	86	$C_3H_8{}^{18}OO$	78	$C_3H_8{}^{18}OO$	78
						$^{13}C_2CH_8O_2$	78	$^{13}CC_2D_8O_2$	85	$C_3H_8{}^{18}O_2$	80	$C_3H_8O_2$	76
						$^{13}C_3H_8O_2$	**79**	**$C_3D_8O_2$**	**84**				
$C_4H_6O_2$	86	$C_4D_6O_2$	92	$C_4H_6{}^{18}O_2$	90	$C_4H_6O_2$	86	$^{13}C_4D_6O_2$	96	**$C_4H_6O_2$**	**86**	**$C_4H_6{}^{18}O_2$**	**90**
						$^{13}CC_3H_6O_2$	87	$^{13}C_3CD_6O_2$	95	$C_4H_6{}^{18}OO$	88	$C_4H_6{}^{18}OO$	88
						$^{13}C_2C_2H_6O_2$	**88**	**$^{13}C_2C_2D_6O_2$**	**94**	$C_4H_6{}^{18}O_2$	90	$C_4H_6O_2$	86
						$^{13}C_3CH_6O_2$	89	$^{13}CC_3D_6O_2$	93				
						$^{13}C_4H_6O_2$	90	$C_4D_6O_2$	92				
$C_4H_8O_2$	88	$C_4D_8O_2$	96	$C_4H_8{}^{18}O_2$	92	$C_4H_8O_2$	88	$^{13}C_4D_8O_2$	100	$C_4H_8O_2$	88	$C_4H_8{}^{18}O_2$	92
						$^{13}CC_3H_8O_2$	89	$^{13}C_3CD_8O_2$	99	**$C_4H_8{}^{18}OO$**	**90**	**$C_4H_8{}^{18}OO$**	**90**
						$^{13}C_2C_2H_8O_2$	90	$^{13}C_2C_2D_8O_2$	98	$C_4H_8{}^{18}O_2$	92	$C_4H_8O_2$	88
						$^{13}C_3CH_8O_2$	**91**	**$^{13}CC_3D_8O_2$**	**97**				
						$^{13}C_4H_8O_2$	92	$C_4D_8O_2$	96				
Products with three oxygen atoms													
$C_3H_4O_3$	88	$C_3D_4O_3$	92	$C_3H_4{}^{18}O_3$	94	$C_3H_4O_3$	88	$^{13}C_3D_4O_3$	95	$C_3H_4O_3$	88	$C_3H_4{}^{18}O_3$	94
						$^{13}CC_2H_4O_3$	**89**	**$^{13}C_2CD_4O_3$**	**94**	**$C_3H_4{}^{18}OO_2$**	**90**	**$C_3H_4{}^{18}O_2O$**	**92**
						$^{13}C_2CH_4O_3$	90	$^{13}CC_2D_4O_3$	93	$C_3H_4{}^{18}O_2O$	92	$C_3H_4{}^{18}OO_2$	90
						$^{13}C_3H_4O_3$	91	$C_3D_4O_3$	92	$C_3H_4{}^{18}O_3$	94	$C_3H_4O_3$	88
$C_3H_6O_3$	90	$C_3D_6O_3$	96	$C_3H_6{}^{18}O_3$	96	$C_3H_6O_3$	90	$^{13}C_3D_6O_3$	99	$C_3H_6O_3$	90	$C_3H_6{}^{18}O_3$	96
						$^{13}CC_2H_6O_3$	91	$^{13}C_2CD_6O_3$	98	$C_3H_6{}^{18}OO_2$	92	$C_3H_6{}^{18}O_2O$	94
						$^{13}C_2CH_6O_3$	**92**	**$^{13}CC_2D_6O_3$**	**97**	**$C_3H_6{}^{18}O_2O$**	**94**	**$C_3H_6{}^{18}OO_2$**	**92**
						$^{13}C_3H_6O_3$	93	$C_3D_6O_3$	96	$C_3H_6{}^{18}O_3$	96	$C_3H_6O_3$	90
$C_4H_6O_3$	102	$C_4D_6O_3$	108	$C_4H_6{}^{18}O_3$	108	$C_4H_6O_3$	102	$^{13}C_4D_6O_3$	112	$C_4H_6O_3$	102	$C_4H_6{}^{18}O_3$	108
						$^{13}CC_3H_6O_3$	103	$^{13}C_3CD_6O_3$	111	**$C_4H_6{}^{18}OO_2$**	**104**	**$C_4H_6{}^{18}O_2O$**	**106**
						$^{13}C_2C_2H_6O_3$	**104**	**$^{13}C_2C_2D_6O_3$**	**110**	$C_4H_6{}^{18}O_2O$	106	$C_4H_6{}^{18}OO_2$	104
						$^{13}C_3CH_6O_3$	105	$^{13}CC_3D_6O_3$	109	$C_4H_6{}^{18}O_3$	108	$C_4H_6O_3$	102
						$^{13}C_4H_6O_3$	106	$C_4D_6O_3$	108				
$C_4H_8O_3$	104	$C_4D_8O_3$	112	$C_4H_8{}^{18}O_3$	110	$C_4H_8O_3$	104	$^{13}C_4D_8O_3$	116	$C_4H_8O_3$	104	$C_4H_8{}^{18}O_3$	110
						$^{13}CC_3H_8O_3$	105	$^{13}C_3CD_8O_3$	115	$C_4H_8{}^{18}OO_2$	106	$C_4H_8{}^{18}O_2O$	108
						$^{13}C_2C_2H_8O_3$	106	$^{13}C_2C_2D_8O_3$	**114**	**$C_4H_8{}^{18}O_2O$**	**108**	**$C_4H_8{}^{18}OO_2$**	**106**
						$^{13}C_3CH_8O_3$	**107**	**$^{13}CC_3D_8O_3$**	113	$C_4H_8{}^{18}O_3$	110	$C_4H_8O_3$	104
						$^{13}C_4H_8O_3$	108	$C_4D_8O_3$	112				
Products with four oxygen atoms													
$C_4H_4O_4$	116	$C_4D_4O_4$	120	$C_4H_4{}^{18}O_4$	124	$C_4H_4O_4$	116	$^{13}C_4D_4O_4$	124	$C_4H_4O_4$	116	$C_4H_4{}^{18}O_4$	124
						$^{13}CC_3H_4O_4$	**117**	**$^{13}C_3CD_4O_4$**	**123**	**$C_4H_4{}^{18}OO_3$**	**118**	**$C_4H_4{}^{18}O_3O$**	**122**
						$^{13}C_2C_2H_4O_4$	118	$^{13}C_2C_2D_4O_4$	122	$C_4H_4{}^{18}O_2O_2$	120	$C_4H_4{}^{18}O_2O_2$	120
						$^{13}C_3CH_4O_4$	119	$^{13}CC_3D_4O_4$	121	$C_4H_4{}^{18}O_3O$	122	$C_4H_4{}^{18}OO_3$	118
						$^{13}C_4H_4O_4$	122	$C_4D_4O_4$	120	$C_4H_4{}^{18}O_4$	124	$C_4H_4O_4$	116
$C_4H_6O_4$	118	$C_4D_6O_4$	124	$C_4H_6{}^{18}O_4$	126	$C_4H_6O_4$	118	$^{13}C_4D_6O_4$	128	$C_4H_6O_4$	118	$C_4H_6{}^{18}O_4$	126
						$^{13}CC_3H_6O_4$	119	$^{13}C_3CD_6O_4$	127	$C_4H_6{}^{18}OO_3$	120	$C_4H_6{}^{18}O_3O$	124
						$^{13}C_2C_2H_6O_4$	**120**	**$^{13}C_2C_2D_6O_4$**	**126**	**$C_4H_6{}^{18}O_2O_2$**	**122**	**$C_4H_6{}^{18}O_2O_2$**	**122**
						$^{13}C_3CH_6O_4$	121	$^{13}CC_3D_6O_4$	125	$C_4H_6{}^{18}O_3O$	124	$C_4H_6{}^{18}OO_3$	120
						$^{13}C_4H_6O_4$	122	$C_4D_6O_4$	124	$C_4H_6{}^{18}O_4$	126	$C_4H_6O_4$	118

Table 4 (*continued*)

(B)

$CH_3OH–CO$		$CD_3OD–CO$		$CH_3{}^{18}OH–C^{18}O$		$^{13}CH_3OH–CO$		$CD_3OD–{}^{13}CO$		$CH_3{}^{18}OH–CO$		$CH_3OH–C^{18}O$	
Formula	*m*/*z*	Formula	*m*/*z*	Formula	*m*/*z*	Formula	*m*/*z*	Formula	*m*/*z*	Formula	*m*/*z*	Formula	*m*/*z*
$C_4H_8O_4$	120	$C_4D_8O_4$	128	$C_4H_8{}^{18}O_4$	128	$C_4H_8O_4$	120	$^{13}C_4D_8O_4$	132	$C_4H_8O_4$	120	$C_4H_8{}^{18}O_4$	128
						$^{13}CC_3H_8O_4$	121	$^{13}C_3CD_8O_4$	131	$C_4H_8{}^{18}OO_3$	122	$C_4H_8{}^{18}O_3O$	126
						$^{13}C_2C_2H_8O_4$	122	$^{13}C_2C_2D_8O_4$	130	$C_4H_8{}^{18}O_2O_2$	124	$C_4H_8{}^{18}O_2O_2$	124
						$\mathbf{^{13}C_3CH_8O_4}$	**123**	$\mathbf{^{13}CC_3D_8O_4}$	**129**	$\mathbf{C_4H_8{}^{18}O_3O}$	**126**	$\mathbf{C_4H_8{}^{18}OO_3}$	**122**
						$^{13}C_4H_8O_4$	124	$C_4D_6O_8$	128	$C_4H_8{}^{18}O_4$	128	$C_4H_8O_4$	120
$C_5H_6O_4$	130	$C_5D_6O_4$	136	$C_5H_6{}^{18}O_4$	138	$C_5H_6O_4$	130	$^{13}C_5D_6O_4$	141	$C_5H_6O_4$	130	$C_5H_6{}^{18}O_4$	138
						$^{13}CC_4H_6O_4$	131	$^{13}C_4CD_6O_4$	140	$\mathbf{C_5H_6{}^{18}OO_3}$	**132**	$\mathbf{C_5H_6{}^{18}O_3O}$	**136**
						$\mathbf{^{13}C_2C_3H_6O_4}$	**132**	$\mathbf{^{13}C_3C_2D_6O_4}$	**139**	$C_5H_6{}^{18}O_2O_2$	134	$C_5H_6{}^{18}O_2O_2$	134
						$^{13}C_3C_2H_6O_4$	133	$^{13}C_2C_3D_6O_4$	138	$C_5H_6{}^{18}O_3O$	136	$C_5H_6{}^{18}OO_3$	132
						$^{13}C_4CH_6O_4$	134	$^{13}CC_4D_6O_4$	137	$C_5H_6{}^{18}O_4$	138	$C_5H_6O_4$	130
						$^{13}C_5H_6O_4$	135	$C_5D_6O_4$	136				
$C_5H_8O_4$	132	$C_5D_8O_4$	140	$C_5H_8{}^{18}O_4$	140	$C_5H_8O_4$	132	$^{13}C_5D_8O_4$	145	$C_5H_8O_4$	132	$C_5H_8{}^{18}O_4$	140
						$^{13}CC_4H_8O_4$	133	$^{13}C_4CD_8O_4$	144	$C_5H_8{}^{18}OO_3$	134	$C_5H_8{}^{18}O_3O$	138
						$^{13}C_2C_3H_8O_4$	134	$^{13}C_3C_2D_8O_4$	143	$\mathbf{C_5H_8{}^{18}O_2O_2}$	**136**	$\mathbf{C_5H_8{}^{18}O_2O_2}$	**136**
						$\mathbf{^{13}C_3C_2H_8O_4}$	**135**	$\mathbf{^{13}C_2C_3D_8O_4}$	**142**	$C_5H_8{}^{18}O_3O$	138	$C_5H_8{}^{18}OO_3$	134
						$^{13}C_4CH_8O_4$	136	$^{13}CC_4D_8O_4$	141	$C_5H_8{}^{18}O_4$	140	$C_5H_8O_4$	132
						$^{13}C_5H_8O_4$	137	$C_5D_8O_4$	140				
Products with five oxygen atoms													
$C_5H_6O_5$	146	$C_5D_6O_5$	152	$C_5H_6{}^{18}O_5$	156	$C_5H_6O_5$	146	$^{13}C_5D_6O_5$	157	$C_5H_6O_5$	146	$C_5H_6{}^{18}O_5$	156
						$^{13}CC_4H_6O_5$	147	$^{13}C_4CD_6O_5$	156	$C_5H_6{}^{18}OO_4$	148	$C_5H_6{}^{18}O_4O$	154
						$\mathbf{^{13}C_2C_3H_6O_5}$	**148**	$\mathbf{^{13}C_3C_2D_6O_5}$	**155**	$\mathbf{C_5H_6{}^{18}O_2O_3}$	**150**	$\mathbf{C_5H_6{}^{18}O_3O_2}$	**152**
						$^{13}C_3C_2H_6O_5$	149	$^{13}C_2C_3D_6O_5$	154	$C_5H_6{}^{18}O_3O_2$	152	$C_5H_6{}^{18}O_2O_3$	150
						$^{13}C_4CH_6O_5$	150	$^{13}CC_4D_6O_5$	153	$C_5H_6{}^{18}O_4O$	154	$C_5H_6{}^{18}OO_4$	148
						$^{13}C_5H_6O_5$	151	$C_5D_6O_5$	152	$C_5H_6{}^{18}O_5$	156	$C_5H_6O_5$	146
$C_5H_8O_5$	148	$C_5D_8O_5$	156	$C_5H_8{}^{18}O_5$	158	$C_5H_8O_5$	148	$^{13}C_5D_8O_5$	161	$C_5H_8O_5$	148	$C_5H_8{}^{18}O_5$	158
						$\mathbf{^{13}CC_4H_8O_5}$	**149**	$\mathbf{^{13}C_4CD_8O_5}$	**160**	$\mathbf{C_5H_8{}^{18}OO_4}$	**150**	$\mathbf{C_5H_8{}^{18}O_4O}$	**156**
						$^{13}C_2C_3H_8O_5$	150	$^{13}C_3C_2D_8O_5$	159	$C_5H_8{}^{18}O_2O_3$	152	$C_5H_8{}^{18}O_3O_2$	154
						$\mathbf{^{13}C_3C_2H_8O_5}$	**151**	$\mathbf{^{13}C_2C_3D_8O_5}$	**158**	$\mathbf{C_5H_8{}^{18}O_3O_2}$	**154**	$\mathbf{C_5H_8{}^{18}O_2O_3}$	**152**
						$^{13}C_4CH_8O_5$	152	$^{13}CC_4D_8O_5$	157	$C_5H_8{}^{18}O_4O$	156	$C_5H_8{}^{18}OO_4$	150
						$^{13}C_5H_8O_5$	153	$C_5D_8O_5$	156	$C_5H_8{}^{18}O_5$	158	$C_5H_8O_5$	148

only one isotope of each element is present and thus only one isotopic mass for each product is observed as expected. As an example, C_2H_4O isotopomers were detected at *m*/*z* = 44 amu (C_2H_4O), 48 amu (C_2D_4O), 46 amu ($^{13}C_2H_4O$) and 46 amu ($C_2H_4{}^{18}O$) in the exposed CH_3OH, CD_3OD, $^{13}CH_3OH$ and $CH_3{}^{18}OH$ systems, respectively. Similarly, in the mixed isotopically pure methanol–carbon monoxide ices, *e.g.* $CH_3OH–CO$, $CD_3OD–CO$, and $CH_3{}^{18}OH–C^{18}O$, only one isotopomer of each product is detected. However, in the case of isotopically mixed ices such as $^{13}CH_3OH–CO$, $CD_3OD–{}^{13}CO$, $CH_3{}^{18}OH–CO$ and $CH_3OH–C^{18}O$, several isotopomers corresponding to one molecular formula are observed (Table 4B). Again for the sake of clarity, consider the three distinct C_2H_4O isomers that were observed in the processed $^{13}CH_3OH–CO$ ice, *i.e.* at *m*/*z* = 44 amu (C_2H_4O), 45 amu ($^{13}CCH_4O$), and 46 amu ($^{13}C_2H_4O$).

Furthermore, we should mention here that several mass peaks were observed simultaneously at about 124 K, 145 K and 203 K as can be seen in Fig. 2A and B in both irradiated methanol and methanol–carbon monoxide isotopologue ices. Note for simplicity that the uncertainty associated with peak sublimation temperatures is ± 2 K, unless otherwise noted. For example, the sublimation of molecules with mass-to-charge ratios corresponding to C_2H_2O, C_2H_4O, C_2H_6O, C_3H_6O, and C_3H_8O is observed at 124 K in both irradiated methanol and methanol–carbon monoxide ices. The above observations are an indication of either co-sublimation of several different products at a specific temperature and/or fragmentation of a high mass organic from photoionization. During the warm-up phase, the amorphous ice of methanol experiences a phase change within the temperature range of 100–125 K as reported earlier[53,63,78,79] and may trigger the sublimation of the products formed *via* a 'molecular volcano' process as reported before with frozen amorphous water[80] resulting in the observation of several products with an identical sublimation temperature of 124 K. Further, peak methanol sublimation occurs at 145 K in both irradiated methanol and methanol–carbon monoxide ice systems. As such, the observed sublimation of C_2H_4O, C_3H_6O, C_4H_8O, C_2H_6O, C_3H_8O and $C_2H_2O_2$ at 145 K can be correlated with co-sublimation of methanol molecules. Similarly, the sublimation of a group of products peaking at 203 K is correlated with co-sublimation of ethylene glycol (formed in the radiolysis process). A detailed discussion of these products is provided in the following sections.

3.2.1. Molecules with definitive assignments

3.2.1.1. Single oxygen bearing molecules. Evidence from the ReTOF mass spectrometry data combined with isotopic labeling led to the identification of molecules which can be formally classified as carbonyl, alcohol, and/or ether. The corresponding sublimation profiles along with their respective shifted isotopologue masses are shown in Fig. 3A and Fig. S2 and S3 (ESI†). In the case of methanol–carbon monoxide ices we have also identified two additional high mass organics C_3H_4O and $C_4H_{10}O$ as shown in Fig. 3B and ESI,† Fig. S4 and S5. A detailed analysis of the identification of these products is provided in the following section; please note that the stated energy in electron volts (eV) is the adiabatic ionization energy (IE) of the molecule for the sake of clarity.

Ketene (H_2CCO). Temperature programmed desorption spectra at m/z = 42 amu in the irradiated ice samples are attributed to molecular formula C_2H_2O and have been assigned to ketene (H_2CCO; 9.6 eV, ref. 81). The sublimation profile at m/z = 42 amu in irradiated methanol ice is observed with a single peak centered at 121 K as shown in Fig. 3A along with the mass shifted isotopomers at m/z = 44 amu for D_2CCO in CD_3OD ice, $H_2CC^{18}O$ in $CH_3{}^{18}OH$ ice and $H_2{}^{13}C^{13}CO$ in $^{13}CH_3OH$ ice. All are in excellent agreement with each other as shown, confirming the assignment of this molecular formula. With regard to the irradiated methanol–carbon monoxide ice systems, the sublimation profile at m/z = 42 amu (H_2CCO) in CH_3OH–CO ice (Fig. 3B) also depicts a single peak centered at 123 K.

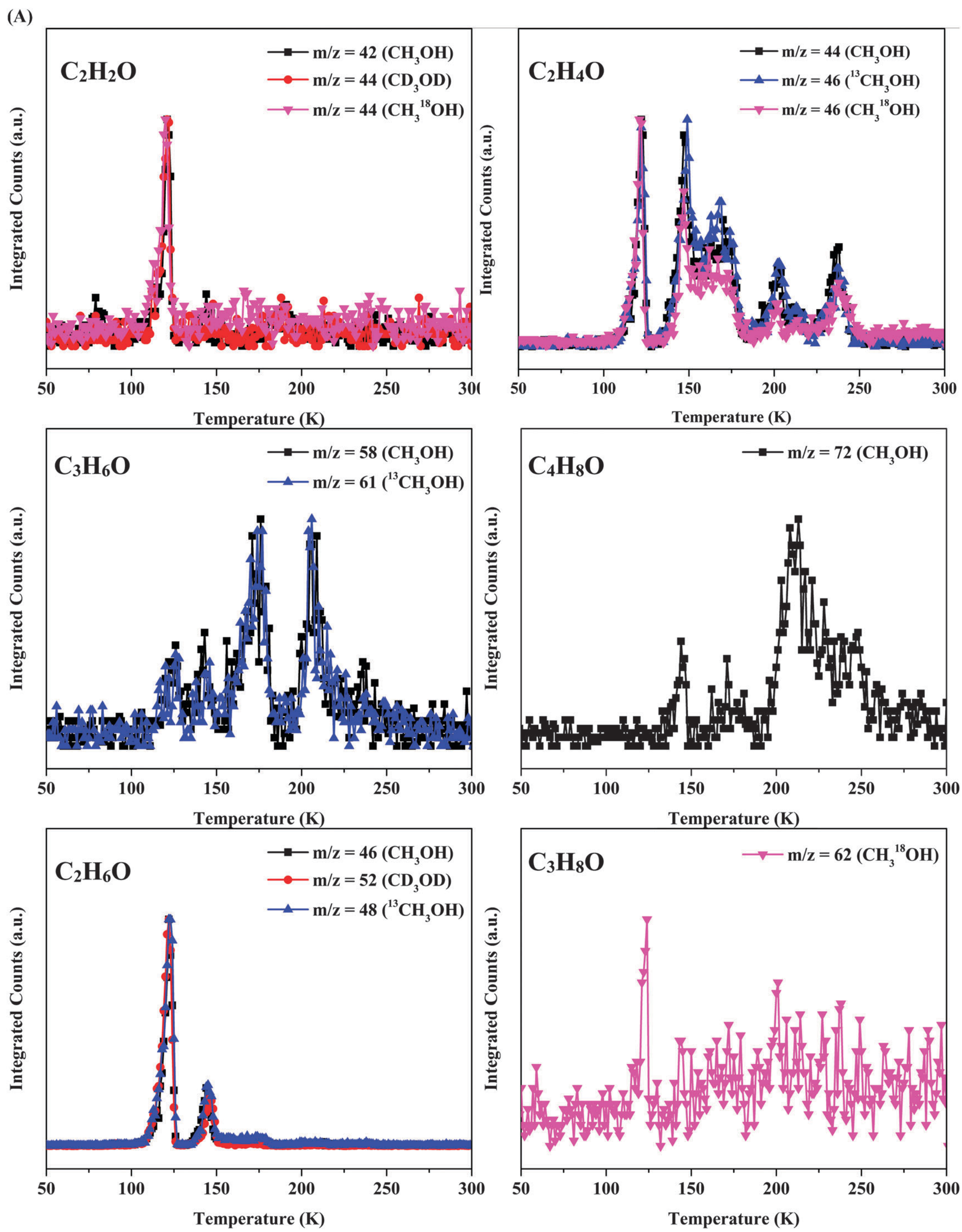

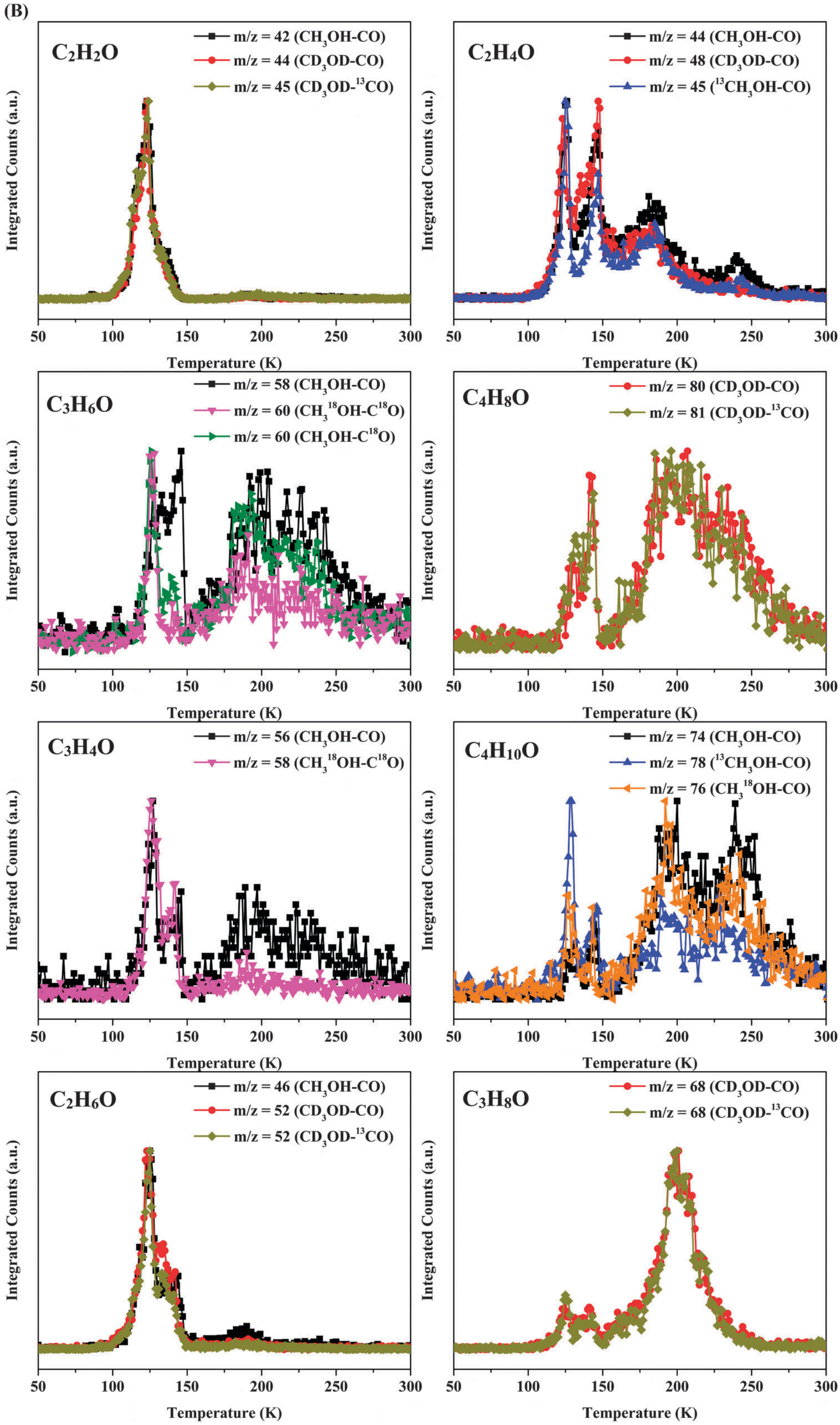
(B)
C_2H_2O
m/z = 42 (CH_3OH-CO)
m/z = 44 (CD_3OD-CO)
m/z = 45 (CD_3OD-^{13}CO)
C_2H_4O
m/z = 44 (CH_3OH-CO)
m/z = 48 (CD_3OD-CO)
m/z = 45 ($^{13}CH_3OH$-CO)
C_3H_6O
m/z = 58 (CH_3OH-CO)
m/z = 60 ($CH_3{}^{18}OH$-$C^{18}O$)
m/z = 60 (CH_3OH-$C^{18}O$)
C_4H_8O
m/z = 80 (CD_3OD-CO)
m/z = 81 (CD_3OD-^{13}CO)
C_3H_4O
m/z = 56 (CH_3OH-CO)
m/z = 58 ($CH_3{}^{18}OH$-$C^{18}O$)
$C_4H_{10}O$
m/z = 74 (CH_3OH-CO)
m/z = 78 ($^{13}CH_3OH$-CO)
m/z = 76 ($CH_3{}^{18}OH$-CO)
C_2H_6O
m/z = 46 (CH_3OH-CO)
m/z = 52 (CD_3OD-CO)
m/z = 52 (CD_3OD-^{13}CO)
C_3H_8O
m/z = 68 (CD_3OD-CO)
m/z = 68 (CD_3OD-^{13}CO)
Integrated Counts (a.u.)
Temperature (K)
50 100 150 200 250 300

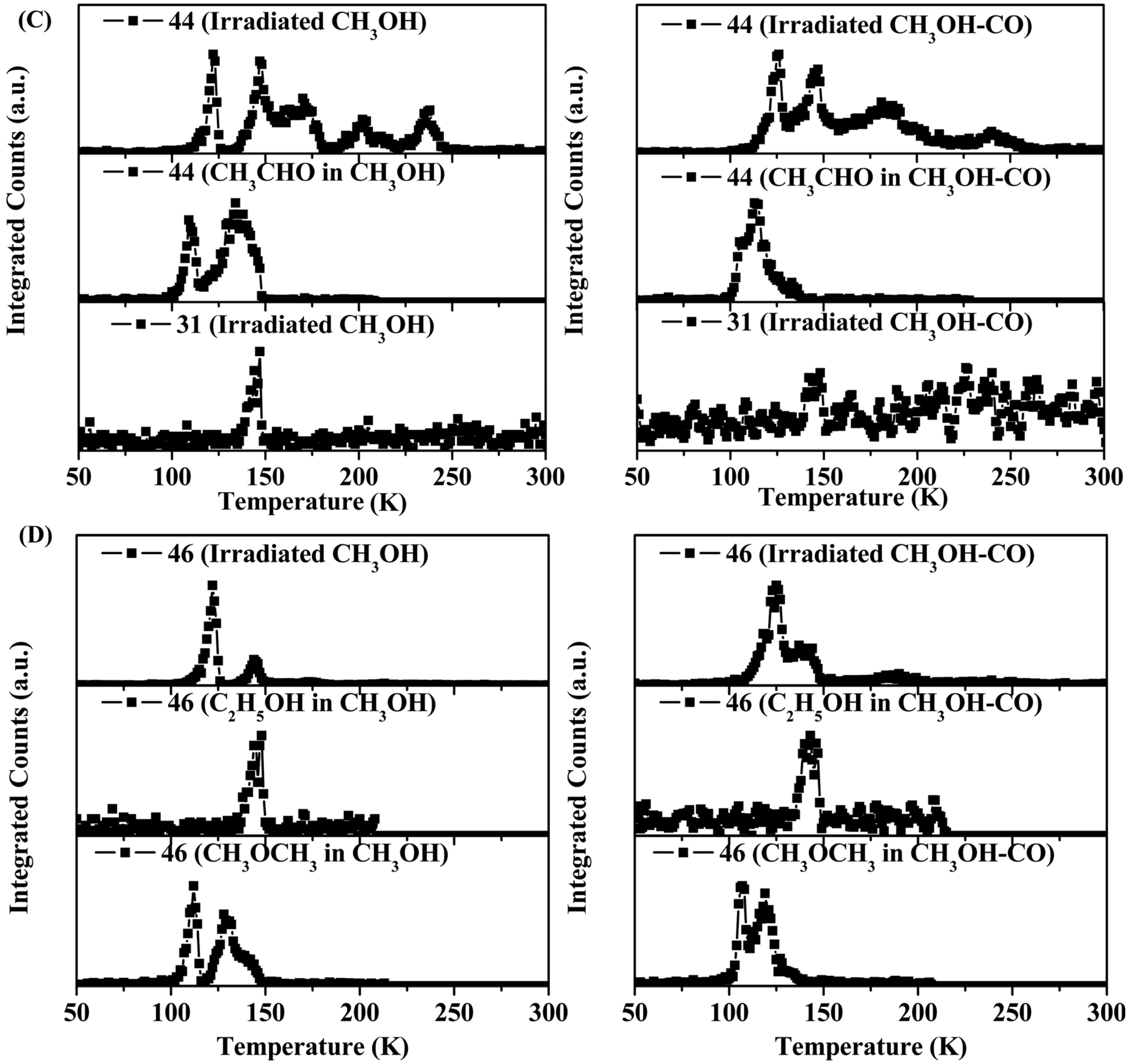

Fig. 3 (A) Sublimation profiles of newly formed products with a single oxygen atom observed in irradiated methanol ices. (B) Sublimation profiles of newly formed products detected with a single oxygen atom observed in irradiated methanol–carbon monoxide (4 : 5) ice systems. (C) Sublimation profiles of the calibration samples containing acetaldehyde (CH_3CHO; m/z = 44 amu) in (left) CH_3OH (Sample 1) and (right) CH_3OH–CO (4 : 5) (Sample 2) are compared with the sublimation profiles of $C_2H_4O^+$ ion counts recorded in irradiated CH_3OH and CH_3OH–CO (4 : 5) ices. Sublimation profiles of the photoionization fragment CH_3O^+ of methanol at m/z = 31 amu are also shown. (D) Sublimation profiles of the calibration samples containing C_2H_6O isomers [ethanol (CH_3CH_2OH) and methoxymethane (CH_3OCH_3); m/z = 46 amu] in (left) CH_3OH (Samples 3 and 5) and (right) CH_3OH–CO (4 : 5) (Samples 4 and 6) ices are compared with the sublimation profiles of m/z = 46 amu recorded in irradiated CH_3OH and CH_3OH–CO (4 : 5) ices.

Similarly, ketene isotopomers were observed in the irradiated labeled ices as shown in Fig. 3B. Recall that we have also identified the ν_2 fundamental of ketene isotopomers $H_2CC^{18}O$ in irradiated $CH_3{}^{18}OH$ ices and $H_2{}^{13}C^{13}CO$ in irradiated $^{13}CH_3OH$ ices using infrared spectroscopy (Fig. 1A, Table 2), along with the observation of the ν_2 fundamental of ketene isotopomer $H_2CC^{18}O$ in both $CH_3{}^{18}OH$–$C^{18}O$ and CH_3OH–$C^{18}O$ ices at 2107 cm^{-1} and 2106 cm^{-1}, respectively, as shown in Fig. 1B and Table 2 as discussed previously. Note that all masses corresponding to the *in situ* identified isotopomers of ketene *via* FTIR spectroscopy were observed following warm-up.

Acetaldehyde (CH_3CHO). Sublimation profiles for masses corresponding to C_2H_4O isomers formed in both irradiated methanol and methanol–carbon monoxide isotopologue ices are shown in Fig. 3A and B, respectively. In both irradiated ice systems the agreement between the sublimation profiles of C_2H_4O isotopomers confirms the identification of a radiolytic product with the molecular formula C_2H_4O. Here we should mention that, among the three possible isomers with the molecular formula C_2H_4O [ethylene oxide (c-C_2H_4O, IE = 10.56 eV), acetaldehyde (CH_3CHO, IE = 10.23 eV) and vinyl alcohol (CH_2CHOH), IE = 9.33 eV], only the latter two can contribute to the signal at the corresponding masses observed. Sublimation profiles of C_2H_4O isotopomers from the irradiated methanol ices reveal five distinct peaks centered at 122 K, 147 K, 170 K, 203 K and 238 K. The multiple sublimation peak temperatures imply the possibility of (i) sublimation of different isomers with different functional groups and overall polarity, (ii) co-sublimation of a specific isomer at different temperatures due to intermolecular interactions with neighboring molecules and/or (iii) photo-fragmentation of a higher mass product producing a fragment ion related to $C_2H_4O^+$. As mentioned above, only two isomers, acetaldehyde (CH_3CHO) and vinyl alcohol (CH_2CHOH), can be ionized at 10.49 eV. Here, the sublimation of acetaldehyde is expected at a lower temperature than that for vinyl alcohol (if formed) due to the less polar functional group (CO) compared to the OH functional group in vinyl alcohol. In order to verify the identification of acetaldehyde (CH_3CHO) in the irradiated methanol ices, calibration experiments were conducted by simply depositing a sample containing $1.0 \pm 0.2\%$ of acetaldehyde (CH_3CHO) in CH_3OH (Sample 1; ESI,† Table S3). The subsequent sublimation profile of m/z = 44 amu (Fig. 3C) does indeed display two peaks centered at slightly lower temperatures of 109 K and 134 K. Coincidentally, methanol begins a phase transition from amorphous to crystalline at 100–125 K (ref. 79) forcing the acetaldehyde to escape *via* a molecular volcano type mechanism.[80] Here, the first peak at 109 K is due to sublimation of acetaldehyde induced from the phase change of methanol. However, some acetaldehyde is trapped within the methanol matrix, hence the appearance of the second peak at 134 K as it co-sublimates with methanol. Here, the sublimation of acetaldehyde is observed until about 150 K, which clearly suggests that the trapped acetaldehyde molecules are subliming together with the methanol matrix. A comparison of sublimation profiles from both the calibration sample and the irradiated CH_3OH ices (Fig. 3C) suggests that the first two peaks at 122 K and 147 K in irradiated methanol ices are due to the sublimation of acetaldehyde. Although the peak temperatures do not match perfectly, the overall trend does match in that acetaldehyde sublimates as methanol changes from amorphous to crystalline, followed by co-sublimation with methanol. To further strengthen the latter point, the sublimation profile of the photoionization fragment CH_3O^+ (appearance energy = 10.4 eV)[81,82] of methanol at m/z = 31 amu is shown in Fig. 3C which displays a sublimation peak at 147 K. Note that the difference in peak temperatures between the irradiated methanol ice and the acetaldehyde–methanol-doped calibration sample is 13 K warmer for both peaks; the shift towards a higher temperature (higher binding energy) may be attributed to intermolecular interactions resulting from the additional large complex organics that were synthesized in the irradiated ice compared to the simple simulation sample. The peak sublimation temperatures at 170 K and 203 K are discussed below along with their tentative assignments. Recall that evidence of acetaldehyde was confirmed *via* infrared absorption at 1724 cm^{-1} (ν_4) together with the isotopically labeled counterparts as discussed in Section 3.1.1. Finally, the sublimation peak at 238 K can be assigned to fragmentation of $C_3H_8O_3$ (glycerol) which shows a prominent fragmentation pattern at 10.49 eV.[83] Note that due to the astrobiological importance pertaining to the prebiotic formation of glycerol, we chose to focus on this specific molecule in a separate publication.

In the case of methanol–carbon monoxide systems, the sublimation profiles of C_2H_4O isotopomers are shown in Fig. 3B and display four distinct sublimation peaks centered at 125 K, 147 K, 183 K, and 240 K. Similar calibration experiments were conducted with a sample containing $0.5 \pm 0.1\%$ of acetaldehyde in a mixed CH_3OH–CO (4 : 5) ice system (Sample 2). Here, the sublimation profile at m/z = 44 amu recorded during the calibration experiment (Fig. 3C) depicts a sharp peak at 114 K with two shoulders at 105 K and 136 K. The shoulder at 105 K can be correlated to sublimation of acetaldehyde induced *via* the phase change similar to that observed in methanol/acetaldehyde simulation that peaked at 109 K; however, this observation is the only similarity. A highly porous methanol ice results from carbon monoxide having already sublimated at these temperatures allowing for more binding sites of the acetaldehyde within the pores of the methanol matrix. The lack of two distinct peaks as observed in the methanol calibration sample is most likely a reflection of the initial porosity of the methanol matrix. Here, most of the acetaldehyde was allowed to sublimate in the mixed methanol–carbon monoxide ice from a combination of high initial porosity followed by phase transition, whereas the pure methanol ice simulation sample trapped more of the acetaldehyde during the phase transition resulting in significant co-sublimation. However, some of the acetaldehyde did remain trapped, thereby explaining the small shoulder at 136 K. Note that the difference of sublimation temperatures between the observed peaks of the irradiated binary mixture and calibration sample is 11 K warmer. Again, this shift towards higher temperatures and thus higher binding energies is attributed to the intermolecular interactions with other complex organics left in the refractory material. The large difference in the sublimation profiles of the calibration and irradiated sample may simply be due to the inherent effect that these large organics acting as 'impurities' have on the phase change behavior of the ice sample.

C_2H_6O isomers: identification of ethanol (C_2H_5OH) and dimethyl ether (CH_3OCH_3). Integrated ion counts at mass-to-charge ratios corresponding to isotopomers of C_2H_6O products were observed in both irradiated methanol and methanol–carbon monoxide isotopologue ices and are shown in Fig. 3A and B, respectively. In irradiated methanol ices, sublimation of C_2H_6O depicts two distinct sublimation peaks centered at 122 K and 144 K as shown in Fig. 3A. The sublimation profile of the product C_2H_6O from irradiated methanol–carbon monoxide ices depicts a pronounced peak at 124 K with a shoulder at 143 K (Fig. 3B). Note that both C_2H_6O isomers, ethanol (C_2H_5OH; 10.48 eV) and dimethyl ether (CH_3OCH_3; 10.0 eV), can be ionized with the 10.49 eV VUV photons. In order to ensure the assignment of these isomers, calibration experiments were performed with ethanol and dimethyl ether in both methanol (Samples 3 and 5) and methanol–carbon monoxide

(Samples 4 and 6) ices and were compared with the sublimation profiles of the C_2H_6O irradiation product obtained from both irradiated methanol and methanol–carbon monoxide ices shown in Fig. 3D.

In the calibration experiments with methanol ices, the sublimation of dimethyl ether started at 102 K and the sublimation profile shows two peaks positioned at 112 K and 128 K with a shoulder at 142 K. The lower sublimation temperature of dimethyl ether is reasonable due to its lower polarity compared to methanol. Here, the peak at 112 K can be correlated to the sublimation of dimethyl ether (CH_3OCH_3) from methanol ices whereas the peak at 128 K follows the same pattern as observed with acetaldehyde ($HCOCH_3$), *i.e.* methanol phase change from amorphous to crystalline resulting in a molecular volcano. Finally, the shoulder at 145 K is the result of co-sublimation of trapped dimethyl ether (CH_3OCH_3) within the methanol matrix. Note that the temperature difference between the irradiated methanol ice sample and the dimethyl ether calibration sample is similar to that observed for the acetaldehyde sample (about 12 K); again this shift in temperature is attributed to intermolecular forces of the large refractory organics formed in the process of irradiation. In the case of methanol–carbon monoxide ices, the calibration experiment with dimethyl ether displays two peaks at 108 K and 119 K with a small shoulder at 145 K. In a similar way, the first peak can be assigned to the sublimation of dimethyl ether (CH_3OCH_3) molecules followed by sublimation of trapped dimethyl ether (CH_3OCH_3) molecules during the phase change, and finally co-sublimation with methanol at 145 K; as discussed above, the residual methanol matrix at these temperatures is most likely of higher porosity compared to the pure methanol samples due to the prior sublimation of carbon monoxide, as such allowing most of the dimethyl ether to leave. We are again attributing the differences in the sublimation profiles of the irradiated and calibration sample to the intrinsic effects of what could be considered contamination from the remaining organics on the phase change behavior of methanol.

The calibration experiments (Fig. 3D) also depict that the sublimation of ethanol (C_2H_5OH) with both peaks positioned at 145 K in the methanol and methanol–carbon monoxide ices matches well the observed profile of the irradiated samples. This observation is not unexpected as ethanol is completely miscible with methanol. In addition, QMS traces of $C_2H_6{}^{18}O^+$ (m/z = 48 amu) and $C_2H_5{}^{18}O^+$ (m/z = 47 amu) ions show two peaks at temperatures of 122 K and 144 K in irradiated $CH_3{}^{18}OH$ ice and at 124 K and 146 K in irradiated $CH_3{}^{18}OH–C^{18}O$ ice (ESI,† Fig. S6). Note that both ethanol ($CH_3CH_2{}^{18}OH$) and dimethyl ether ($CH_3{}^{18}OCH_3$) show prominent fragment ion with formula $C_2H_5{}^{18}O^+$ during the electron impact ionization,[81] providing further evidence in support of our assignment of dimethyl ether and ethanol formed in irradiated methanol and methanol–carbon monoxide ices.

3.2.1.2. Complex organic molecules with two oxygen atoms. By comparing the sublimation profiles of the integrated ion counts observed from the isotopically labeled ices of both methanol and methanol–carbon monoxide, products with the molecular formula $C_2H_2O_2$, $C_2H_4O_2$, and $C_2H_6O_2$ are identified. It is worth mentioning that the sublimation profiles of the products in the irradiated methanol ices are relatively narrow with sharp peaks compared to the sublimation profiles observed in irradiated methanol–carbon monoxide ices as can be seen in Fig. 4–8 and ESI,† Fig. S7 and S8. The broad sublimation features observed in the latter mixed ices are most likely due to the intermolecular interactions with the residual high mass organics (up to 150 amu) formed within the processed mixed ices (Fig. 2B). In comparison, the radiation induced chemical processing of methanol isotopologue ices resulted in the identification of fewer products with mass-to-charge ratios of up to 90 amu only (Fig. 2A), which explains the diminished dipole–dipole interactions of the subliming molecules with the residual organic matrix resulting in the relatively narrow sublimation profiles observed in the case of methanol systems.

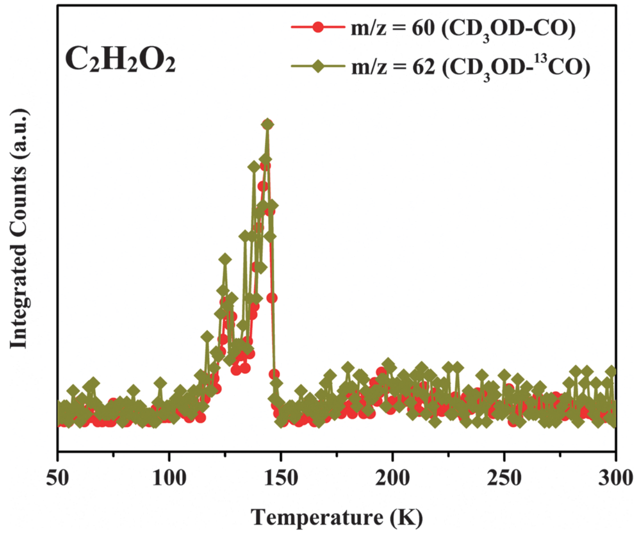

Fig. 4 Sublimation profile of $C_2H_2O_2$ isotopomers identified as glyoxal (HCOCOH), only in the processed mixed methanol–carbon monoxide (4 : 5) ice systems.

Identification of glyoxal ($C_2H_2O_2$). A product with the molecular formula $C_2H_2O_2$ and the respective mass shifted isotopomers were observed only in the irradiated mixed methanol–carbon monoxide isotopologue ices with a sublimation peak at 145 K as shown in Fig. 4. We are assigning this sublimation of the molecule to glyoxal (HCOCHO) for two reasons. First, note that 2-oxiranone [Cyc(CH_2OC)O] (an isomer of glyoxal) is 38 kJ mol^{-1} less stable than the glyoxal and holds an ionization energy of 10.96 eV (calculated),[84] and therefore should not be attributed for any ion signal collected at this particular photon energy whereas glyoxal could be with its ionization energy at 10.2 eV. Second, the third most stable isomer (63 kJ mol^{-1} less stable than glyoxal) ethyne-1,2-diol (HOCCOH) has an ionization energy of 9.3 eV (ref. 84) and can be ionized; however, this diol isomer is expected to sublime at temperatures greater than the sublimation temperature of ethylene glycol ($HOCH_2CH_2OH$) which displays a sublimation peak at about 200 K (see below) because ethyne-1,2-diol (530 K) holds a higher boiling point than ethylene glycol (471 K).

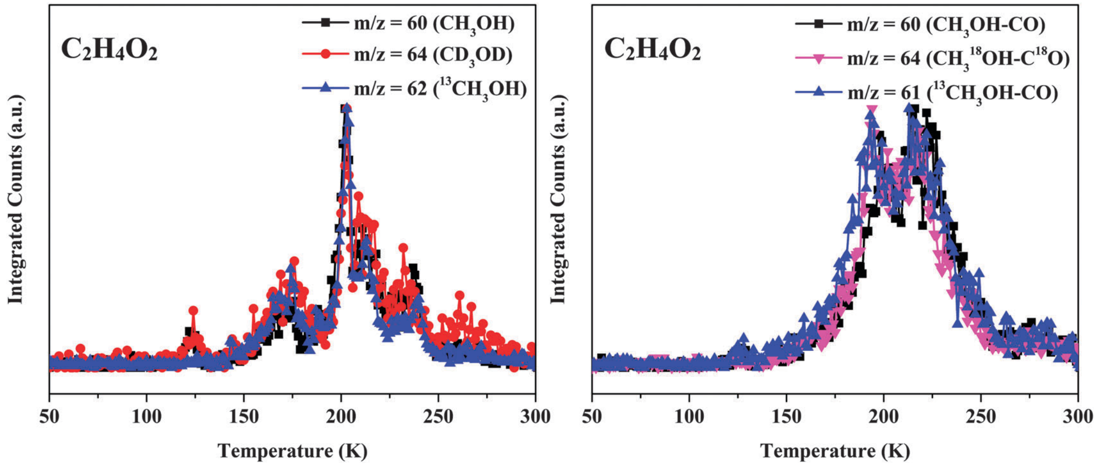

Fig. 5 Sublimation profiles of $C_2H_4O_2$ isotopomers of irradiated methanol ice systems (left) and methanol–carbon monoxide systems (right). Molecular isomers, glycolaldehyde and ethane-1,2-diol, are assigned to the observed ion signal. For a detailed discussion on the assignment, please see the main text.

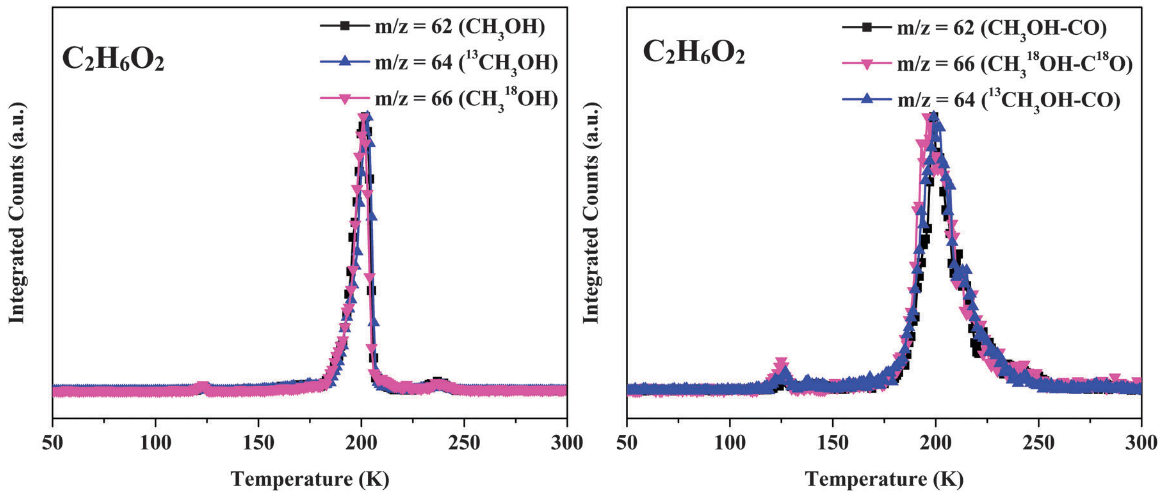

Fig. 6 Sublimation profiles of $C_2H_6O_2$ isotopomers of irradiated methanol ice systems (left) and methanol–carbon monoxide systems (right). Ethylene glycol $HOCH_2CH_2OH$ is assigned to the observed ion signal. For a detailed discussion on the assignment, please see the main text.

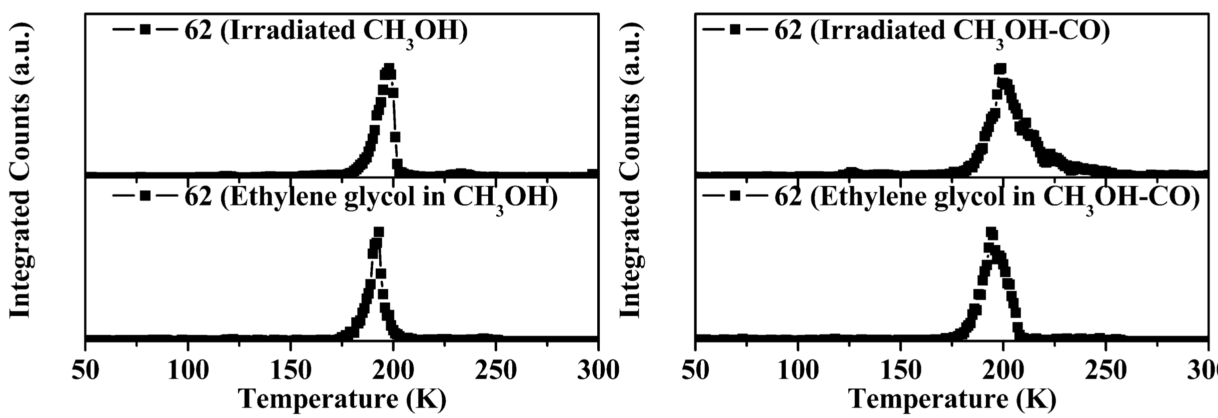

Fig. 7 Sublimation profiles of the calibration samples containing ethylene glycol ($HOCH_2CH_2OH$; m/z = 62 amu) in (left) CH_3OH (Sample 11) and (right) CH_3OH–CO (4 : 5) (Sample 12) are compared with the sublimation profiles of $C_2H_6O_2^+$ ion counts recorded in irradiated CH_3OH and CH_3OH–CO (4 : 5) ices.

However, no detectable signal was collected for $C_2H_2O_2$ at temperatures greater than 200 K. Therefore, we can conclude that in irradiated methanol–carbon monoxide ices ethyne-1,2-diol did not form or was below the detection limit. Finally, please note the

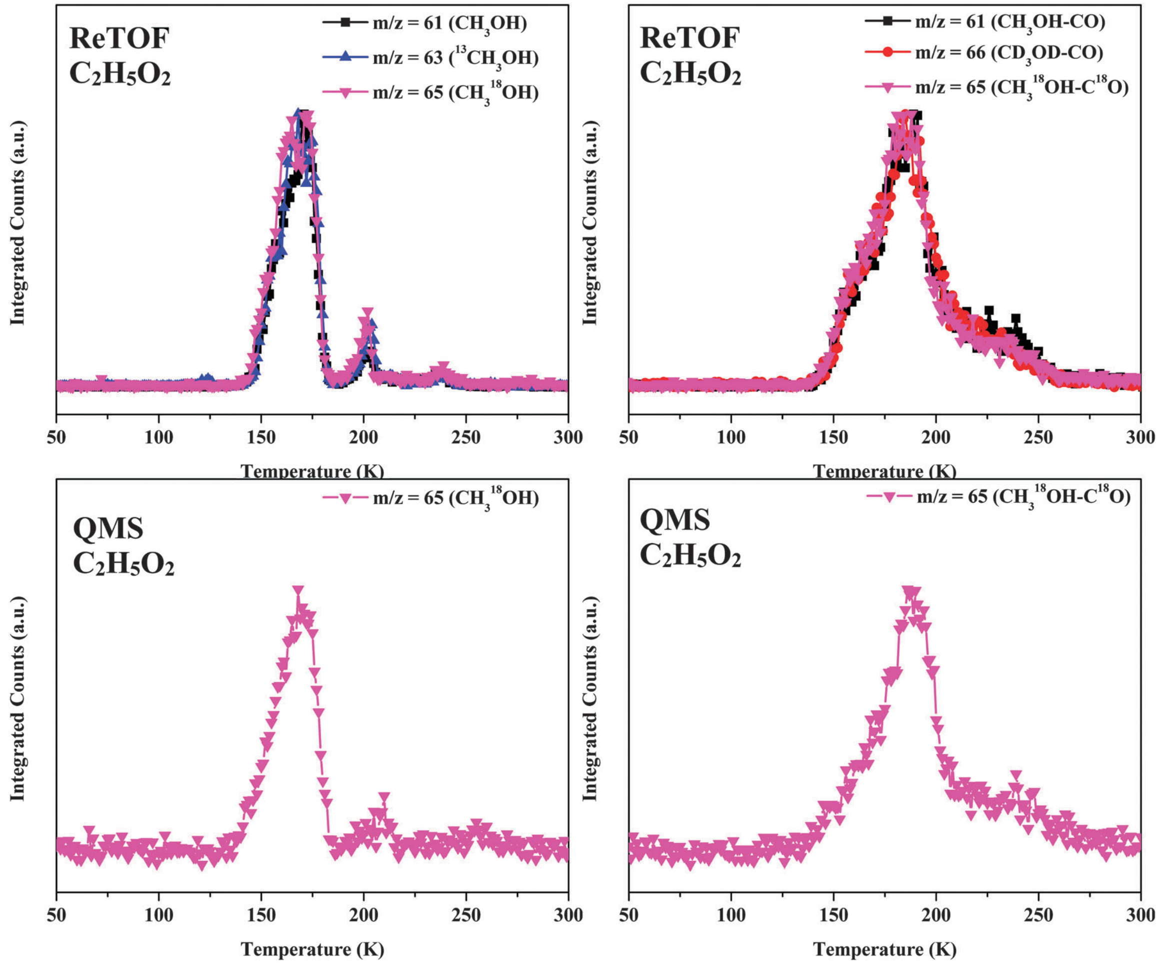

Fig. 8 ReTOF sublimation profiles and QMS traces of $C_2H_5O_2$ isotopomers of irradiated methanol ice systems (left) and methanol–carbon monoxide systems (right). Methoxy methanol (CH_3OCH_2OH) is assigned to the observed ion signal.

similar trend in sublimation peaks as discussed above; here, the weak sublimation peak observed at 125 K is related to the phase change of methanol followed by co-sublimation at 145 K.

$C_2H_4O_2$ isomers: identification of glycolaldehyde and ethene-1,2-diol. Among the four stable isomers of $C_2H_4O_2$, glycolaldehyde ($HOCH_2CHO$; 10.2 eV), ethene-1,2-diol (HOCHCHOH; 9.62 eV), acetic acid (CH_3COOH; 10.65 eV) and methyl formate ($HCOOCH_3$; 10.84 eV), only glycolaldehyde and ethene-1,2-diol can be ionized with 10.49 eV VUV photons used in the present study. A significantly more detailed discussion related to assignment of glycolaldehyde and ethene-1,2-diol can be found in a previous publication.[63] Very briefly though, five sublimation peaks at 123 K, 166 K, 200 K, 210 K and 234 K in each isotopically labeled methanol ice (Fig. 5) were observed for the sublimation of $C_2H_4O_2$ isomers in the irradiated methanol ices. The first peak at 123 K is most likely due to the induced sublimation of $C_2H_4O_2$ isomers resulting from the amorphous to crystalline phase change inducing a molecular cryo-volcano. Following this is the sublimation peak at 166 K which is assigned to the sublimation of glycolaldehyde based on the coincidently decreasing ν_{14} band from *in situ* FTIR observations. Next, the observed peak at 200 K is from co-sublimation with ethylene glycol followed by direct sublimation of ethene-1,2-diol at 210 K.[63] Finally, the distinct peak around 234 K is assigned to the fragmentation from glycerol ($C_3H_8O_3$) based on a recent study on the photoionization of glycerol ($C_3H_8O_3$) in which a prominent photo ion fragment ($C_2H_4O_2$) was identified with an appearance energy of 9.9 eV.[83] In the case of irradiated methanol–carbon monoxide isotopologue ices, the $C_2H_4O_2$ product was confirmed sublimating at 125 K, 195 K and 218 K (Fig. 5) with the latter two peaks assigned to glycolaldehyde and ethene-1,2-diol, respectively, and the first peak related to the sublimation due to phase change of methanol at 125 K.

Identification of ethylene glycol ($HOCH_2CH_2OH$). The sublimation profiles of $C_2H_6O_2$ in both irradiated methanol and methanol–carbon monoxide ices show a prominent peak at 198 K along with a weak sublimation peak at 125 K as shown in Fig. 6. In the case of irradiated methanol systems, the sublimation profiles also display a slight peak at 236 K. Here, the intense peak at 198 K suggests the sublimation of a single isomer with the molecular formula $C_2H_6O_2$. In order to ensure the assignment of ethylene glycol ($HOCH_2CH_2OH$; IE = 10.16 eV)[81] in both methanol and methanol–carbon monoxide ices, calibration experiments were performed with ethylene glycol in CH_3OH and CH_3OH–CO ices as displayed in Fig. 7. The sublimation profiles of the ion counts at m/z = 62 amu recorded from the calibration experiments were compared with the sublimation profiles of $C_2H_6O_2$ observed in both irradiated CH_3OH and CH_3OH–CO ices. The sublimation of ethylene glycol (Fig. 7) shows a single peak at 193 K in CH_3OH ice (Sample 11; ESI,† Table S3) and at 194 K in CH_3OH–CO (Sample 12) ice. As expected and observed, ethylene glycol holds two hydroxyl groups and will sublime at a higher temperature than methanol. The sublimation profile of the $C_2H_6O_2$ product obtained in both irradiated methanol and methanol–carbon monoxide ices is in reasonable agreement with the desorption profile of ethylene glycol obtained from the calibration experiments. In addition, QMS traces corresponding to $C_2H_6O^+$ are also observed at about 198 K in both irradiated methanol and methanol–carbon monoxide ices. Also observed are ion fragments typical of ethylene glycol due to electron impact ionization at the mass-to-charge ratios correspond to $C_2H_3O^+$, $C_2H_4O^+$, $C_2H_5O^+$, and $C_2H_5O_2^+$, as shown in ESI,† Fig. S6. Therefore, the sublimation peak at 198 K recorded using ReTOF mass spectrometry in irradiated methanol and methanol–carbon monoxide ices is assigned to ethylene glycol ($HOCH_2CH_2OH$). Also recall that we have identified ethylene glycol *via* the observation of the ν_9 band of ethylene glycol at 1094 cm^{-1} using *in situ* infrared spectroscopy.

As mentioned, a weak peak is also observed at about 125 K (Fig. 6) in both irradiated methanol and methanol–carbon monoxide ices. As this temperature is well below the sublimation temperature of methanol ($\sim$145 K) and is correlated with the amorphous to crystalline phase change, the peak observed at this temperature could indicate either a 'cyro-volcano' of ethylene glycol or possibly the sublimation of a less polar $C_2H_6O_2$ isomer. Among the isomers are ethylene glycol (470 K), ethylhydroperoxide (368 K), methoxymethanol (356 K), and dimethyl peroxide (239 K) with the boiling points given in parentheses. Of these isomers, dimethyl peroxide is expected to sublime at temperatures below the sublimation temperature of methanol (338 K). Consequently, the weak sublimation peak at 125 K may be related to dimethyl peroxide (CH_3OOCH_3; 9.1 eV). Finally, the sublimation peak at 236 K (Fig. 7) in the irradiated methanol isotopologue ices is once again attributed to glycerol ($C_3H_8O_3$) in which a prominent photo fragment at m/z = 62 amu ($C_2H_6O_2$) has been identified with an appearance energy of 9.9 eV.[83]

Identification of methoxymethanol (CH_3OCH_2OH). Methoxymethanol is a rather interesting radiation by-product as it has been previously identified only in the low energy electron radiolysis of methanol ices.[57,85] Based on the functional groups present in methoxymethanol (CH_3OCH_2OH) and a comparison of the trends in boiling points, methoxymethanol (356 K) is expected to sublime at a temperature higher than methanol (338 K) but at a lower temperature compared to ethylene glycol (470 K). However, there are no significant ion counts of $C_2H_6O_2$ (Fig. 8) at temperatures between the sublimation of methanol and ethylene glycol (140–170 K) that would normally indicate the sublimation of a different molecular isomer. Previously, methoxymethanol was assigned as a low energy electron radiolysis product of methanol ice from the combination of a unique sublimation profile and the fragmentation pattern. The justification was based heavily on a previous mass spectroscopic analysis of synthesized methoxymethanol which identified a prominent ion fragment at m/z = 61 amu corresponding to $C_2H_5O_2^+$, whereas the expected parent molecular ion peak at m/z = 62 amu ($C_2H_6O_2^+$) was not observed or determined to be within the noise level.[86] Following a similar approach here, we concur with the previous identification of methoxymethanol in energetically processed methanol ices and present the novel identification of this product in the irradiated binary ice mixture of methanol and carbon monoxide. Evidence supporting the identification of methoxymethanol is twofold as presented here. First, upon examination of the QMS data, isotopomers connected with $C_2H_5O_2^+$ were observed subliming with peak ion counts at 170 K, with no detectable signal being contributed from the parent ($C_2H_6O_2$) at these temperatures, in agreement with the previous studies.[57,85] Second, $C_2H_5O_2^+$ isotopomers that were detected utilizing single photoionization ReTOF mass spectrometry have *identical sublimation profiles* to that derived from the QMS data. Sublimation profiles observed at these mass-to-charge ratios are shown in Fig. 8 for irradiated methanol and methanol–carbon monoxide ices. Note that the possibility of radicals sublimating is discounted as the applied thermal energy would allow for any trapped radicals to diffuse and easily react at these temperatures. Also, previous attempts at dosing the irradiated methanol ice with oxygen atoms did not decrease the overall TPD signal of $C_2H_5O_2^+$ further implying that $C_2H_5O_2$ radicals are not directly sublimating.[57] From our observations, *i.e.* the direct correlation between two different gas phase detection methods, methoxymethanol is suggested to be an extremely thermally labile compound or photoionization at 10.49 eV leads to fragmentation thereby explaining the lack of parent ion signal in the TPD analysis. In both irradiated methanol and methanol–carbon monoxide ices, the sublimation of $C_2H_5O_2^+$ started at 143 K with a prominent peak positioned at 170 K and 184 K, respectively. Additional sublimation peaks observed at this m/z linked to $C_2H_5O_2^+$ in irradiated CH_3OH ices (Fig. 8) at 202 K and 238 K are attributed to the co-sublimation of methoxymethanol (CH_3OCH_2OH) with ethylene glycol ($HOCH_2CH_2OH$) and photofragmentation of glycerol ($C_3H_8O_3$),[83] respectively. The sublimation peak at 202 K is excluded as due to fragmentation of ethylene glycol ($HOCH_2CH_2OH$) as the calibration experiments with ethylene glycol did not exhibit any fragmentation at m/z = 61 amu ($C_2H_5O_2$).

3.2.2. Molecules with tentative assignments

3.2.2.1. Vinyl alcohol (CH_2CHOH). Vinyl alcohol (CH_2CHOH; 9.3 eV) is tentatively assigned to account for the ion signal (m/z = 44 amu) observed at the sublimation temperature (peak) of 170 $\pm$ 2 K in the irradiated methanol ice systems and at 185 $\pm$ 2 K in the processed methanol–carbon monoxide systems (Fig. 3A and B). Here, the sublimation of vinyl alcohol at temperatures higher than for acetaldehyde is reasonable since the molecule is overall more polar, and thus will have a higher energy of desorption. The sublimation peak at 203 ± 2 K observed in the TPD spectra of the processed methanol ices coincides with the sublimation of ethylene glycol and thus may possibly be attributed to co-sublimation of vinyl alcohol with ethylene glycol due to the similar polarity. Photo-fragmentation from ethylene glycol is excluded since photoionization of the ethylene glycol calibration sample did not show any fragmentation. Unfortunately, similar calibration experiments with vinyl alcohol could not be conducted due to the inherent instability of the molecule (and commercial unavailability) which will tautomerize to acetaldehyde.

3.2.2.2. C_3H_4O isomers. A radiolysis by-product with the molecular formula C_3H_4O was identified only in the irradiated methanol–carbon monoxide ices. In Fig. 3A, the sublimation profile of C_3H_4O isotopomers shows two distinct peaks centered at 127 K and 144 K which again is attributed to the phase change induced molecular volcano followed by co-sublimation with methanol. However, a broad sublimation profile that extends up to 300 K is observed and again is most likely a combination of sublimation of different isomers and photofragmentation of high mass organics. Molecular isomers that may contribute to the ion counts at the derived molecular formula are propenal (CH_2CHCHO; 10.1 eV), cyclopropanone ($CH_2(CO)CH_2$; 9.1 eV), and methyl ketene (CH_3CHCO; 8.95 eV). Of these, only propenal (CH_2CHCHO) is readily available and was used as a calibration sample at 1.5 ± 0.5% in methanol–carbon monoxide ice in order to help with the possible identification. The sublimation profile at m/z = 56 amu of propenal recorded from the calibration sample together with the sublimation profile of C_3H_4O isomers observed in irradiated CH_3OH–CO ices is shown in ESI,† Fig. S9. The sublimation profile at m/z = 56 amu shows two peaks at 128 K and 138 K and these temperatures can be correlated to the sublimation of propenal during the phase change and the sublimation of the methanol matrix as discussed above. The correlation of the TPD spectra would suggest sublimation of propenal; however, we again cannot eliminate the possibility of cyclopropanone ($CH_2(CO)CH_2$) and methyl ketene (CH_3CHCO) isomers and therefore can only present a tentative assignment here.

3.2.2.3. C_3H_6O isomers. Products with the molecular formula C_3H_6O were identified in both irradiated methanol and methanol–carbon monoxide ices. The sublimation profiles at m/z corresponding to isotopologues of C_3H_6O isomers are shown in Fig. 3A and B. Of the molecular isomers, acetone (CH_3COCH_3; 9.7 eV), propanal (C_2H_5CHO; 10.0 eV), and allyl alcohol (CH_2CHCH_2OH; 9.7 eV) can account for the observed ion signal as these have ionization energies below the 10.49 eV threshold. The TPD spectra of the C_3H_6O molecular product depict four distinct peaks centered at 125 K, 145 K, 172 K, and 203 K in irradiated methanol ices. In the irradiated mixed methanol–carbon monoxide ices, two sharp peaks are displayed at 126 K and 146 K together with a broad peak centered at about 187 K. Similar to that previously discussed, the first sublimation peaks at about 125 K and 145 K are associated with the phase transition of amorphous to crystalline (125 K) inducing a molecular volcano followed by co-sublimation of methanol near 145 K. To help identify which isomers were sublimating, calibration experiments (ESI,† Table S3) were performed with acetone (CH_3COCH_3; Samples 1 and 2), propanal (CH_3CH_2CHO; Samples 3 and 4) and allyl alcohol (CH_2CHCH_2OH; Samples 5 and 6) in both methanol and methanol–carbon monoxide ices. The sublimation profiles of ion counts at m/z = 58 amu ($C_3H_6O^+$) recorded from the calibration experiments are shown in ESI,† Fig. S10 in comparison with the sublimation profile at m/z = 58 amu recorded from both irradiated CH_3OH and CH_3OH–CO ices. The sublimation temperatures of these molecules are lower than the sublimation temperature of methanol as expected based on their polarity and subsequent boiling point trends, whereas allyl alcohol (CH_2CHCH_2OH) is expected to sublime at a higher temperature than methanol. Here, acetone and propanal both exhibited peak sublimation temperatures of 137 K from methanol ice and 128 K and 126 K, respectively, in the mixed methanol–carbon monoxide ice and the sublimation profiles of allyl alcohol from both methanol and methanol–carbon monoxide ices depict a single sublimation peak at 154 K and 152 K, respectively. Unfortunately, the TPD profiles of the calibration samples are not adequately unique to disentangle for a definitive assignment. Moreover, *in situ* IR spectroscopy did not yield strong evidence for the formation of these molecules to allow for certainty in the assignment, in agreement with previous examinations on the energetic processing of methanol rich ices.[53,74,79] However, ion counts were observed corresponding to the molecular formula C_3H_6O and thus we can only suggest the possibility that acetone, propanal, and/or allyl alcohol were/was formed. In addition possible contributions from photofragmentation of the higher mass products (such as $C_4H_8O_2$) may contribute to the ion counts observed at higher temperatures, namely the broad sublimation profile extending from 170 to 250 K in the irradiated methanol–carbon monoxide ice along with the peaks at 172 K and 203 K in the TPD spectra of irradiated methanol ices. For example, the appearance energies of $C_3H_6O^+$ from $C_4H_8O_2$ isomers, 3-methoxypropanal and methoxymethyloxirane, are 8.5 eV and 10.2 eV, respectively. The sublimation of the product with the derived molecular formula $C_4H_8O_2$ (discussed below) resulted in three peaks at 179 K, 208 K and 254 K in irradiated methanol ices and a broad sublimation feature within the 175–275 K temperature range in irradiated methanol–carbon monoxide ices. Future experiments using tunable vacuum ultraviolet light for selective photoionization will allow us make specific assignments based upon their ionization energies.

3.2.2.4 C_3H_8O isomers. Products were identified in the TPD spectra of the irradiated ice systems with the molecular formula C_3H_8O as shown in Fig. 3A and B. The molecular isomers of this group are either alcohols such as 1-propanol ($CH_3CH_2CH_2OH$; 10.2 eV), 2-propanol ($CH_3CH(OH)CH_3$; 10.2 eV) or an ether molecule such as methoxyethane ($CH_3OCH_2CH_3$; 9.7 eV). In irradiated methanol ices, the sublimation of C_3H_8O is identified *via* a distinct sublimation peak at 124 K. In the case of methanol–carbon monoxide ices, C_3H_8O isomers are observed sublimating at 125 K and 142 K. In order to assist in the determination of which C_3H_8O isomers were detected, calibration experiments were performed with only 1-propanol and 2-propanol in both methanol and methanol–carbon monoxide ices as methoxyethane is not commercially available. The TPD profiles of 1-propanol and 2-propanol peak at 155 K and 153 K, respectively, in CH_3OH ices and at 152 K and 149 K, respectively, in CH_3OH–CO ices, as shown in ESI,† Fig. S11. The above information clearly suggests that 1-propanol and 2-propanol isomers sublime at higher temperatures than methanol. Furthermore, the sublimation profiles of C_3H_8O radiolytic by-product isomers (m/z = 60 amu) do not agree with those of the alcohol calibration samples. As such we can only postulate the possible formation of methoxy ethane with the observed peaks attributed to the molecular volcano induced by the amorphous to crystalline phase change at 125 K and co-sublimation of C_3H_8O isomers with methanol at 145 K.

3.2.2.5. C_4H_8O isomers. Ion counts associated with the molecular formula C_4H_8O are observed in the TPD spectra of both irradiated methanol and methanol–carbon monoxide ices (Fig. 3A and B). Molecules such as butanal (C_3H_7CHO; 9.8 eV), iso-butanal ($CH_3CH(CH_3)CHO$; 9.7 eV), butanone ($C_2H_5COCH_3$; 9.1 eV), and 2-buten-1-ol ($HOCH_2CHCHCH_3$; 9.1 eV) can contribute to the observed signal here. As mentioned previously, both irradiated ices exhibited peaks at the sublimation temperature of methanol, and thus ion counts for these masses correspond again to co-sublimation with methanol. However, the broad peak positioned at about 208 K is most likely due to photofragmentation of higher mass organics, such as $C_3H_4O_2$ (m/z = 72 amu) isomers as discussed below. Similarly in the irradiated methanol–carbon monoxide ices (Fig. 3B), the sublimation profiles of C_4D_8O display a broad sublimation feature centered at $\sim$200 K which may be attributed again to the photofragmentation of higher mass organics. Calibration experiments were once again conducted in an effort to remove some of the ambiguity observed in the TPD spectra of the potential carriers for the observed C_4H_8O isomers. Here, calibration samples contained butanal (Samples 3 and 4), iso-butanal (Samples 7 and 8) and butanone (Samples 5 and 6) in both CH_3OH and CH_3OH–CO (4 : 5) ices. The sublimation profiles of the ion counts of C_4H_8O isomers at m/z = 72 amu are shown in ESI,† Fig. S12 and are compared with the sublimation profiles observed at m/z = 72 amu (C_4H_8O) in irradiated CH_3OH ices and at m/z = 80 amu (C_4D_8O) in irradiated CD_3OD–CO ices. As shown in ESI,† Fig. S12, all TPD spectra are again not sufficiently unique to make a definitive assignment and the isomers typically sublimate with methanol. Based on the above information alone, we can only suggest that at least one of these molecules is formed within irradiated methanol ices.

3.2.2.6. $C_4H_{10}O$ isomers. We have also identified $C_4H_{10}O$ molecular isomers; however, this observation is only in irradiated methanol–carbon monoxide ices. The sublimation profiles of integrated ion counts corresponding to $C_4H_{10}O$ isotopomers are shown in Fig. 3B and are observed with peaks at 128 K and 143 K. Alcohols and ethers are possible isomers and include 1-butanol ($CH_3CH_2CH_2CH_2OH$; 10.0 eV), 2-butanol ($CH_3CH_2CH(OH)CH_3$; 9.9 eV), iso-butanol ($(CH_3)_2CHCH_2OH$; 10.0 eV), *tert*-butanol ($(CH_3)_3COH$; 9.9 eV), methoxypropane ($CH_3OC_3H_7$; 9.41 eV) and ethoxyethane ($C_2H_5OC_2H_5$; 9.51 eV). In order to quantify which isomers were detected in the irradiated samples calibration experiments were performed with 1-butanol, 2-butanol, iso-butanol and *tert*-butanol in CH_3OH–CO ices. The sublimation profiles of these $C_4H_{10}O$ isomers at m/z = 74 amu are compared with the sublimation profile of the irradiation product $C_4H_{10}O$ (m/z = 74 amu) and are shown in ESI,† Fig. S13. The TPD profiles of 1-butanol, 2-butanol, iso-butanol and *tert*-butanol peak at 159 K, 154 K, 159 K and 155 K, respectively, and are not in agreement with the observed profile or peak positions recorded in irradiated CH_3OH–CO ice (128 K and 143 K). Consequently, we once more can only suggest the possible identification of less polar ether molecules methoxypropane ($CH_3OC_3H_7$) and ethoxyethane ($C_2H_5OC_2H_5$) isomers, while again is attributed to the compaction of the methanol phase change at $\sim$125 K inducing a cryovolcano along with co-sublimation of $C_4H_{10}O$ alcohols and ethers with methanol at $\sim$145 K.

3.2.2.7. $C_3H_4O_2$ isomers. Ion counts attributed to the molecular formula $C_3H_4O_2$ have been detected in both irradiated methanol and methanol–carbon monoxide ices. The TPD spectra of irradiated methanol ices show $C_3H_4O_2$ isomers sublimating with peaks at 208 K and 236 K in irradiated methanol ices (ESI,† Fig. S7) and at 183 K and 236 K in irradiated methanol–carbon monoxide ices (ESI,† Fig. S14). These observations suggest the formation of isomers with at least two different functional groups resulting in different polarities and subsequently different desorption energies. Molecules such as methyl glyoxal (CH_3COCHO; 9.6 eV) and 1,3-propanedial ($HCOCH_2CHO$) can account for the $C_3H_4O_2$ isomers. In addition, more polar en-ol isomers, such as 2-hydroxyacrylaldehyde ($HCOC(OH)CH_2$) and 3-hydroxyacrylaldehyde ($HOCHCHCHO$), can also be correlated to this product as well. Here, the sublimation peaks at 203 K in irradiated methanol ice and at 183 K in irradiated methanol–carbon monoxide ices can be correlated to the less polar isomers (possibly methyl glyoxal and 1,3-propanedial) and the sublimation peaks centered at 236 K in both methanol and methanol–carbon monoxide ices can be assigned to the sublimation of glycerol, as photoionization of this molecule at 10.49 eV results in ion fragmentation.[83]

3.2.2.8. $C_3H_6O_2$ isomers. The sublimation profiles recorded in connection with $C_3H_6O_2$ isotopomers in methanol ices (ESI,† Fig. S7) depict three prominent peaks at 173 K, 210 K and 236 K. The peak at 236 K has been assigned to photofragmentation of glycerol ($C_3H_8O_3$).[83] In irradiated methanol–carbon monoxide ices, $C_3H_6O_2$ isotopomers were identified *via* a broad sublimation profile (150–300 K) with two peaks at 192 K and 244 K (ESI,† Fig. S14). Methyl sugar molecules such as hydroxyacetone (CH_3COCH_2OH; 10.0 eV), 2-hydroxypropanal ($CH_3CH(OH)CHO$) and 3-hydroxypropanal ($HOCH_2CH_2CHO$) can be linked to the product $C_3H_6O_2$ with one hydroxyl and one carbonyl functional groups. In addition, isomers bearing acid and ester functional groups such as propionic acid (C_2H_5COOH; 10.44 eV) and methyl acetate (CH_3COOCH_3; 10.25 eV) can also be linked to $C_3H_6O_2$ isomers.

3.2.2.9. $C_3H_8O_2$ isomers. Isomers with the molecular formula $C_3H_8O_2$ have been identified in both irradiated methanol and methanol–carbon monoxide ices as shown in ESI,† Fig. S7 and S14, respectively. In irradiated methanol ices, the sublimation profile shows two prominent peaks at 171 K and 203 K. Molecules such as methoxyethanol ($CH_3OCH_2CH_2OH$) and ethoxymethanol ($CH_3CH_2OCH_2OH$) may be responsible for the observed ion counts at 171 K as these molecules are expected to sublime at temperatures similar to that of methoxymethanol. Similarly, the sublimation of di-ol isomers is expected to be at temperatures close to that of ethylene glycol. Hence, 1,2-propanediol and/or 1,3-propanediol isomers may be responsible for the signal at 203 K. In the case of irradiated methanol–carbon monoxide ices, the sublimation of $C_3H_8O_2$ (ESI,† Fig. S14) shows a broad profile extending from 150 K to at least 270 K. The broad sublimation profile is most likely due to possible intermolecular interactions with higher mass organics, as we have mentioned before. Here, the peak at ~185 K may possibly be attributed to the sublimation of methoxyethanol ($CH_3OCH_2CH_2OH$) or ethoxymethanol ($CH_3CH_2OCH_2OH$) isomers as the peak position is close to the observed temperature for methoxymethanol (184 K). On the other hand, more polar di-ol isomers such as 1,2-propanediol and/or 1,3-propanediol may account for the extended sublimation tail due to their higher desorption energies.

3.2.2.10. $C_4H_6O_2$ isomers. Products with the formula $C_4H_6O_2$ were only detected in the TPD spectra of irradiated methanol–carbon monoxide ices and are shown in ESI,† Fig. S14 which shows a broad sublimation profile with two subtle peaks at 192 K and 236 K which again suggest that isomers of $C_4H_6O_2$ with different polarities are sublimating. The weak features observed at ~145 K can be linked to the co-sublimation of $C_4H_6O_2$ isomers with the methanol matrix. Isomers of $C_4H_6O_2$ can be associated to dicarbonyl molecules such as butane-2,3-dione ($CH_3COCOCH_3$; 9.3 eV), 2-oxobutanal ($HCOCOCH_2CH_3$), and molecules bearing single carbonyl (CO) and single hydroxyl (OH) groups such as 2-hydroxybut-3-enal ($HCOCH(OH)CHCH_2$) and 4-hydroxybut-2-enal ($HCOCHCHCH_2OH$). The dicarbonyl isomers are expected to sublime at lower temperatures (~ 192 K) due to their less polar functional group compared to isomers bearing hydroxyl groups. Fragmentation of glycerol at 10.49 eV (ref. 83) is once again attributed to the peak at 236 K.

3.2.2.11. $C_4H_8O_2$ isomers. The sublimation profiles due to $C_4H_8O_2$ isomers are depicted in ESI,† Fig. S15 and S16. In irradiated methanol ices, the sublimation of $C_4H_8O_2$ displays three peaks at 179 K, 207 K and 254 K; however, in irradiated methanol–carbon monoxide ices, the sublimation profile of $C_4H_8O_2$ shows a broad profile with a slight peak positioned at 236 K. These observations again suggest the possible formation of multiple isomers of $C_4H_8O_2$ with different polarities. Hydroxyl-carbonyl isomers of hydroxybutanal and hydroxybutanone, ester molecules such as methyl propionate ($CH_3CH_2COOCH_3$; 10.2 eV) and ethyl acetate ($CH_3COOCH_2CH_3$; 10.0 eV) and di-ol molecules such as but-2-ene-1,4-diol ($HOCH_2CHCHCH_2OH$) can be considered as the possible isomers of the product $C_4H_8O_2$.

3.2.3. Complex organic molecules bearing three, four and five oxygen atoms

3.2.3.1. $C_3H_6O_3$. Isomers corresponding to the molecular formula $C_3H_6O_3$ were observed in the TPD spectra of the irradiated methanol and mixed methanol–carbon monoxide isotopologue ice systems as shown in ESI,† Fig. S15 and S16, respectively. The sublimation profiles of $C_3H_6O_3$ molecular isomers in both irradiated ice systems are broad and show two slight sublimation peaks at ~210 K and ~240 K and imply different isomers with various polarities. Molecular isomers with $C_3H_6O_3$ formula consist of astrobiologically important C3-sugar molecules such as glyceraldehyde ($HOCH_2CH(OH)CHO$) and 1,3-dihydroxyacetone ($HOCH_2COCH_2OH$). In addition, molecules with an ester functional such as methyl-2-hydroxyacetate (CH_3OCOCH_2OH; 10.42 eV) and methoxymethylformate (CH_3OCH_2OCHO) can also be associated to the product $C_3H_6O_3$. Additional complex organics bearing three oxygen atoms ($C_3H_4O_3$) were identified only in irradiated methanol–carbon monoxide isotopologue ices (ESI,† Fig. S16).

3.2.3.2. $C_4H_{6,8}O_3$. In the case of methanol–carbon monoxide systems, a product with the molecular formula $C_4H_8O_3$ was observed with the TPD profile of $C_4H_8O_3$ shown in ESI,† Fig. S17. The sublimation of $C_4H_8O_3$ in irradiated methanol–carbon monoxide ices depicts a profile similar to that of $C_3H_6O_3$ (ESI,† Fig. S16), but extending up to 300 K. Among the $C_4H_8O_3$ isomers include sugar molecules with a methyl group such as 2,3-dihydroxybutanal ($HCOCH(OH)CH(OH)CH_3$) and 1,3-dihydroxy-2-butanone ($HOCH_2COCH(OH)CH_3$). In addition, molecules with an ester functional such as 1-hydroxyethylacetate ($CH_3COOCH(OH)CH_3$), methyl-2-hydroxypropanoate ($CH_3OCOCH(OH)CH_3$), and 2-hydroxyethylacetate ($CH_3COOCH_2CH_2OH$) are also possible $C_4H_8O_3$ isomers; the chemical structures of these isomers are shown in ESI,† Fig. S19. Additional complex organics bearing three oxygen atoms ($C_4H_6O_3$) were only identified in irradiated methanol–carbon monoxide isotopologue ices (ESI,† Fig. S16). The TPD spectra of these products are broad implying the formation of an abundant mixture of isomers with various desorption energies.

3.2.3.3. $C_nH_mO_{4,5}$. Molecules bearing four and five oxygen atoms are only detected in the TPD spectra of irradiated methanol–carbon monoxide ice systems. The ReTOF mass spectroscopic analysis resulted in the identification of five products bearing four oxygen atoms which include isomers of the molecular formula $C_4H_4O_4$, $C_4H_6O_4$, $C_4H_8O_4$, $C_5H_6O_4$, $C_5H_8O_4$, $C_5H_6O_5$ and $C_5H_8O_5$ with their respective sublimation profiles shown in ESI,† Fig. S17 and S18. Astrobiologically relevant sugar related molecules shown in ESI,† Fig. S19 could possibly make up a subset of sublimating molecules. However, numerous molecules can be associated with these products; therefore no specific assignment can be made as the result would be ambiguous. A summary of molecular formula observed in this study and the corresponding chemical structures, with identified molecules marked in bold, is presented in ESI,† Fig. S20.

4. Discussion

4.1. Formation pathways based on ReTOF mass spectrometry

Within the irradiated mixed isotopologue binary ice systems of methanol and carbon monoxide ($^{13}CH_3OH$–CO, CD_3OD–^{13}CO, $CH_3{}^{18}OH$–CO and CH_3OH–$C^{18}O$), products with mixed isotopes of the same molecular formula were observed (see Table 4). However, in the irradiated methanol isotopologue ices (CH_3OH, CD_3OD, $^{13}CH_3OH$ and $CH_3{}^{18}OH$) and the mixed isotopically pure methanol–carbon monoxide ices (CH_3OH–CO, CD_3OD–CO, and $CH_3{}^{18}OH$–$C^{18}O$), only products containing one isotope were identified, as expected. From these observations, we can comment on the reaction pathways as discussed below. The most intense isotopomers are marked in Table 4. A detailed discussion of the most likely formation pathways is provided in the following sections.

4.1.1. Ketene (H_2CCO). Evidence for the synthesis of ketene *via* three competing formation pathways in irradiated methanol–carbon monoxide ices was observed in this study. For the sake of clarity, these pathways are labelled as (i) "$2CH_3OH$", (ii) "$1CH_3OH$ + 1CO" and (iii) "2CO". The resultant isotopomers of ketene *via* each pathway are listed in Table 5. It should be noted that several of the ketene isotopomers observed have an identical mass at 44 amu in the $^{13}CH_3OH$–CO system ($H_2{}^{13}C^{13}CO$), the $CH_3{}^{18}OH$–CO system ($H_2CC^{18}O$) and the CH_3OH–$C^{18}O$ system ($H_2CC^{18}O$) and overlap in mass with other possible C_2H_4O molecular isotopomers. However, in the irradiated CD_3OD–^{13}CO ice system, isotopomers of ketene were observed at distinctive mass-to-charge ratios [m/z = 44 amu (D_2CCO), 45 amu ($D_2C^{13}CO$) and 46 amu ($D_2{}^{13}C^{13}CO$)] allowing for a quantitative contribution of each formulation pathway. Specifically, the isotopically labeled carbon atom in this system can act as a tracer thereby elucidating the reaction pathways. Here for example, D_2CCO can only be produced stemming from a "$2CH_3OH$" pathway whereas $D_2C^{13}CO$ and $D_2{}^{13}C^{13}CO$ isotopomers are the products formed *via* "$1CH_3OH$ + 1CO" and "2CO" reaction mechanisms respectively. Ion counts at m/z = 44 amu (D_2CCO), 45 amu ($D_2C^{13}CO$) and 46 amu ($D_2{}^{13}C^{13}CO$) in irradiated CD_3OD–^{13}CO ice are indeed observed and shown in Fig. 9. The most intense ion counts occur at m/z = 45 ($D_2C^{13}CO$) as shown in Fig. 9 and imply that the most prominent pathway is the "$1CH_3OH$ + 1CO" reaction pathway. Surprisingly, the ion signal at m/z = 46 amu ($D_2{}^{13}C^{13}CO$) is about $70 \pm 5\%$ of the total ion counts observed at m/z = 45 amu implying the overall significance of the "2CO" formulation pathway. On the other hand, the isotopomer D_2CCO (m/z = 44 amu) formed *via* the "$2CH_3OH$" formulation pathway was observed at only $6 \pm 2\%$ of the total ion counts at m/z = 45 amu in the methanol–carbon monoxide ices.

4.1.2. Acetaldehyde (CH_3CHO). Following compelling evidence on the formation of acetaldehyde in both irradiated pure methanol ice and binary ices of methanol–carbon monoxide together with their isotopologue ices, we can discuss formulation pathways. Here, building blocks for the formation of acetaldehyde in pure methanol ices (CH_4 and CO) can only originate from radiolysis of CH_3OH and both have been identified as products in the irradiated methanol systems as shown in Fig. 1 and Table 2. In the case of mixed methanol–carbon monoxide systems, the introduction of carbon monoxide can further enhance the formation of acetaldehyde in a similar manner to the formation of ketene described above. Here, evidence of acetaldehyde formation *via* the three identified formulation pathways "$2CH_3OH$", "$1CH_3OH$ + 1CO" and "2CO" is observed as well. Again in the isotopically pure ices (CH_3OH–CO, CD_3OD–CO and $CH_3{}^{18}OH$–$C^{18}O$) acetaldehyde was only detected at a single mass-to-charge ratio such as m/z = 44 amu (CH_3CHO), 48 amu (CD_3CDO), and 46 amu ($CH_3CH^{18}O$), respectively. However, in the mixed isotopic ices, especially in the case of CD_3OD–^{13}CO ice, acetaldehyde isotopomers formed *via*

Table 5 List of isotopomers of the products C_2H_2O, C_2H_4O and C_2H_6O together with their mass-to-charge ratios formulated *via* (i) "$2CH_3OH$" (ii) "$1CH_3OH$ + 1CO" and (iii) "2CO" pathways in mixed isotopic ices ($^{13}CH_3OH$–CO, CD_3OD–^{13}CO, $CH_3{}^{18}OH$–CO and CH_3OH–$C^{18}O$). The mass-to-charge ratios shown in bold for CD_3OD–^{13}CO ice depict distinctiveness

	"$2CH_3OH$"		"$1CH_3OH$ + 1CO"		"2CO"	
Ices	Formula	m/z (amu)	Formula	m/z (amu)	Formula	m/z (amu)
C_2H_2O						
$^{13}CH_3OH$–CO	$H_2{}^{13}C^{13}CO$	44	$H_2{}^{13}CCO$	43	H_2CCO	42
CD_3OD–^{13}CO	**D_2CCO**	**44**	**$D_2C^{13}CO$**	**45**	**$D_2{}^{13}C^{13}CO$**	**46**
$CH_3{}^{18}OH$–CO	$H_2CC^{18}O$	44	H_2CCO	42	H_2CCO	42
CH_3OH–$C^{18}O$	H_2CCO	42	$H_2CC^{18}O$	44	$H_2CC^{18}O$	44
C_2H_4O						
$^{13}CH_3OH$–CO	$^{13}CH_3{}^{13}CHO$	46	$^{13}CH_3CHO$	45	CH_3CHO	44
CD_3OD–^{13}CO	**CD_3CDO**	**48**	**$CD_3{}^{13}CDO$**	**49**	**$^{13}CD_3{}^{13}CDO$**	**50**
$CH_3{}^{18}OH$–CO	$CH_3CH^{18}O$	46	CH_3CHO	44	CH_3CHO	44
CH_3OH–$C^{18}O$	CH_3CHO	44	$CH_3CH^{18}O$	46	$CH_3CH^{18}O$	46
C_2H_6O						
$^{13}CH_3OH$–CO	$^{13}C_2H_5OH$	48	$^{13}CCH_5OH$	47	C_2H_5OH	46
CD_3OD–^{13}CO	**C_2D_5OD**	**52**	**$C^{13}CD_5OD$**	**53**	**$^{13}C_2D_5OD$**	**54**
$CH_3{}^{18}OH$–CO	$C_2H_5{}^{18}OH$	48	C_2H_5OH	46	C_2H_5OH	46
CH_3OH–$C^{18}O$	C_2H_5OH	46	$C_2H_5{}^{18}OH$	48	$C_2H_5{}^{18}OH$	48

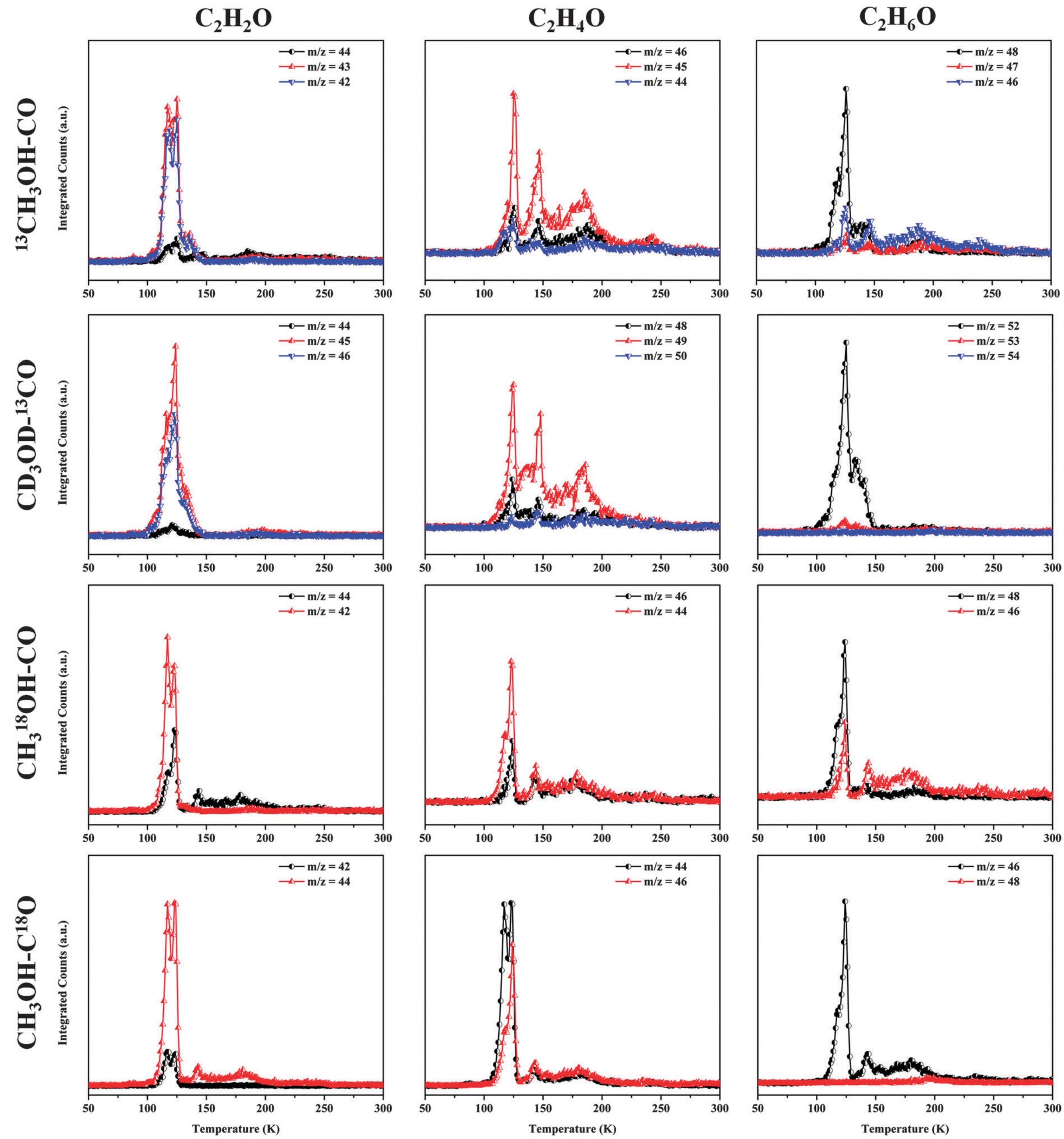

Fig. 9 Sublimation profiles of the integrated ion counts of (left) C_2H_2O, (center) C_2H_4O and (right) C_2H_6O isotopomers subliming from irradiated mixed isotopic ices: $^{13}CH_3OH$–CO, CD_3OD–^{13}CO, $CH_3{}^{18}OH$–CO and CH_3OH–$C^{18}O$.

these three established formulation pathways are observed at m/z = 48 amu (CD_3CDO), 49 amu ($CD_3{}^{13}CDO$), and 48 amu ($^{13}CD_3{}^{13}CDO$) as highlighted in Table 5 and shown in Fig. 9. The ion signals shown in Fig. 9 are quite intense at m/z = 49 ($CD_3{}^{13}CDO$), further implying a predominant "1CH$_3$OH + 1CO" reaction pathway. Unlike ketene formation however, acetaldehyde shows a stronger ion peak corresponding to the "2CH$_3$OH" formulation pathway (CD_3CDO) with a weak "2CO" formulation product ($^{13}CD_3{}^{13}CDO$).

4.1.3. C_2H_6O isomers. The detection of ethanol (C_2H_5OH) and dimethyl ether (CH_3OCH_3) in the irradiated ices of methanol and methanol–carbon monoxide is discussed in Section 3.2.1.2. Following a similar discussion as above for ketene and acetaldehyde, we can comment on the formation pathways of these isomers based on the integrated ion counts of C_2H_6O isotopomers observed in the mixed isotopic ices. The isotopomers of C_2H_6O formed *via* "2CH$_3$OH", "1CH$_3$OH + 1CO" and "2CO" formulation pathways are listed in Table 5. It should be noted from Table 5 that the mass-to-charge ratios of C_2H_6O isotopomers are again unique only in the processed CD_3OD–^{13}CO ice system. Here, C_2H_6O isotopomers are expected at m/z = 52 amu (C_2D_6O), 53 amu ($^{13}CCD_6O$) and 54 amu ($^{13}C_2D_6O$) with their sublimation profiles shown in Fig. 9. Here, the strong

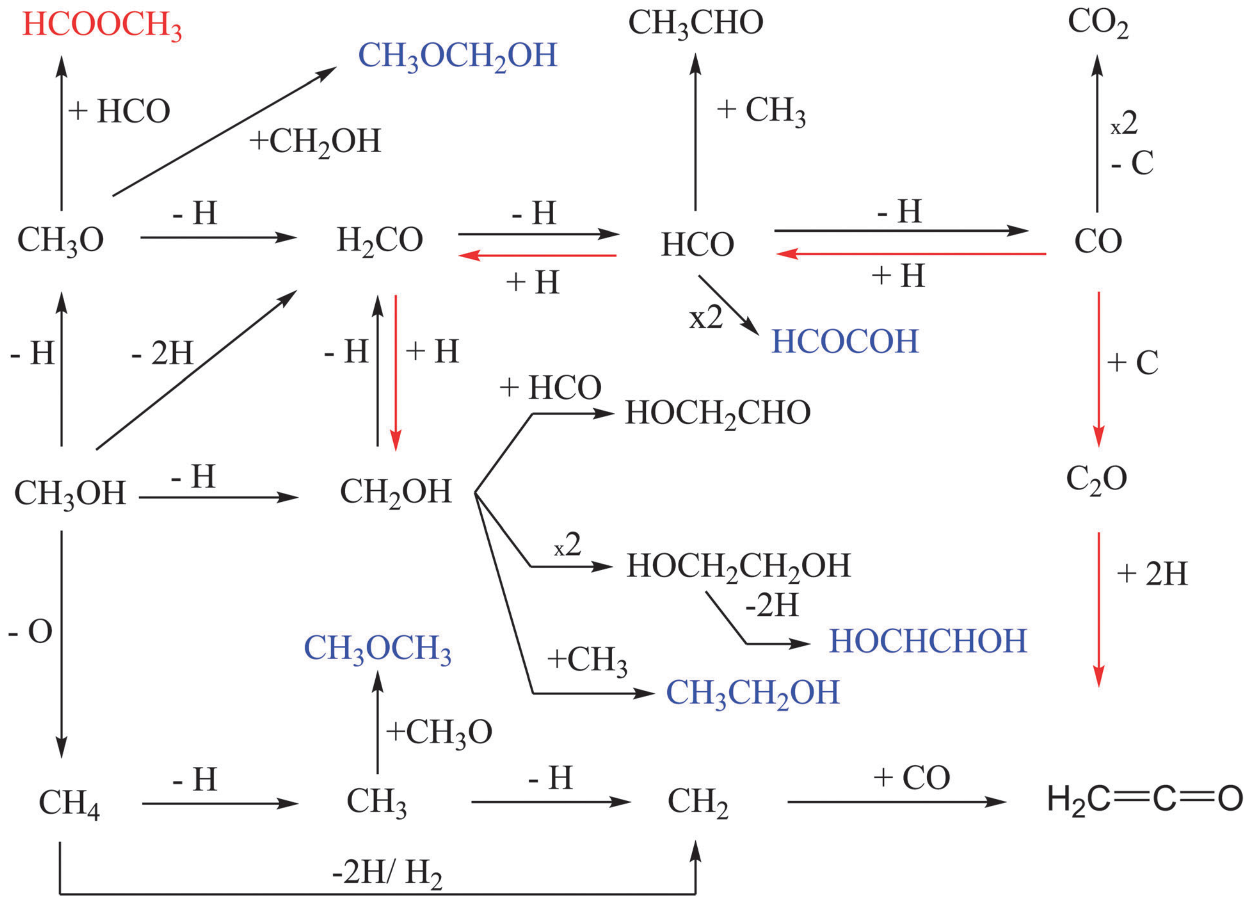

Fig. 10 Formation pathways of ketene (H_2CCO), acetaldehyde (CH_3CHO), methyl formate ($HCOOCH_3$), ethanol (CH_3CH_2OH), dimethyl ether (CH_3OCH_3), glyoxal (HCOCOH), ethene-1,2-diol (HOCHCHOH), glycolaldehyde ($HOCH_2CHO$), ethylene glycol ($HOCH_2CH_2OH$) and methoxy methanol (CH_3OCH_2OH) in irradiated methanol and methanol–carbon monoxide ices, determined previously.[48,54,61] The molecules presented in red have been identified based upon IR spectroscopy alone, in blue are those molecules based on gas phase detection *via* single photoionization ReTOF mass spectrometry, and in black are those identified with both analytical techniques.

integrated ion counts at m/z = 52 amu (C_2D_6O) indicate a predominant "2CH_3OH" formulation pathway as the integrated ion counts at m/z = 53 amu ($^{13}CCD_6O$) and 54 amu ($^{13}C_2D_6O$) are only 7 ± 3% and 2 ± 1% compared to the dominant ion counts at m/z = 52 amu. In this particular scenario, the "2CH_3OH" formulation pathway to the formation of C_2H_6O product isomers is the most prevalent.

4.2. Reaction pathways

Here, we would like to discuss the reaction mechanism underlying the formation of ketene (H_2CCO), acetaldehyde (CH_3CHO), methyl formate ($HCOOCH_3$), glycolaldehyde ($HOCH_2CHO$) and ethylene glycol ($HOCH_2CH_2OH$) identified in irradiated methanol and methanol–carbon monoxide ices.[53,54,63] Fig. 10 compiles the reaction pathways which have previously been identified mostly in irradiated CH_3OH and CH_3OH–CO ices based on the temporal evolution of the products recorded using infrared spectroscopy.[53,54] In addition, the formation mechanism of both ketene (H_2CCO) and acetaldehyde (CH_3CHO) is also included in Fig. 10. Formation pathways of ketene and acetaldehyde are not verified based on their temporal evolution in both irradiated methanol and methanol–carbon monoxide ices. However, these molecules were identified in the irradiated CH_4–CO ices.[61,64] Since both CH_4 and CO are present within irradiated CH_3OH and CH_3OH–CO ices (Fig. 1 and Table 2), we tried to discuss the validity of the reported formation pathways of both ketene (H_2CCO) and acetaldehyde (CH_3CHO) in the present experiments.

Previous experiments on the radiation induced decomposition of methanol have identified four reaction pathways as follows:[53,54] (i) unimolecular decomposition to the hydroxymethyl (CH_2OH) radical and a suprathermal hydrogen atom, (ii) unimolecular decomposition to the methoxy (CH_3O) radical and a suprathermal hydrogen atom, (iii) decomposition to formaldehyde (H_2CO) and molecular hydrogen and/or two hydrogen atoms and (iv) decomposition to form methane (CH_4) and atomic oxygen (term symbols have been omitted for clarity).

$$CH_3OH \rightarrow CH_2OH + H \quad \text{(i)}$$

$$CH_3OH \rightarrow CH_3O + H \quad \text{(ii)}$$

$$CH_3OH \rightarrow H_2CO + 2H/H_2 \quad \text{(iii)}$$

$$CH_3OH \rightarrow CH_4 + O \quad \text{(iv)}$$

Further, both hydroxymethyl radical and methoxy radical were found to undergo subsequent unimolecular decomposition to produce formaldehyde (H_2CO) and atomic hydrogen *via* reactions v and vi, respectively.[53,54]

$$CH_2OH \rightarrow H_2CO + H \quad \text{(v)}$$

$$CH_3O \rightarrow H_2CO + H \quad \text{(vi)}$$

Formaldehyde may further undergo successive unimolecular decompositions *via* atomic hydrogen elimination to form the formyl (HCO) radical (reaction vii) and carbon monoxide (CO) (reaction viii).

$$H_2CO \rightarrow HCO + H \quad \text{(vii)}$$

$$HCO \rightarrow CO + H \quad \text{(viii)}$$

In summary, the radiolysis of frozen methanol results in the formation of formyl radical (HCO), carbon monoxide (CO), methane (CH_4), formaldehyde (H_2CO), methoxy radical (CH_3O) and hydroxymethyl radical (CH_2OH). Save for the methoxy radical (CH_3O), all of the radiolysis products have been identified *via in situ* infrared spectroscopy in the irradiated methanol isotopologue ices as presented in this study and in previous examinations.

Previous experiments demonstrated that the newly formed products within irradiated methanol ices predominantly follow radical–radical reaction pathways.[53,54] Here, the radicals formed through reactions (i)–(viii) undergo a barrierless reaction resulting in the formation of larger and more complex organics. Consider for example the reaction of the formyl (HCO) radical with the hydroxymethyl (CH_2OH) radical resulting in the formation of glycolaldehyde ($HOCH_2CHO$) as shown in reaction ix.

$$CH_2OH + HCO \rightarrow HOCH_2CHO \quad \text{(ix)}$$

A radical–radical recombination of a formyl radical (HCO) with a methoxy (CH_3O) radical (reaction (x)) can lead to the formation of methyl formate ($HCOOCH_3$).

$$CH_3O + HCO \rightarrow HCOOCH_3 \quad \text{(x)}$$

Similarly, ethylene glycol ($HOCH_2CH_2OH$) can be formed *via* the dimerization of the hydroxymethyl (CH_2OH) radical as shown below (reaction (xi)).

$$CH_2OH + CH_2OH \rightarrow HOCH_2CH_2OH \quad \text{(xi)}$$

The above observations suggest that these molecules are most likely formed within the same matrix cage and a subsequent radical–radical reaction pathway is most plausible at 5.5 K where diffusion of these radicals is severally inhibited.[53,54]

In the case of methanol–carbon monoxide ices, the decomposition of methanol follows reaction pathways (i)–(viii), as discussed above. In addition, hydrogenation of carbon monoxide (CO) is also possible since the suprathermal atomic hydrogen produced during the decomposition of methanol (reactions (i)–(viii)) can add stepwise to carbon monoxide leading to the formation of the formyl radical *via* reaction (xii) with successive hydrogenation (reactions (xiii) and (xiv)) of the formyl radical ultimately producing formaldehyde and the CH_2OH radical as well.

$$CO + H \rightarrow HCO \quad \text{(xii)}$$

$$HCO + H \rightarrow H_2CO \quad \text{(xiii)}$$

$$H_2CO + H \rightarrow CH_2OH \quad \text{(xiv)}$$

Recall that in mixed isotopic ices of methanol–carbon monoxide, $^{13}CH_3OH$–CO, $CH_3{}^{18}OH$–CO, CD_3OD–^{13}CO and CH_3OH–$C^{18}O$, two isotopomers of formaldehyde were identified (Table 2) in each system *via in situ* IR spectroscopy. As an example, in $CH_3{}^{18}OH$–CO ices, formaldehyde was identified at 1692 cm^{-1} and 1724 cm^{-1} and these band positions agree within experimental uncertainty with the formaldehyde bands observed in irradiated $CH_3{}^{18}OH$ ices ($H_2C^{18}O$; 1693 cm^{-1}) and CH_3OH ices (H_2CO; 1726 cm^{-1}). Therefore, we can confidently state that $H_2C^{18}O$ is formed following two distinct reaction pathways: first *via* decomposition of methanol ($CH_3{}^{18}OH$) following reactions (iii) and (v) and second *via* the hydrogenation reaction of carbon monoxide (CO) following reactions (xii) and (xiii). Similarly, glycolaldehyde ($HOCH_2CHO$) and methyl formate ($HCOOCH_3$) are formed *via* reactions (ix) and (x) which show the radical–radical recombination of a CH_2OH unit with the HCO unit. As such, inclusion of two different isotopically labeled HCO units in both glycolaldehyde ($HOCH_2CHO$) and methyl formate ($HCOOCH_3$) is expected in the processed mixed isotope systems ($^{13}CH_3OH$–CO, $CH_3{}^{18}OH$–CO, CD_3OD–^{13}CO and CH_3OH–$C^{18}O$). Indeed, the deconvolution of infrared spectra in the carbonyl absorption stretching region did reveal vibrational frequencies associated with isotopomers of glycolaldehyde and methyl formate, thereby supporting the proposed "$1CH_3OH + 1CO$" mechanism identified above.

Next is a discussion on the identified formation mechanism of acetaldehyde (CH_3CHO) and ketene (H_2CCO). Since both of these products were identified in irradiated CH_4–CO ices[61] similar reaction pathways are expected as both CH_4 and CO have been identified in all of the processed ice systems. Here, the decomposition of methane produces the methyl radical (CH_3) and the methylene radical (CH_2) following reactions (xv)–(xvii).

$$CH_4 \rightarrow CH_3 + H \quad \text{(xv)}$$

$$CH_4 \rightarrow CH_2 + 2H/H_2 \quad \text{(xvi)}$$

$$CH_3 \rightarrow CH_2 + H \quad \text{(xvii)}$$

In the irradiated methanol ices, acetaldehyde can then be formed *via* the radical–radical recombination of the CH_3 radical and the HCO radical.

$$CH_3 + HCO \rightarrow CH_3CHO \quad \text{(xviii)}$$

In the case of isotopologue ices of CH_3OH–CO, HCO can be produced *via* either decomposition of methanol (reactions (iii) and (vii)) or hydrogenation of carbon monoxide *via* reaction (xii). Consequently, two different carbonyl stretching frequencies for acetaldehyde isotopomers are expected with evidence of this confirmed through *in situ* IR spectroscopy shown in Table 3. As an example, the formyl unit (HCO) of CH_3CHO (1726 cm^{-1}) and $CH_3CH^{18}O$ (1695 cm^{-1}) must have originated from CH_3OH and $C^{18}O$, respectively, in the irradiated $CH_3OH–C^{18}O$ ice. Further, evidence of this is also supported by ReTOF mass spectrometry as discussed above. Here, acetaldehyde synthesis *via* the "$1CH_3OH$ + 1CO" formulation was found to be the dominant reaction pathway. In addition, we have also identified acetaldehyde formation following the "$2CH_3OH$" reaction pathway using ReTOF mass spectrometry implying the formation of the HCO radical *via* decomposition of a methanol molecule as shown in reactions (iii) and (vii).

In the irradiated methanol ices, ketene (H_2CCO) can be formed *via* the reaction of the CH_2 radical (reactions (xvi) and (xvii)) with CO formed *via* the decomposition of the CH_3OH molecule (reactions (i) and (v)–(viii)).

$$CH_2 + CO \rightarrow H_2CCO \quad \text{(xix)}$$

In addition, ketene can also be formed *via* reactions (xx)–(xxii) in carbon monoxide rich ices, as identified previously.[64]

$$CO + CO \rightarrow CO_2 + C \quad \text{(xx)}$$

$$C + CO \rightarrow CCO \quad \text{(xxi)}$$

$$CCO + 2H \rightarrow H_2CCO \quad \text{(xxii)}$$

The validity of reaction (xx) is verified *via* the detection of CO_2 in the present experiment (Fig. 1 and Table 2). In addition, CCO has been previously observed following 5 keV electron irradiation of pure carbon monoxide ices[87] at 1988 cm^{-1} and post broadband UV photolysis of carbon monoxide ice at 1990 cm^{-1}.[88] Further evidence in support of the proposed reaction pathway to ketene is also provided by ReTOF mass spectroscopic analysis. The ReTOF mass spectroscopic analysis resulted in the identification of ion counts at three different mass-to-charge ratios, m/z = 44 amu (D_2CCO), 45 amu ($D_2C^{13}CO$) and 46 amu ($D_2{}^{13}C^{13}CO$), as shown in Fig. 9. Here, in the processed $CD_3OD–^{13}CO$ ice system, two ketene isotopomers, D_2CCO (m/z = 44 amu) and $D_2C^{13}CO$ (45 amu), are expected to form *via* reaction (xix) and (xx) is expected to produce $D_2{}^{13}C^{13}CO$ (m/z = 46 amu) since both the carbon atoms have originated from ^{13}CO molecules.

Finally, we would like to comment on the general reaction pathways ultimately producing larger molecules identified above. Here, radical–radical recombination of a methyl radical (CH_3) with a methoxy radical (CH_3O) (reaction (xxiii)) and a hydroxymethyl radical (CH_2OH) (reaction (xxiv)) can lead to the formation of C_2H_6O isomers, dimethyl ether (CH_3OCH_3) and ethanol (CH_3CH_2OH), respectively.

$$CH_3 + CH_3O \rightarrow CH_3OCH_3 \quad \text{(xxiii)}$$

$$CH_3 + CH_2OH \rightarrow CH_3CH_2OH \quad \text{(xxiv)}$$

Similarly, dimerization of the CH_3O radical (reaction (xxv)) and reaction with CH_2OH (reaction (xxvi)) can result in the formation of dimethyl peroxide (CH_3OOCH_3) and methoxymethanol (CH_3OCH_2OH), respectively.

$$CH_3O + CH_3O \rightarrow CH_3OOCH_3 \quad \text{(xxv)}$$

$$CH_3O + CH_2OH \rightarrow CH_3OCH_2OH \quad \text{(xxvi)}$$

In addition, dimerization of the HCO radical can also form the product glyoxal (HCOCHO) *via* reaction (xxvii).

$$HCO + HCO \rightarrow HCOCHO \quad \text{(xxvii)}$$

A schematic summary of the overall formation routes of the products identified using ReTOF mass spectroscopic analysis and *in situ* IR spectroscopy is presented in Fig. 11. Among them, the possible formation pathways mostly *via* radical–radical recombination pathways are discussed above for ketene (C_2H_2O), acetaldehyde (C_2H_4O), glycolaldehyde ($C_2H_4O_2$) and ethylene glycol ($C_2H_6O_2$). Also, a possible formation route to methoxymethane (C_2H_6O), ethanol (C_2H_6O), dimethyl peroxide ($C_2H_6O_2$), methoxymethanol ($C_2H_6O_2$) and glyoxal ($C_2H_2O_2$) is discussed.

5. Summary

The present experiments demonstrated that complex organics are formed in methanol and mixed methanol–carbon monoxide ices exposed to ionizing radiation at 5.5 K. Frozen methanol and carbon monoxide have long been identified as key constituents within the molecular clouds of the interstellar medium in addition to ubiquitous water along with minor amounts of methane, ammonia and carbon dioxide.[35–41] The molecular abundance of methanol within the icy mantles varies from 5% to 30% relative to water in several low mass star-forming regions or dark molecular clouds.[36,89,90] In addition, carbon monoxide is often present with methanol in numerous sources with its abundance in icy mantles typically around 20% with respect to water.[35–41] These icy mantles are constantly being bombarded with high energy galactic cosmic rays and/or exposed to the interstellar UV field. Consequently, an understanding of the radiation induced chemical modifications of methanol and mixed methanol–carbon monoxide ices remains extremely important in understanding the chemical evolution of molecular clouds. In the current study presented here, a combined *in situ* infrared spectroscopic (solid state) and mass spectroscopic (gas phase) detection scheme was employed to identify the endogenous products formed within methanol and methanol–carbon monoxide ices exposed to energetic electrons simulating the equivalent exposure of chemical processing *via* galactic cosmic rays.[91–93] Experiments with isotopically labeled methanol (CH_3OH, CD_3OD, $^{13}CH_3OH$, and $CH_3{}^{18}OH$) and methanol–carbon monoxide ices (CH_3OH–CO, CD_3OD–CO, $^{13}CH_3OH$–CO, $CH_3{}^{18}OH$–CO, $CD_3OD–^{13}CO$, $CH_3{}^{18}OH–C^{18}O$, and $CH_3OH–C^{18}O$) were conducted to help identify products and reaction pathways *via* the observed frequency shifts of functional groups and mass shifts in gas phase detection of TPD spectra. The infrared spectroscopic analysis resulted in the identification of the following radiolysis products: hydroxymethyl radical (CH_2OH), formyl radical (HCO), methane (CH_4), formaldehyde

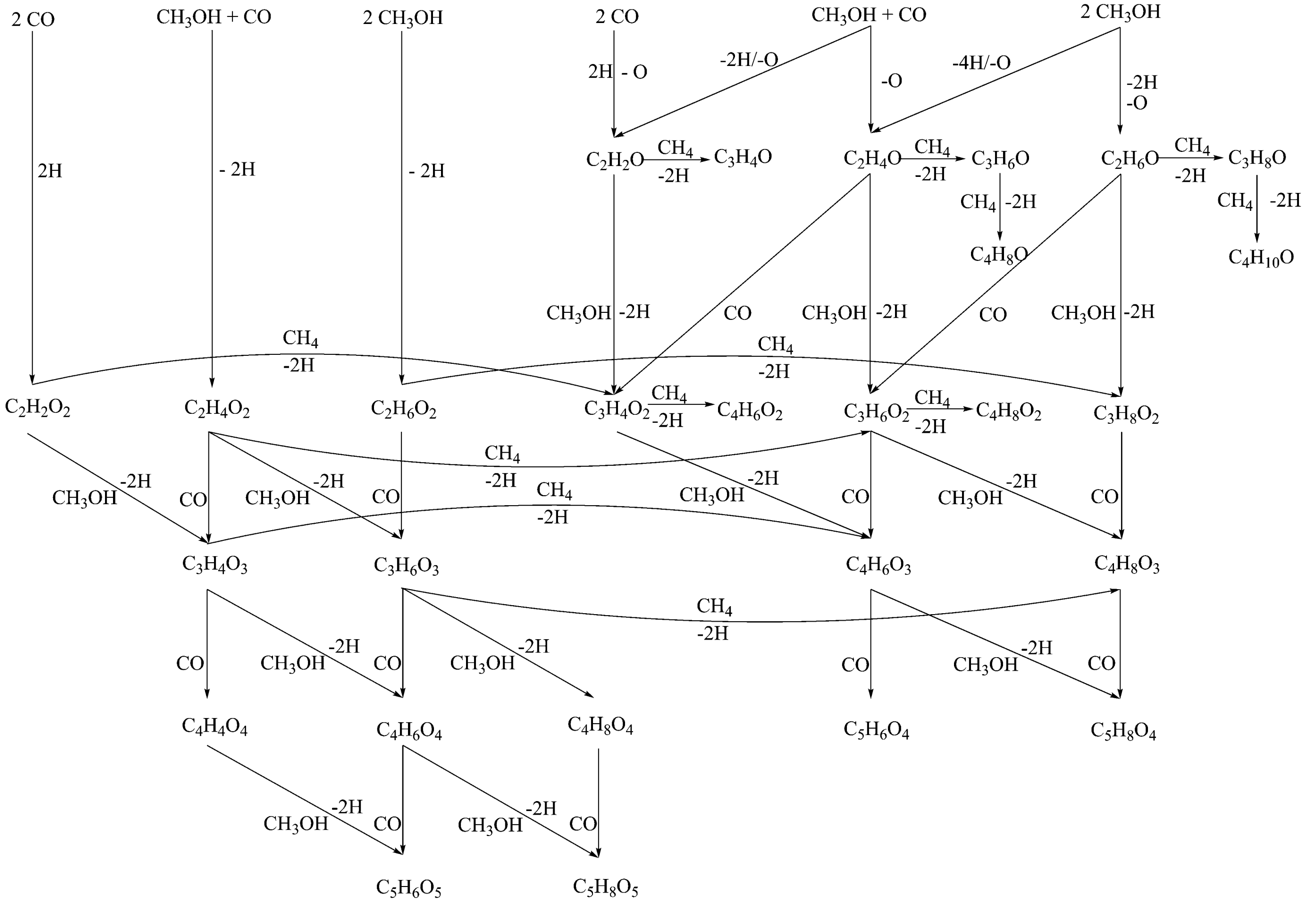

Fig. 11 Schematic representation of the formation routes of the newly formed products detected in the irradiated methanol and methanol–carbon monoxide ices.

(H_2CO), carbon dioxide (CO_2), ethylene glycol ($HOCH_2CH_2OH$), glycolaldehyde ($HOCH_2CHO$), methyl formate ($HCOOCH_3$), and ketene (H_2CCO). Also of note is the suggested formation of large and complex carbonyl bearing organics such as acetaldehyde, saturated/unsaturated high mass aldehydes (*e.g.* propanal and propenal) and ketones (*e.g.* acetone) through deconvolution of the carbonyl absorption bands, observed in both methanol and methanol–carbon monoxide isotopologue ices. However, the infrared spectroscopic analysis is limited as similar functional groups overlap resulting in an ambiguous assignment. Subsequently, we conducted temperature programmed desorption (TPD) complemented with single photon ionization ReTOF mass spectrometry at 10.49 eV to monitor the endogenous products sublimating. Using ReTOF mass spectrometry of the sublimating species, we have definitively identified ketene (H_2CCO), acetaldehyde (CH_3COH), ethanol (C_2H_5OH), dimethyl ether (CH_3OCH_3), glyoxal ($HCOCOH$), glycolaldehyde ($HOCH_2CHO$), ethene-1,2-diol ($HOCHCHOH$), ethylene glycol ($HOCH_2CH_2OH$), methoxy methanol (CH_3OCH_2OH) and glycerol ($CH_2OHCHOHCH_2OH$) in the irradiated ice systems. Moreover, we were able to identify molecules containing up to *five oxygen* atoms sublimating from the processed ices; however, no specific assignments of these large organics could be made at this time.

Here it is worth comparing the identified products in the present experiments with the C/H/O bearing molecules detected in the interstellar medium which are displayed in Fig. 12. All of the alcohols that have been observed in the ISM have been identified in this study, save for that of vinyl alcohol (CH_2CHOH) which has at this time been labelled as tentatively identified. Among the aldehydes detected in the ISM, formaldehyde (H_2CO) and acetaldehyde (CH_3CHO) were confirmed as endogenous synthesized products following exposure to ionizing radiation. Higher mass aldehydes such as propanal (CH_3CH_2CHO) and propenal (CH_2CHCHO) have been tentatively identified as possible isomers of C_3H_6O and C_3H_4O identified *via* ReTOF spectrometry. Within the group of ester type molecules, methyl formate ($HCOOCH_3$) was confirmed *via* only infrared spectroscopy as the ionization energy (10.84 eV) is greater than the available ionization energy (10.49 eV) used in the present study while methyl acetate (CH_3COOCH_3) and ethyl formate ($HCOOC_2H_5$) were only tentatively assigned as possible $C_3H_6O_2$ isomers. The only sugar molecule observed thus far in the ISM is glycolaldehyde ($HOCH_2CHO$) and has been confirmed *via* both infrared spectroscopy and ReTOF mass spectrometry in all ice systems upon exposure to ionizing radiation presented here. Both of the ether type molecules that have been detected in the interstellar medium, dimethyl ether (CH_3OCH_3) and methoxyethane ($CH_3OCH_2CH_3$),

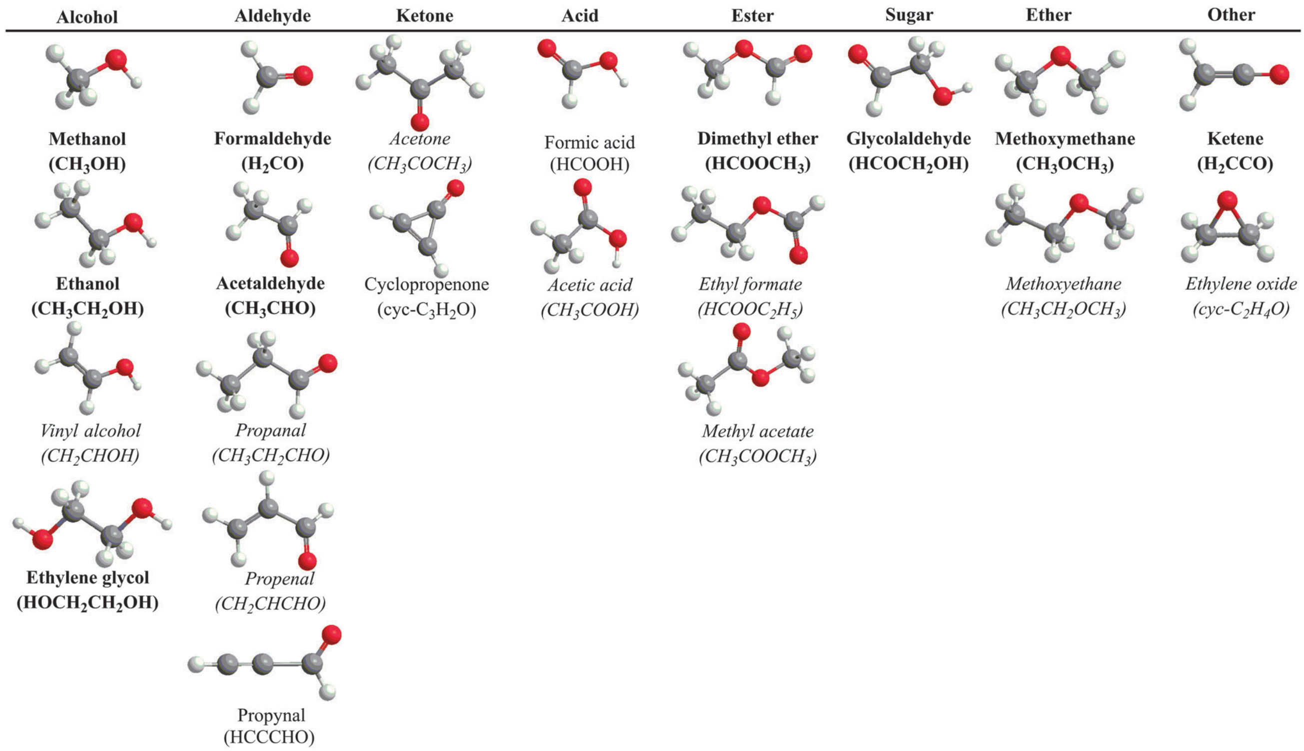

Fig. 12 List of C/H/O bearing stable molecules detected in the interstellar medium (ISM). The molecules indicated in bold letters are identified in the present study. The molecules indicated in *italics* are the possible isomers of the products identified in the present study.

are identified as well in both the irradiated methanol and methanol–carbon monoxide ices using ReTOF mass spectrometry. Finally, ketene (H_2CCO) has been identified as a radiolytic by-product in all ice systems, *via* both FTIR spectroscopy and ReTOF mass spectrometry. Unfortunately, in the present study we could not elucidate the majority of the higher mass organics containing anywhere from three to five oxygen atoms as the calibration experiments were not unique enough to disentangle the contribution from each possible isomer. However, future experimental investigations with tunable vacuum ultraviolet light for selective ionization will allow the specific assignment of isomers based on the unique ionization energy, complemented with their m/z ratios and unique temperature or energy of desorption.

Several novel reaction pathways have been identified in this study as well. These reaction pathways have been classified for the sake of simplicity as (i) "$2CH_3OH$", (ii) "$1CH_3OH + 1CO$" and (iii) "2CO" and are summarized in Fig. 10 and 11. By conducting experiments with mixed isotopes of a specific atom, we were able to trace the isotope in the observed m/z shift in the TPD spectra and frequency shift *via in situ* IR spectroscopy. As anticipated, in the processed mixed ices the "$1CH_3OH + 1CO$" is the most prominent reaction pathway producing the expected isotopologues as is correlated (Table 4B) with the most intense ion peaks. However, the "$2CH_3OH$" and "2CO" reaction pathways as described in Section 4.2 did result in enough products with high enough column densities to be observed *via* IR spectroscopy and ionized in the gas phase during TPD ReTOF analysis, as such they are not inconsequential in the formation of complex organics. Future experiments will explore the possibility of isotopic fractionation resulting from these identified pathways.

Finally, we would like to comment on the astrobiological relevance of the present reaction products. We have identified several products associated with the sugar related molecules formed within methanol and methanol–carbon monoxide ice systems exposed to ionizing radiation. As mentioned, the simplest form of sugar, glycolaldehyde ($HOCH_2CHO$), has been identified. In addition, the sugar alcohol (ethylene glycol; $HOCH_2CH_2OH$) and the dehydrogenated form of glycolaldehyde (glyoxal; HCOCHO) were also identified in irradiated methanol ice (only ethylene glycol) and methanol–carbon monoxide ice (both ethylene glycol and glyoxal). We have also found evidence for the possible formation of higher mass sugar molecules as shown in Fig. 13. Here, we observed products sublimating with the molecular formula $C_3H_6O_3$ in all of the processed ice systems. Unfortunately we can only suggest that within this group of isomers C3 sugar molecules (glyceraldehyde and 1,3-dihydroxyacetone) are formed. Previous searches for these C3-sugar molecules, glyceraldehyde ($HOCH_2CH(OH)CHO$)[21] and 1,3-dihydroxyacetone ($(HOCH_2)_2CO$),[22–24] in the ISM have been remained inconclusive until now. However, these molecules were found on the recovered carbonaceous meteorites on Earth,[9] implying the presence of an extraterrestrial origin and the possibility of an *ex situ* delivery to a prebiotic earth. In addition, the survivability of glycolaldehyde has recently been demonstrated in simulated meteoric impacts.[94] Finally, we have also identified $C_4H_8O_4$ and $C_5H_8O_5$ in irradiated methanol–carbon monoxide ices. These products can be linked to

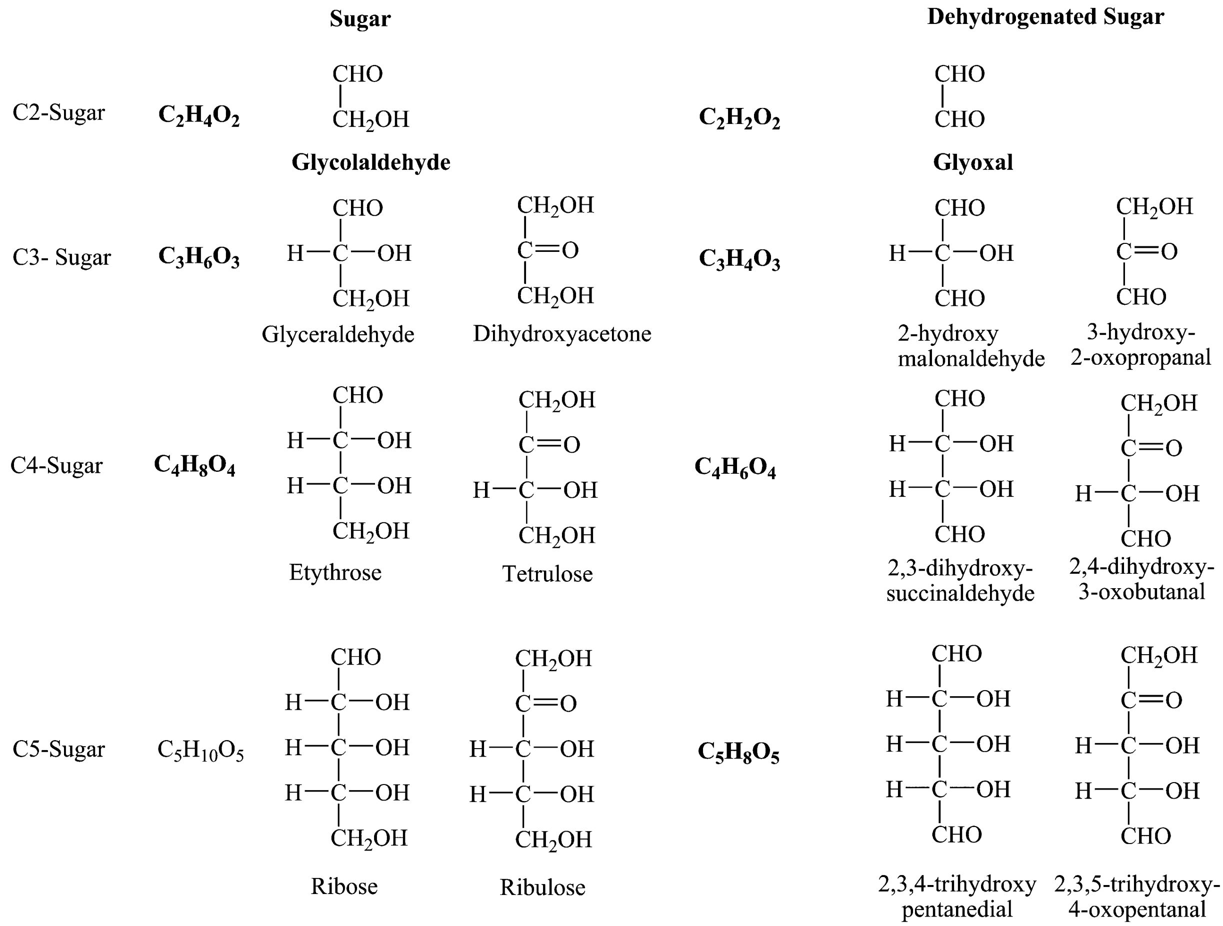

Fig. 13 Examples of C2–C5 sugar and dehydrogenated sugar with the corresponding molecular formula. Molecules with these potential molecular structures that have been identified in irradiated methanol and methanol–carbon monoxide mixed ices are depicted in bold.

the C4-sugar molecules erythrose ($CH_2OH(CHOH)_2CHO$) and tetrulose ($CH_2OHCHOHC(O)HCH_2OH$) and dehydrated forms of ribose and ribulose (C5-sugars) as shown in Fig. 13. These molecules are key components of RNA, DNA and cell membranes, as well as important energy sources. Consequently, the prebiotic origin of large sugar molecules is essential for aiding in the overall understanding of the origin of life.

The results presented here demonstrate that significantly large complex organics are synthesized as a result of exposure to ionizing radiation at relatively low doses, *i.e.* a few eV per molecule as typical for an ice-covered grain within a cold molecular cloud. Furthermore, our results imply that state-of-the-art experimental techniques are necessary to fully elucidate the rich and complex chemistry that is induced within these simulated astrophysical environments. As described above, many of the molecules were masked within the *in situ* FTIR spectroscopy due to the similar functional groups and subsequent overlapping frequencies. Utilizing temperature programmed desorption coupled with single photoionization reflectron time-of-flight mass spectrometry, a plethora of large complex organics were detected. Unfortunately, many of the molecules could not specifically be identified based on their TPD profile alone. Next generation experiments are currently being designed to reveal the exact molecular structure of the tentatively assigned molecules based upon their unique ionization energies correlated with their distinct temperature of desorption. Exploiting each molecules exclusive ionization energy will be accomplished from the use of *tunable* vacuum ultraviolet light photons generated *via* four wave mixing. This technique has recently been successfully implemented with promising results to be disseminated in the near future and will be used more extensively with upcoming experimental studies.

Acknowledgements

The authors would like to thank the NASA Exobiology Program MNX13AH62G, the W. M. Keck Foundation and the University of Hawaii at Manoa for their financial support.

References

1 Cologne, The Cologne Database for Molecular Spectroscopy: http://www.astro.uni-koeln.de/cdms, 2013, DOI: The Cologne Database for Molecular Spectroscopy.

2 E. Herbst, *Phys. Chem. Chem. Phys.*, 2014, **16**, 3344–3359.

3 E. Herbst and E. F. van Dishoeck, *Annu. Rev. Astron. Astrophys.*, 2009, **47**, 427–480.
4 A. I. Vasyunin and E. Herbst, *Astron. J.*, 2013, **769**, 34.
5 Å. Hjalmarson, P. Bergman and A. Nummelin, *Proc. 1st European Workshop on Exo-/astro-biology (ESA SP-496)*, Noordwijk, ESA, 2001.
6 D. T. Halfen, V. Ilyushin and L. M. Ziurys, *Astron. J.*, 2011, **743**, 60.
7 A. F. Jalbout, *Origins Life Evol. Biospheres*, 2008, **38**, 489–497.
8 J. E. Elsila, J. P. Dworkin, M. P. Bernstein, M. P. Martin and S. A. Sandford, *Astrophys. J.*, 2007, **660**, 911.
9 G. Cooper, N. Kimmich, W. Belisle, J. Sarinana, K. Brabham and L. Garrel, *Nature*, 2001, **414**, 879–883.
10 M. H. Engel and S. A. Macko, *Precambrian Res.*, 2001, **106**, 35–45.
11 M. H. Engel and S. A. Macko, *Nature*, 1997, **389**, 265–268.
12 H. Busemann, A. F. Young, C. M. D. Alexander, P. Hoppe, S. Mukhopadhyay and L. R. Nittler, *Science*, 2006, **312**, 727–730.
13 O. Botta, D. Glavin, G. Kminek and J. Bada, *Origins Life Evol. Biospheres*, 2002, **32**, 143–163.
14 J. M. Hollis, F. J. Lovas and P. R. Jewell, *Astrophys. J., Lett.*, 2000, **540**, L107–L110.
15 J. M. Hollis, S. N. Vogel, L. E. Snyder, P. R. Jewell and F. J. Lovas, *Astrophys. J., Lett.*, 2001, **554**, L81–L85.
16 D. T. Halfen, A. J. Apponi, N. Woolf, R. Polt and L. M. Ziurys, *Astrophys. J.*, 2006, **639**, 237–245.
17 M. A. Requena-Torres, J. Martín-Pintado, S. Martín and M. R. Morris, *Astrophys. J.*, 2008, **672**, 352.
18 J. K. Jørgensen, C. Favre, S. E. Bisschop, T. L. Bourke, E. F. van Dishoeck and M. Schmalzl, *Astrophys. J., Lett.*, 2012, **757**, L4.
19 J. M. Hollis, F. J. Lovas, P. R. Jewell and L. H. Coudert, *Astrophys. J., Lett.*, 2002, **571**, L59–L62.
20 J. Crovisier, D. Bockelee-Morvan, N. Biver, P. Colom, D. Despois and D. C. Lis, *Astron. Astrophys.*, 2004, **418**, L35–L38.
21 J. M. Hollis, P. R. Jewell, F. J. Lovas, A. Remijan and H. Mollendal, *Astrophys. J., Lett.*, 2004, **610**, L21.
22 W. S. L. Weaver and G. A. Blake, *Astrophys. J.*, 2005, **624**, L33–L36.
23 S. L. Widicus, R. Braakman, D. R. Kent Iv and G. A. Blake, *J. Mol. Spectrosc.*, 2004, **224**, 101–106.
24 A. J. Apponi, D. T. Halfen, L. M. Ziurys, J. M. Hollis, A. J. Remijan and F. J. Lovas, *Astrophys. J., Lett.*, 2006, **643**, L29–L32.
25 M. A. Requena-Torres, J. Martin-Pintado, A. Rodriguez-Franco, S. Martin, N. J. Rodrmguez-Fernandez and P. De Vicente, *Astron. Astrophys.*, 2006, **455**, 971–985.
26 A. Bacmann, V. Taquet, A. Faure, C. Kahane and C. Ceccarelli, *Astron. Astrophys.*, 2012, **541**, L12.
27 A. G. G. M. Tielens and W. Hagen, *Astron. Astrophys.*, 1982, **114**, 245–260.
28 D. P. Ruffle and E. Herbst, *Mon. Not. R. Astron. Soc.*, 2001, **322**, 770.
29 R. T. Garrod and E. Herbst, *Astron. Astrophys.*, 2006, **457**, 927–936.
30 R. T. Garrod, S. L. W. Weaver and E. Herbst, *Astrophys. J.*, 2008, **682**, 283.
31 A. Belloche, R. T. Garrod, H. S. P. Muller, K. M. Menten, C. Comito and P. Schilke, *Astron. Astrophys.*, 2009, **499**, 215–232.
32 R. T. Garrod and S. L. Widicus Weaver, *Chem. Rev.*, 2013, **113**, 8939–8960.
33 T. G. Robin, *Astrophys. J.*, 2013, **765**, 60.
34 H. G. Arce, J. Santiago-Garcia, J. K. Jorgensen, M. Tafalla and R. Bachiller, *Astrophys. J., Lett.*, 2008, **681**, L21–L24.
35 E. L. Gibb, D. C. B. Whittet, W. A. Schutte, A. C. A. Boogert, J. E. Chiar, P. Ehrenfreund, P. A. Gerakines, J. V. Keane, A. G. G. M. Tielens, E. F. v. Dishoeck and O. Kerkhof, *Astrophys. J.*, 2000, **536**, 347.
36 E. L. Gibb, D. C. B. Whittet, A. C. A. Boogert and A. G. G. M. Tielens, *Astrophys. J., Suppl. Ser.*, 2004, **151**, 35–73.
37 A. C. A. Boogert, K. M. Pontoppidan, C. Knez, F. Lahuis, J. Kessler-Silacci, E. F. Van Dishoeck, G. A. Blake, J. C. Augereau, S. E. Bisschop and S. Bottinelli, *Astrophys. J.*, 2008, **678**, 985.
38 K. I. Öberg, A. C. A. Boogert, K. M. Pontoppidan, G. A. Blake, N. J. Evans, F. Lahuis and E. F. v. Dishoeck, *Astrophys. J.*, 2008, **678**, 1032.
39 K. M. Pontoppidan, A. C. A. Boogert, H. J. Fraser, E. F. van Dishoeck, G. A. Blake, F. Lahuis, K. I. Oberg, N. J. Evans Ii and C. Salyk, *Astrophys. J.*, 2008, **678**, 1005.
40 K. I. Öberg, A. C. A. Boogert, K. M. Pontoppidan, B. Saskia van den, E. F. v. Dishoeck, B. Sandrine, A. B. Geoffrey, I. Neal and J. Evans, *Astrophys. J.*, 2011, **740**, 109.
41 W. T. Reach, M. S. Kelley and J. Vaubaillon, in ArXiv e-prints, 2013, vol. 1306, p. 2381.
42 R. I. Kaiser, G. Eich, A. Gabrysch and K. Roessler, *Astrophys. J.*, 1997, **484**, 487–498.
43 R. I. Kaiser and K. Roessler, *Astrophys. J.*, 1998, **503**, 959.
44 M. Garozzo, D. Fulvio, Z. Kanuchova, M. E. Palumbo and G. Strazzulla, *Astron. Astrophys.*, 2010, **509**, A67.
45 S. E. Bisschop, G. W. Fuchs, E. F. van-Dishoeck and H. Linnartz, *Astron. Astrophys.*, 2007, **474**, 1061–1071.
46 W. D. Geppert, M. Hamberg and R. D. Thomas, *et al.*, *Faraday Discuss.*, 2006, **133**, 177.
47 N. J. Mason, A. Dawes, P. D. Holtom, R. J. Mukerji, M. P. Davis, B. Sivaraman, R. I. Kaiser, S. V. Hoffmann and D. A. Shaw, *Faraday Discuss.*, 2006, **133**, 311–329.
48 C. J. Bennett, C. S. Jamieson, Y. Osamura and R. I. Kaiser, *Astrophys. J.*, 2005, **624**, 1097–1115.
49 C. J. Bennett, Y. Osamura, M. D. Lebar and R. I. Kaiser, *Astron. J.*, 2005, **634**, 698–711.
50 L. Zhou, R. I. Kaiser, L. G. Gao, A. H. H. Chang, M. C. Liang and Y. Y. Yung, *Astrophys. J.*, 2008, **686**, 1493–1502.
51 C. J. Bennett, T. Hama, Y. S. Kim, M. Kawasaki and R. I. Kaiser, *Astrophys. J.*, 2011, **727**, 27–37.
52 C. J. Bennett and R. I. Kaiser, *Astrophys. J.*, 2007, **660**, 1289–1295.
53 C. J. Bennett, S.-H. Chen, B.-J. Sun, A. H. H. Chang and R. I. Kaiser, *Astrophys. J.*, 2007, **660**, 1588.
54 C. J. Bennett and R. I. Kaiser, *Astrophys. J.*, 2007, **661**, 899–909.

55 P. A. Gerakines, W. A. Schutte and P. Ehrenfreund, *Astron. Astrophys.*, 1996, **312**, 289–305.
56 K. I. Öberg, R. T. Garrod, E. F. van Dishoeck and H. Linnartz, *Astron. Astrophys.*, 2009, **504**, 891–913.
57 T. D. Harris, D. H. Lee, M. Q. Blumberg and C. R. Arumainayagam, *J. Phys. Chem.*, 1995, **99**, 9530–9535.
58 P. Modica and M. E. Palumbo, *Astron. Astrophys.*, 2010, **519**, 22.
59 P. Modica, M. E. Palumbo and G. Strazzulla, *Planet. Space Sci.*, 2012, **73**, 425–429.
60 Y. J. Chen, A. Ciaravella, G. M. M. Caro, C. Cecchi-Pestellini, A. Jimenez-Escobar, K. J. Juang and T. S. Yih, *Astrophys. J.*, 2013, **778**, 162.
61 R. I. Kaiser, S. Maity and B. M. Jones, *Phys. Chem. Chem. Phys.*, 2014, **16**, 3399–3424.
62 B. M. Jones and R. I. Kaiser, *J. Phys. Chem. Lett.*, 2013, **4**, 1965–1971.
63 S. Maity, R. I. Kaiser and B. M. Jones, *Faraday Discuss.*, 2014, **168**, 485–516.
64 S. Maity, R. I. Kaiser and B. M. Jones, *Astron. J.*, 2014, **788**, 36.
65 M. S. Westley, G. A. Baratta and R. A. Baragiola, *J. Chem. Phys.*, 1998, **108**, 3321–3326.
66 R. Brunetto, G. Caniglia, G. A. Baratta and M. E. Palumbo, *Astrophys. J.*, 2008, **686**, 1480–1485.
67 A. M. Goodman, *Appl. Opt.*, 1978, **17**, 2779–2787.
68 W. R. M. Rocha and S. Pilling, *Spectrochim. Acta, Part A*, 2014, **123**, 436–446.
69 R. Luna, M. Á. Satorre, M. Domingo, C. Millán and C. Santonja, *Icarus*, 2012, **221**, 186–191.
70 P. Hovington, D. Drouin and R. Gauvin, *Scanning*, 1997, **19**, 1–14.
71 D. Drouin, A. R. Couture, D. Joly, X. Tastet, V. Aimez and R. Gauvin, *Scanning*, 2007, **29**, 92–101.
72 R. Hilbig and R. Wallenstein, *IEEE J. Quantum Electron.*, 1981, **17**, 1566–1573.
73 W. A. VonDrasek, S. Okajima and J. P. Hessler, *Appl. Opt.*, 1988, **27**, 4057–4061.
74 R. L. Hudson and M. H. Moore, *Icarus*, 2000, **145**, 661–663.
75 R. L. Hudson and M. J. Loeffler, *Astrophys. J.*, 2013, **77**, 109.
76 A. Aspiala, J. Murto and P. Sten, *Chem. Phys.*, 1986, **106**, 399–412.
77 J. Ceponkus, W. Chin, M. Chevalier, M. Broquier, A. Limongi and C. Crépin, *J. Chem. Phys.*, 2010, **133**, 094502.
78 R. L. Hudson and M. H. Moore, *Radiat. Phys. Chem.*, 1995, **45**, 779–789.
79 G. A. Baratta, A. C. Castorina, G. Leto, M. E. Palumbo, F. Spinella and G. Strazzulla, *Planet. Space Sci.*, 1994, **42**, 759–766.
80 M. P. Collings, J. W. Dever, H. J. Fraser and M. R. S. McCoustra, *Astrophys. Space Sci.*, 2003, **285**, 633–659.
81 H. Y. Afeefy, J. F. Liebman and S. E. Stein, in *Neutral Thermochemical Data*, ed. P. J. Linstrom and W. G. Mallard, National Institute of Standards and Technology, Gaithersburg, MD, 2013, vol. 69.
82 Y. J. Shi, S. Consta, A. K. Das, B. Mallik, D. Lacey and R. H. Lipson, *J. Chem. Phys.*, 2002, **116**, 6990–6999.
83 F. Bell, Q. N. Ruan, A. Golan, P. R. Horn, M. Ahmed, S. R. Leone and M. Head-Gordon, *J. Am. Chem. Soc.*, 2013, **135**, 14229–14239.
84 D. Vijay and G. N. Sastry, *THEOCHEM*, 2005, **714**, 199–207.
85 M. D. Boamah, K. K. Sullivan, K. K. Shulenberger, C. M. Soe, L. M. Jacob, F. C. Yhee, K. E. Atkinson, M. C. Boyer, D. R. Haines and C. R. Arumainayagam, *Faraday Discuss.*, 2014, **168**, 1–18.
86 R. A. Johnson and A. E. Stanley, *Appl. Spectrosc.*, 1991, **45**, 218–222.
87 C. S. Jamieson, A. M. Mebel and R. I. Kaiser, *Astrophys. J., Suppl. Ser.*, 2006, **163**, 184–206.
88 P. A. Gerakines and M. H. Moore, *Icarus*, 2001, **154**, 372.
89 E. Dartois, W. Schutte, T. R. Geballe, K. Demyk, P. Ehrenfreund and L. d'Hendecourt, *Astron. Astrophys.*, 1999, **342**, L32–L35.
90 K. M. Pontoppidan, E. Dartois, E. F. van Dishoeck, W.-F. Thi and L. d'Hendecourt, *Astron. Astrophys.*, 2003, **404**, L17–L20.
91 M. H. Moore, R. L. Hudson and P. A. Gerakines, *Spectrochim. Acta*, 2001, **57**, 843–858.
92 R. I. Kaiser and K. Roessler, *Astrophys. J.*, 1997, **475**, 144–154.
93 G. Strazzulla, A. C. Castorina and M. E. Palumbo, *Planet. Space Sci.*, 1995, **43**, 1247–1251.
94 V. P. McCaffrey, N. E. B. Zellner, C. M. Waun, E. R. Bennett and E. K. Earl, *Origins Life Evol. Biospheres*, 2014, 1–14, DOI: 10.1007/s11084-014-9358-5.

